**Polish Society of Theoretical and Applied Electrical Engineering**
**Częstochowa Branch**

# *XII SYMPOSIUM*
# *OF MAGNETIC MEASUREMENTS & MODELING*


*Częstochowa – Siewierz, 17th – 19th October 2016*

*in memory of*
*Professor Kazimierz Zakrzewski (1938 – 2016)*

# *ABSTRACTS*

**Under the auspices of**

**Polish Academy of Science**
**Committee of Electrical Engineering**

**Professor Krzysztof Kluszczyński**
**President of Polish Society of Theoretical and Applied Electrical Engineering (PTETiS)**

**Organized in the jubilee year of**

**55th anniversary of**
**Polish Society of Theoretical and Applied Electrical Engineering**

**15th anniversary of**
**Polish Society of Theoretical and Applied Electrical Engineering, Częstochowa Branch**

**50th anniversary of**
**Faculty of Electrical Engineering**
**Częstochowa University of Technology**

# XII SYMPOSIUM OF MAGNETIC MEASUREMENTS & MODELING

**Częstochowa – Siewierz, 17th – 19th October 2016**

## *ORGANIZED BY:*

**Polish Society of Theoretical and Applied Electrical Engineering, Częstochowa Branch**

**Częstochowa University of Technology**
**Faculty of Electrical Engineering**

**Tele & Radio Research Institute, Warsaw**

**Ariel University, Ariel, Israel**

**Institute of Materials Science**
**University of Silesia in Katowice**

**Stalprodukt S.A., Bochnia**

**Electrotechnical Institute, Warsaw**

# XII SYMPOSIUM OF MAGNETIC MEASUREMENTS & MODELING

**Częstochowa – Siewierz, 17th – 19th October 2016**

## SCIENTIFIC COMITTEE

*Chairman:*

| | |
|---|---|
| Kazimierz Zakrzewski | Łódź University of Technology, Poland |

*Honorary Chairman:*

| | |
|---|---|
| Jacek R. Przygodzki | Retired Professor of Warsaw University of Technology, Warsaw, Poland |

*Members:*

| | |
|---|---|
| Jerzy Bajorek | Wrocław University of Technology, Poland |
| Lech Borowik | Częstochowa University of Technology, Poland |
| Adam Bieńkowski | Warsaw University of Technology, Poland |
| Marcos F. de Campos | Fluminense Federal University, Brazil |
| Krzysztof Chwastek | Częstochowa University of Technology, Poland |
| Andrzej Demenko | Poznań University of Technology, Poland |
| Józef Gromek | Tele & Radio Research Institute, Poland |
| Octavio Guzman | Universidad Nacional de Colombia, Colombia |
| Grzegorz Haneczok | University of Silesia, Poland |
| Robert G. Harrison | Carleton University, Canada |
| Andrzej Kapłon | Kielce University of Technology, Poland |
| Andriy Kityk | Częstochowa University of Technology, Poland |
| Ivan Kityk | Częstochowa University of Technology, Poland |
| Krzysztof Kluszczyński | Silesian University of Technology, Poland |
| Marcin Leonowicz | Warsaw University of Technology |
| Aminta Mendoza | Universidad Nacional de Colombia, Colombia |
| Yevgen Melikhov | Wolfson Centre for Magnetics, Cardiff University, UK |
| Waldemar Minkina | Częstochowa University of Technology, Poland |
| Roman Nadolski | Kielce University of Technology, Poland |
| Andrzej Nowakowski | Tele & Radio Research Institute, Poland |
| Ryszard Nowosielski | Silesian University of Technology, Poland |
| Marian Pasko | Silesian University of Technology, Poland |
| Yosef Pinhasi | Ariel University, Israel |
| Andrzej Rusek | Częstochowa University of Technology, Poland |
| Krzysztof Sokalski | Częstochowa University of Technology |
| Jan Szczygłowski | Częstochowa University of Technology, Poland |
| Barbara Ślusarek | Tele & Radio Research Institute, Poland |
| Sławomir Tumański | Warsaw University of Technology, Poland |

| | |
|---|---|
| Manuel Vázquez | Institute of Material Science of Madrid, Spain |
| Andrzej Wac-Włodarczyk | Lublin University of Technology, Poland |
| Wiesław Wilczyński | Electrotechnical Institute, Warsaw |
| Jerzy Wysłocki | Częstochowa University of Technology, Poland |
| Asher Yahalom | Ariel University, Israel |
| Sergey E. Zirka | Dnepropetrovsk National University, Ukraine |
| Stan Żurek | Megger Ltd., United Kingdom |

## ORGANIZING COMITTEE

| | |
|---|---|
| Jan Szczygłowski | Head of the Committee |
| Mariusz Najgebauer | Secretary |
| Adam Jakubas | |

# FRAME PROGRAM OF
# XII SYMPOSIUM OF MAGNETIC MEASUREMENTS & MODELING

**Częstochowa – Siewierz, 17th – 19th October 2016**

| | | |
|---|---|---|
| **Monday 17.10.2016** | | |
| **9.00 – 11.30** | **Registration of the participants** | |
| **11.30 – 11:45** | **Official opening of the Symposium** | |
| **11.45 – 13.00** | **Plennary Session I** | |
| **13.00 – 14.00** | **Lunch** | |
| **14.00 – 16.00** | **Session 1A:**<br>**Magnetic Measurements** | **Session 1B:**<br>**Solid State I** |
| **16.00 – 16.30** | **Coffee break** | |
| **16.30 – 18.30** | **Session 2A:**<br>**Magnetic Modelling** | **Session 2B:**<br>**Solid State II** |
| **19.00 – 22.00** | **Barbeque** | |
| **Tuesday 18.10.2016** | | |
| **7.30 – 9.00** | **Breakfast** | |
| **9.00 – 10.00** | **Plennary Session II** | |
| **10.00 – 10.30** | **Coffee break** | |
| **10.30 – 13.00** | **Session 3A:**<br>**Non-Destructive Testing** | **Session 3B:**<br>**Solid State III** |
| **13.00 – 14.00** | **Lunch** | |
| **14.00 – 15.30** | **Session 4A:**<br>**Sensors and Actuators I** | **Session 4B:**<br>**Electric Machines** |
| **15.30 – 16.00** | **Coffee break** | |
| **16.00 – 17.30** | **Session 5A:**<br>**Sensors and Actuators II** | **Session 5B:**<br>**Magnetic fluids and powders** |
| **18.30 – 24.00** | **Gala dinner with Concert *Film music Kilar & Morricone***<br>**(Beniamin Czech – violino, Magdalena Czech – cello, Tadeusz Trzaskalik – piano)** | |
| **Wednesday 19.10.2016** | | |
| **7.30 – 9.00** | **Breakfast** | |
| **9.00 – 10.45** | **Session 6:**<br>**Novel solutions** | |
| **10.45 – 11.15** | **Coffee break** | |
| **11.00 – 11.15** | **Meeting of the SMMM Scientific Committee** | |
| **11:15** | **Closing remarks of the Symposium** | |
| **12.00 – 13.00** | **Lunch** | |

# PROGRAM OF
# XII SYMPOSIUM OF MAGNETIC MEASUREMENTS & MODELING
**Częstochowa – Siewierz, 17th – 19th October 2016**

| **Monday 17.10.2016** | |
|---|---|
| 9.00 – 11.30 | Registration of the participants |
| 11.30 – 11:45 | **Official opening of the Symposium** |
| 11.45 – 13.00 | **Plennary Session I**<br>***Chairmen: prof. A. Demenko, prof. R. Nadolski***<br>1. **Remembrance of Professor Kazimierz Zakrzewski**<br>2. **Invited talk**: *R. Hiergeist, K. Wagner, G. Ross*, Characterization of softmagnetic materials in AC magnetic fields by digital methods<br>3. **Invited talk**: *R. Szewczyk*, Method of moments in Jiles-Atherton model based magnetostatic modelling of thin layers |
| 13.00 – 14.00 | Lunch |
| 14.00 – 16.00 | **Session 1A: Magnetic Measurements**<br>***Chairmen: prof. R. Szewczyk, dr J. Bajorek***<br>1. *R. Gozdur, P. Szczurek, A. Majocha*, Intercomparison of measurements of magnetic power losses<br>2. *S. Zurek*, Example of vanishing anisotropy at high rotational magnetisation of grain-oriented electrical steel<br>3. *S. Zurek*, Practical implementation of universal digital feedback for characterisation of soft magnetic materials under controlled AC waveforms<br>4. *W.A. Pluta*, Angular and frequency behavior of some properties of electrical steel sheets<br>5. *M. Przybylski, D. Kapelski, B. Ślusarek*, Mechanical properties of soft magnetic composites at the temperature of liquid nitrogen |
| 14.00 – 16.00 | **Session 1B: Solid State I**<br>***Chairmen: prof. J. Wysłocki, dr P. Gębara***<br>1. *K. Kotynia, P. Pawlik, M. Hasiak, M. Pruba, K. Pawlik*, Structural and magnetic studies of the Fe-Co-Zr-Mo-W-B amorphous alloy<br>2. *K. Filipecka, P. Pawlik, A. Kozdraś, J. Filipecki, K. Kotynia, J.J. Wysłocki*, Effect of annealing temperature on phase constitution and magnetic properties of the nanocrystalline Pr-Fe-B alloy ribbons doped with tungsten<br>3. *R. Nowosielski, M. Kądziołka-Gaweł, P. Gębara, R. Babilas*, Magnetic properties and structure after crystallization of $Fe_{80-x}B_{20}Nb_x$ (x=4,6,10) metallic glasses<br>4. *P. Pawlik, M. Pruba, K. Pawlik*, Phase structure and magnetic properties of the Co-precipitated magnetite nanoparticles<br>5. *M. Hasiak, M. Miglierini*, First order reversal curve analysis of annealed Fe-Co-Si-B-Mo-P metallic glass |
| 16.00 – 16.30 | Coffee break |

| | |
|---|---|
| 16.30 – 18.30 | **Session 2A: Magnetic Modelling**<br>***Chairmen: prof. A. Kapłon, dr R. Gozdur***<br>1. *M. Wołoszyn*, *M. Chojnicki*, *M. Nowak*, Magnetic signature of land vehicles<br>2. *R.M. Wojciechowski*, *C. Jędryczka*, Description of sources of magnetic field using edge values of current vector potential<br>3. *M. Najgebauer*, Scaling-based modelling of power losses in amorphous and nanocrystalline alloys<br>4. *R. Jastrzębski*, *K. Chwastek*, *I. Biondić*, *K. Miličević*, A comparison of different estimation methods for hysteresis modelling<br>5. *M. Bereźnicki*, *P. Jabłoński*, *J. Szczygłowski*, Statistical significance of coefficients in the Bertotti model |
| 16.30 – 18.30 | **Session 2B: Solid State II**<br>***Chairmen: prof. A. Mendoza, dr K. Pawlik***<br>1. *P. Gębara*, *M. Hasiak*, Investigation of critical behavior in $Gd_{75}Ge_{15}Si_5Ce_5$ alloy<br>2. *R. Gozdur*, *M. Lebioda*, Magnetic properties and flux distribution in the LaFeCoSi/FeCoV hybrid structures<br>3. *M. Hasiak*, Soft magnetic properties and magnetocaloric effect of irradiated Fe-Mo-Cu-B alloy<br>4. *M. Kubisztal*, *I. Herok*, *M. Karolus*, *K. Prusik*, *G. Haneczok*, Preparation and magnetic characteristics of $Co_{1-\delta}Zn_\delta Fe_2O_4$ ferrite nanopowders<br>5. *K. Prusik, E. Matyja, M. Kubisztal, M. Zubko, A. Chrobak, R. Swadźba,* Magnetic properties and structure and of the Ni-Mn-Co-In with the boron addition |
| 19.00 – 22.00 | Barbeque |

# PROGRAM OF
# XII SYMPOSIUM OF MAGNETIC MEASUREMENTS & MODELING
**Częstochowa – Siewierz, 17th – 19th October 2016**

| Tuesday 18.10.2016 | |
|---|---|
| 7.30 – 9.00 | Breakfast |
| 9.00 – 10.00 | **Plennary Session II**<br>***Chairmen: prof. J. Szczygłowski, prof. B. Ślusarek***<br>1. **Invited talk**: *Y. Melikhov*, Phenomenological modelling of hysteresis: applications and limitations<br>2. **Invited talk**: *A. Stupakov*, How to perform the accurate magnetic measurements – physical interpretation and practical implementaion |
| 10.00 – 10.30 | Coffee break |
| 10.30 – 13.00 | **Session 3A: Non-Destructive Testing**<br>***Chairmen: prof. K. Chwastek, dr A. Stupakov***<br>1. *J. Bajorek*, Issues of magnetic permeability of austenitic stainless steel measurements by non-destructive method<br>2. *T. Garstka*, Comparison of the results of the barkhausen noise invesitigations with using various design of sensors<br>3. *D. Jackiewicz, A. Juś, R. Szewczyk, A. Bieńkowski*, Two methods of magnetoelastic effect utilization to evaluate mechanical strain in the truss structures<br>4. *M. Kachniarz, R. Szewczyk*, Study on Rayleigh hysteresis model and its aplicability in modelling magnetic hysteresis phenomenon in ferromagnetic materials<br>5. *P. Nowak, M. Nowicki, R. Szewczyk*, FEM-based forward eddy current tomography transformation for automotive industry<br>6. *J. Salach*, Recent state of research on compressive and tensile stresses influence on magnetic properties of amorphous materials |
| 10.30 – 13.00 | **Session 3B: Solid State III**<br>***Chairmen: prof. G. Haneczok, dr M. Hasiak***<br>1. *J.F. López, M. Rios, G.A. Mendoza*, Effects of doping on the structural distortion of $La_{0.7}Dy_{0.3}Mn_{1-x}Zn_xO_3$<br>2. *A. Mendoza, J.F. López, O. Guzmán*, Nonequilibrium patterns in spinodal granular matter<br>3. *P. Kwapuliński, J. Gieraltowski, C. Dolabdjian, Z. Stokłosa, G. Haneczok*, Magnetic properties of Co-Fe-Si-B micro-wires<br>4. *T. Gizynski, W. Kaszuwara, M. Kulczyk, M. Leonowicz*, Hydrostatic extrusion at high temperature<br>5. *K. Pawlik*, Effect of heat treatment on the phase transformation and magnetic properties of the rapidly solidified $Pr_9Fe_{58}Co_{13}Zr_1Nb_4B_{15}$ alloy ribbons<br>6. *M. Szymański, B. Michalski, M. Leonowicz, Z. Miazga*, Complex characteristics of sintered Nd-Fe-B magnets from scrap HDDs |

| | |
|---|---|
| 13.00 – 14.00 | Lunch |
| 14.00 – 15.30 | **Session 4A: Sensors and Actuators I**<br>***Chairmen: prof. M. Wołoszyn, prof. A. Nowakowski***<br>1. *D. Gaworska-Koniarek, J. Bajorek, W. Wilczynski*, Magnetic field strength sensor<br>2. *D. Stachowiak, A. Demenko*, Simulation and investigation of the micro-displacement actuator with magnetostrictive rod<br>3. *M. Kurzawa, D. Stachowiak*, Investigation of thermo-mechanical behavior in shape memory alloy actuator<br>4. *M. Nowicki, M. Kachniarz, R. Szewczyk*, Temperature error of Hall-effect and magnetoresistive commercial magnetometers |
| 14.00 – 15.30 | **Session 4B: Electric Machines**<br>***Chairmen: prof. K. Kluszczyński, dr M. Najgebauer***<br>1. *P. Kowol, K. Kluszczyński*, Equivalent-circuit approach to MR multi-disc clutch designing against the background of magnetic field calculation<br>2. *W. Burlikowski, Ł. Kohlbrenner*, Comparison of databases for modelling of nonlinear current - flux linkage characteristics in electromechanical converters<br>3. *Z. Kowalik*, Uncertainty of the magnetic flux linkages measurements performed with the use of the modified current decay test<br>4. *J. Rolek, G. Utrata, A. Kaplon*, An influence of the temperature and magnetic core saturation on the inductance frequency characteristic of an induction machine |
| 15.30 – 16.00 | Coffee break |
| 16.00 – 17.30 | **Session 5A: Sensors and Actuators II**<br>***Chairmen: prof. Y. Pinhasi, dr D. Stachowiak***<br>1. *D. Mazur, R. Smusz, P. Kielan*, Analysis of thermal stratified storage tank<br>2. *A. Majocha, R. Gozdur*, Wiegand sensor as an effective energy source for supplying ultra low power electronics<br>3. *P. Jankowski -Mihułowicz, D. Kawalec, M. Węglarski*, Using the phased antenna array to increase geometric size of the interrogation zone in UHF RFID system |
| 16.00 – 17.30 | **Session 5B: Magnetic fluids and powders**<br>***Chairmen: prof. A. Yahalom, dr R. Wojciechowski***<br>1. *Z. Pilch, J. Domin*, Conception of the throttle-return valve for the magnetorheological fluid<br>2. *M. Szczygieł, Z. Pilch, J. Domin, T. Trawiński, K. Kluszczyński, M. Przybylski, B. Ślusarek*, Analysis of the applicability of 3D magnetic filament technology in electrical and electromechanical devices<br>3. *P. Kielan, Z. Pilch*, MR clutch work control in hil loop using a DSP processor |
| 18.30 – 24.00 | **Gala dinner with Concert *Film music Kilar & Morricone***<br>(Beniamin Czech – violino, Magdalena Czech – cello, Tadeusz Trzaskalik – piano) |

# PROGRAM OF
# XII SYMPOSIUM OF MAGNETIC MEASUREMENTS & MODELING
**Częstochowa – Siewierz, 17th – 19th October 2016**

| **Wednesday 19.10.2016** | |
|---|---|
| 7.30 – 9.00 | Breakfast |
| 9.00 – 10.45 | **Session 6: Novel solutions**<br>***Chairmen: prof. O. Guzman, dr Y. Melikhov***<br>1. *Y. Pinhasi*, Radiative power beaming using high power magneto-static free-electron maser<br>2. *M. Tuval, A. Yahalom*, Relativistic engine based on a permanent magnet<br>3. *A. Jakubas, P. Gębara, A. Gnatowski, K. Chwastek*, Measurements of properties of polymer-metallic composites<br>4. *J. Szałatkiewicz, R. Szewczyk, M. Kalinowski, J. Kataja, P. Råback, J. Ruokolainen, M. Kachniarz*, Open source ELMER software based FEM modelling of waveguides and resonant cavities for microwave heating and drying devices<br>5. *A. Abramowska*, The role of IEEE literature in patented innovation |
| 10.45 – 11.15 | Coffee break |
| 11.00 – 11.15 | **Meeting of the SMMM Scientific Committee** |
| 11.15 | **Closing remarks of the Symposium** |
| 12.00 – 13.00 | Lunch |

# *ABSTRACTS*

# THE ROLE OF IEEE LITERATURE IN PATENTED INNOVATION

A. Abramowska

EBSCO Sp. z o.o.
Krakowskie Przedmieście 79, 00-079 Warszawa, Poland
e-mail: AAbramowska@ebsco.com

IEEE is the world's largest technical professional organization dedicated to advancing technology for the benefit of humanity. IEEE and its members inspire a global community to innovate for a better tomorrow through its highly cited publications, conferences, technology standards, and professional and educational activities. There are more than 420,000 IEEE members in over 160 countries. IEEE publishes a third of the world's technical literature in electrical engineering, computer science, and electronics and is a leading developer of international standards that underpin many of today's telecommunications, information technology, and power-generation products and services. IEEE is the biggest source of scientific prior art to the top patenters. **InnovationQ Plus** is the new discovery and analytics platform from the IEEE and IP.com that combines deep engineering content from the IEEE with IP.com's global patent and non-patent literature.

**InnovationQ Plus** helps:

- Access and identify prior art
- Determine patentability
- Gain global understanding of patent clearance/freedom to operate
- Enable better patent claim & application construction
- Identify industry activity and discover opportunities
- Assess competitive positioning and threats
- Discover partnerships/licensing opportunities
- Analyze your IP's positioning in the market
- Optimize R&D operations

**Why InnovationQ Plus?**

InnovationQ Plus indexes the full text of IEEE publications alongside a comprehensive global patent literature database. IEEE publications are critical to the patent process and cited in patents three times more than any other publisher. The patented semantic engine is uniquely tuned for IP driving comprehensive and accurate results and analytics This combination provides a single, integrated solution that enables discovery of key information to confidently make decisions regarding your IP portfolio.


# ISSUES OF MAGNETIC PERMEABILITY OF AUSTENITIC STAINLESS STEEL MEASUREMENTS BY NON-DESTRUCTIVE METHOD

J. Bajorek

R&J Measurement, Lipowa 48, Borowa, bajorek@rjmeasurement.com.pl

***Abstract.*** *The paper presents the impact of engineering processes on the properties of austenitic stainless steel. In addition, the necessity of measurements of very small changes in magnetic permeability and the way of their realization on the large objects by non-destructive method with the uncertainty of the type "A" is discussed.*

## I. INTRODUCTION

Technology of equipment production in many areas such as physics (particle accelerator), energy industry (generators), shipbuilding (warships), requires the use of materials with high mechanical strength and very low magnetic permeability μ. The tailoring the appropriate mechanical and magnetic properties of austenitic stainless steel requires control of the engineering processes influence on the magnetic properties of the material.

Available publications clearly indicate that magnetic measurements provide an alternative or supplement to the previously used ultrasonic and penetrative methods.

The measurement of the relative magnetic permeability enables a more complete assessment of the degree of the material structure degradation and allows more accurately assess the mechanical and electrical properties of objects under examination.

It also allows assessing the instability of austenite caused by static and dynamic loads in the operating conditions of machines. Among others its concerns generators caps. They are in fact exposed to high centrifugal forces and the presence of large, alternating magnetic fields.

Very low required relative permeability ($\mu \leq 1.05$) and high resistivity is necessary because of limitations of induced eddy currents. Similar requirements provide warships.

Therefore it is necessary to measure the permeability not only for blank material in the laboratory but also in semi- and final products of machines and equipment of large dimensions. This requires the implementation of local measurements of magnetic permeability by non-destructive methods and puts high demands on instrumentation.

In the paper the impact of engineering processes on the properties of austenitic stainless steel is discussed. The possibility of non-destructive measurement of the magnetic permeability is presented. In addition, the necessity of measurements of very small changes in magnetic permeability and the way of their realization on the large objects by non-destructive method with the uncertainty of the type "A" is discussed.

# STATISTICAL SIGNIFICANCE OF COEFFICIENTS IN THE BERTOTTI MODEL

M. Bereźnicki, P. Jabłoński and J. Szczygłowski

Częstochowa University of Technology, Faculty of Electrical Engineering
al. Armii Krajowej 17, 42-200 Częstochowa, Poland

In the paper two formulas for description of loss in the magnetic material subject to alternating field re-magnetization are compared. The comparison is carried out for Bertotti's and Richter's formulas. On the basis of statistical analysis that relies on the statistical assessment of components in both formulas, it is shown that Richter's formula is simpler and more adequate for the description in the considered SMM samples.

## REFERENCES

[1] Bertotti G., Hysteresis in magnetism, *Academic Press*, San Diego, 1998
[2] Barranger J., Hysteresis and Eddy-current losses of a tranfoormer lamination vieved as an application of the Poynting theorem, *NASA Technical note*, TN D-3114, 1965

# COMPARISON OF DATABASES FOR MODELLING OF NONLINEAR CURRENT - FLUX LINKAGE CHARACTERISTICS IN ELECTROMECHANICAL CONVERTERS

W. Burlikowski and Ł. Kohlbrenner

Department of Mechatronics, Faculty of Electrical Engineering, Silesian University of Technology, Akademicka 10A, 44-100 Gliwice, wojciech.burlikowski@polsl.pl

***Abstract.*** *In the paper various types of databases for the current-flux linkage characteristic approximation are presented. In case of Hamiltonian model of the electromechanical converter they are necessary both in simulational model and in practical implementation of control system. The comparison includes uniform database and non-uniform one based on triangulation. The exemplary results are shown for case of 3-phase synchronous reluctance motor without neutral wire (Fig.1). The hybrid type of database, based on sequential linear interpolation (SLI), is proposed.*

## I. INTRODUCTION

Mathematical models of electromechanical converters employ either Lagrangian or Hamiltonian form of equations, depending on the choice of state variables [1]. The equation of electrical circuit of the converter (Fig.1) with flux linkages as state variables, using Hamiltonian formalism, has the following form:

$$\frac{d}{dt}\boldsymbol{\Psi} = \boldsymbol{u} - \boldsymbol{R}\boldsymbol{i}(\varphi, \boldsymbol{\Psi}) \tag{1}$$

while its Lagrangian counterpart can be written as:

$$\frac{d}{dt}\boldsymbol{i} = (\boldsymbol{L_d}(\varphi, \boldsymbol{i}))^{-1}\left(\boldsymbol{u} - \left(\omega\frac{\partial \boldsymbol{\Psi}(\varphi, \boldsymbol{i})}{\partial \varphi} + \boldsymbol{R}\right)\boldsymbol{i}\right) \tag{2}$$

where $\boldsymbol{i}(\varphi, \boldsymbol{\Psi})$ is the function that defines currents $\boldsymbol{i} = [i_\mathrm{A}, i_\mathrm{B}]$ in terms of rotor angular position $\varphi$ and flux linkages $\boldsymbol{\Psi} = [\psi_\mathrm{A} - \psi_\mathrm{C}, \psi_\mathrm{B} - \psi_\mathrm{C}] = [\psi_\mathrm{AC}, \psi_\mathrm{BC}]$; $\boldsymbol{u} = [e_\mathrm{AC}, e_\mathrm{BC}]$ – supply voltages; $\boldsymbol{R}$ – resistance matrix; $\omega$ - mechanical angular velocity; $\boldsymbol{L_d}(\varphi, \boldsymbol{i})$ - dynamic inductance matrix.

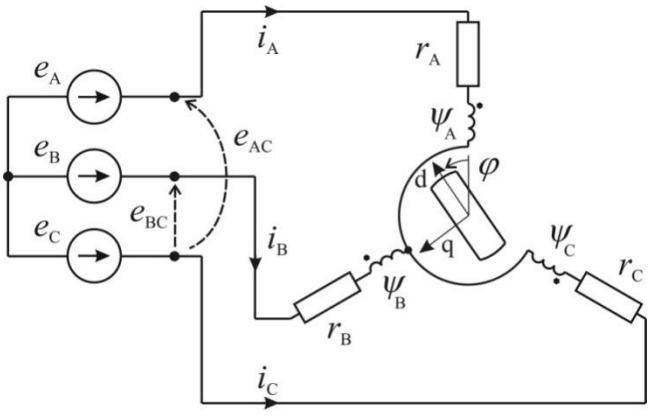


*Fig.1. Electrical circuit of the synchronous reluctance motor (SynRM)*

## II. TYPES OF DATABASES

The quantities which are databases in eq.1,2 are $\boldsymbol{\Psi}(\varphi, \boldsymbol{i})$, $\boldsymbol{i}(\varphi, \boldsymbol{\Psi})$ and $\boldsymbol{L_d}(\varphi, \boldsymbol{i})$. In idealized mathematical description used in these equations they represent continuous functions. However, as

in practice they are obtained either using numerical simulations or measurements, they are discrete in nature [1][4]. They can be divided into two groups:
a) primary database - presenting flux linkages as function of currents $\boldsymbol{\Psi}(\varphi, \boldsymbol{i})$. It is regarded as primary because it can be directly obtained using numerical modeling (e.g. FEM) or measurement,
b) secondary databases - their form depends on the type of equations. In case of Lagrangian equations it is dynamic inductance $\boldsymbol{L_d}(\varphi, \boldsymbol{i})$ obtained using differentiation of primary database $\boldsymbol{\Psi}(\varphi, \boldsymbol{i})$ [5]. In case of Hamiltonian formalism it is $\boldsymbol{i}(\varphi, \boldsymbol{\Psi})$ obtained using inversion of primary database based either on simplical approximation or reinterpolation [1][2].

## III. PROPERTIES OF THE SECONDARY DATABASES

The main problems which arise in practical application of various types of databases is their structure and approximation properties. The paper focuses on drawbacks and advantages of various implementations of current-flux linkage characteristic $\boldsymbol{i}(\varphi, \boldsymbol{\Psi})$ [1]:
a) uniform - which ensures very fast access to data but suffers because of inaccuracy in highly saturated regions leading sometimes to loss of stability (LofS.) of simulations (Fig.2a),
b) triangulated - very accurate in highly saturated regions but suffers because of very slow access to data (Fig.2b).
Authors propose to solve these problems using a hybrid method, based on sequential linear interpolation (SLI) algorithm connected with local triangulation [2][3].

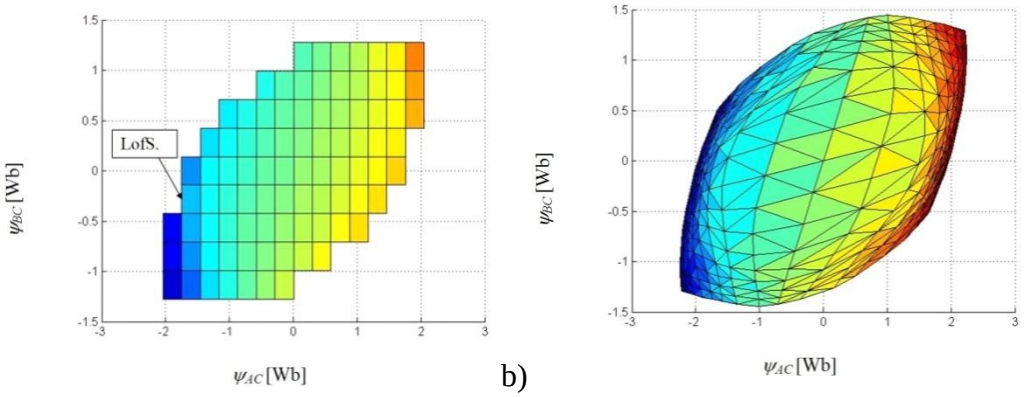


*Fig.2. Domains of uniform (a) and triangulated (b) databases representing current-flux linkage characteristic.*

## REFERENCES


[1] Burlikowski W., Hamiltonian model of electromechanical actuator in natural reference frame, Part 1&2, *Archives of Electrical Engineering*, vol. 60(3), 2011, pp. 317-348
[2] Agoston M.K., Computer Graphics and Geometric Modeling - Mathematics, *Springer*, 2005
[3] Chang J.Z., Allenbach J.P., Bouman Ch.A., Sequential linear interpolation of multidimensional functions. IEEE *Transactions on Image Processing*, vol. 6, no. 9, September 1997. p. 1231-1245
[4] Kowalik Z., Measurement Results Based Approximation of the Nonlinear Flux-Current Characteristic of an Electromechanical Actuator, *Measurement Automation Monitoring*, vol. 02/2016, 2016, pp. 49-54
[5] Herold T. et al., Extension of a d-q model of a permanent magnet excited synchronous machine by including saturation, cross-coupling and slotting effects, 2011 IEEE *International Electric Machines & Drives Conference* (IEMDC), 2011, pp. 1363 – 1367

# EFFECT OF ANNEALING TEMPERATURE ON PHASE CONSTITUTION AND MAGNETIC PROPERTIES OF THE NANOCRYSTALLINE Pr-Fe-B ALLOY RIBBONS DOPED WITH TUNGSTEN

K. Filipecka[1,2], P. Pawlik[1], A. Kozdraś[3], J. Filipecki[2], K. Kotynia[1] and J.J. Wysłocki[1]

[1] Institute of Physics, Faculty of Production Engineering and Materials Technology, Czestochowa University of Technology, Armii Krajowej 19, 42-200 Czestochowa, Poland
[2] Institute of Physics, Faculty of Mathematics and Natural Science, Jan Dlugosz University, Armii Krajowej 13/15, 42-200 Czestochowa, Poland
[3] Department of Physics, Faculty of Production Engineering and Logistics, Opole University of Technology, Ozimska str. 75, 45-370 Opole, Poland

The rapidly solidified bulk RE-Fe-B (RE = rare earth) magnets are of considerable interest due to their potential magnetic applications. Interesting properties in this group of alloys were observed for Pr-Fe-B-type systems, in which $Pr_2Fe_{14}B$ phase is responsible for the high coercivity. In order to improve magnetic properties, many modifications of their chemical composition were worked out. The increase in the magnetic parameters can be obtained by changing the proportions of the basic components (Pr, Fe and B) or by doping the base alloy. One of alloying elements, which is very interesting due to its influence on formation of hard magnetic $RE_2Fe_{14}B$ phase and improving the glass forming ability is tungsten. Furthermore, to obtain optimal magnetic properties, appropriate processing conditions are crucial issue. Therefore, the aim of the present work was to investigate the phase constitution and magnetic properties of the rapidly solidified $Fe_{65}Pr_9B_{18}W_8$ alloy ribbons in as-cast state and subjected to short time annealing.

The base alloy was prepared by arc-melting of the high purity elements, with addition of pre-alloy Fe-B of known composition, under Ar protective atmosphere. The ribbon samples were obtained by melt-spinning technique under low pressure of Ar. The linear speed of the cooper wheel surface of 25 m/s was used. Subsequently, the ribbons were sealed off in a quartz tube under low pressure of Ar to maintain purity of atmosphere during heat treatment. In order to change the magnetic properties and obtain the nanocrystalline microstructure, the samples were annealed at various temperatures ranging from 923 K to 1023 K for 5 min, and subsequently rapidly cooled in the water. Crystallization behavior of the as-cast ribbon was studied using differential scanning calorimeter Netzsch DSC404 at heating rate of 10 K/min. The phase structure analysis was investigated using Bruker D8 Advance diffractometer with Cu Kα radiation. Mössbauer spectra were measured using Polon Mössbauer spectrometer with a 57Co:Rh source in conventional transmission geometry and subsequently analysed using WinNormos for Igor software. Tested samples were crushed to powder in order to obtain a specimens representative for the entire volume of the material. Room temperature hysteresis loops were measured by LakeShore 7307 VSM magnetometer at external magnetic fields up to 2 T.

The DSC studies were used to specify the range of annealing temperatures during heat treatment. The structural and magnetic studies have shown amorphous structure of ribbons in as-cast state and their soft magnetic properties. Short-time annealing (for 5 min) at 923 K did not result in change of phase composition and magnetic properties. Heat treatment of specimens at the 943 K and higher temperatures for 5 min led to nucleation and growth of crystalline phases and allowed to obtain a nanocrystalline structure. The volume fraction of amorphous phase decreases in expense of growing grains of crystalline phases. The phase analysis of XRD spectra revealed presence of the hard magnetic $Pr_2Fe_{14}B$ and the paramagnetic $Pr_{1+x}Fe_4B_4$ phases. Due to the overlap of diffraction peaks it was difficult to determine presence of particular phases. Therefore, for explicit phase identification the Mössbauer studies were performed. Analysis of Mössbauer spectrum for the as-cast sample confirmed its amorphous structure. These studies carried out on ribbon annealed at 923 K for 5 min have shown presence of component corresponding to

amorphous and paramagnetic crystalline phases. The corresponding volume fractions of constituent phases were 94 vol. % of the amorphous and 6 vol. % of the $Pr_{1+x}Fe_4B_4$ phases. Annealing at 983 K led to significant change of Mössbauer spectrum that suggests a presence a major fraction of crystalline phases. The quantitative analysis of this spectrum has shown that the annealed ribbon consists of 45 vol. % of the $Pr_2Fe_{14}B$ phase, 40 vol. % of the $Pr_{1+x}Fe_4B_4$ phase and 15 vol. % of the disordered component. The wasp-waisted shape of hysteresis loop measured for ribbon annealed at 943 K is typical for alloys, where formation of isolated grains of hard magnetic phase within the amorphous matrix occurs during heat treatment. With the increase of annealing temperature hysteresis loops characteristic for hard magnetic materials were measured, which is related to evolution of microstructure and phase constitution of the samples. Large volume fraction of the paramagnetic $Pr_{1+x}Fe_4B_4$ phase resulted in relatively low values of $(BH)_{max}$. With increasing of annealing temperature, a slight increase of the coercivity is observed. The maximum value of coercivity ${}_JH_c$ = 974 kA/m was obtained for sample annealed at 1003 K for 5 min. However, the heat treatment at 983 K for 5 min resulted in the maximum values of remanence $J_r$ = 0.39 T and maximum energy product $(BH)_{max}$ = 23.3 kJ/m$^3$.

# COMPARISON OF THE RESULTS OF THE BARKHAUSEN NOISE INVESITIGATIONS WITH USING VARIOUS DESIGN OF SENSORS

T. Garstka

Częstochowa University of Technology, Faculty of Production Engineering and Materials Technology
Al. Armii Krajowej 19, 42-200 Częstochowa, Poland, e-mail: tomasz.garstka@wip.pcz.pl

***Abstract.*** *The paper present results of the Barkhausen noise investigations of the steel samples, conducted with using three different design of the measurement sensors, at the same reference conditions. The character and scale of the obtained differences were discussed.*

## I. INTRODUCTION

Nondestructive methods based on Barkhausen noise measurement are widely used for ferromagnetic materials testing. It allows to rapid control of properties of manufactured products in process of metal forming, rolling, welding or heat treatment. Also the automation of control procedures is easy and measuring equipment is relatively cheap and safely to the staff. The physical principle of these testing methods relies on well-known effect (discovered by H. Barkhausen in 1919) of jerky motion of the magnetic domains' walls between pinning sites during magnetization process. It result in discontinuous magnetic flux density changes inside the material, inducing in a pick-up coil series of electrical pulses, which after conditioning take characteristic form called magnetic Barkhausen Noise (BN). Course of this phenomenon is determined by a lot of materials properties as microstructure type, grain size, texture and mechanical stress level [1]. Also the magnetization conditions as well as measuring set-up parameters have considerable impact on the results of its measurements. Individual research teams use own measuring set-up and commercial solutions are cryptic. Especially, due to lack of detailed standards of Barkhausen noise sensors construction, results received in laboratory investigations as well as industrial applications with different measuring head may be various. For this reasons, to conduct research on construction of detection sensor seems to be right to check and recognize differences caused by its sensitivity and measurement resolutions. This issue was analyzed in [2, 3], but due to various magnetization conditions, the results cannot be fully compared and clear.

## II. EXPERIMENT AND MATERIAL

The magnetic Barkhausen noise measurements were carried out using the stand-alone measurement equipment for excitation, detection and processing of BN developed at Technical University of Częstochowa by author [4]. During the investigations, the raw Barkhausen noise signal and its root mean square value, envelope as well as the magnetization conditions was recorded. For the tests, different surface detection sensors of BN were examined, as:

- air coil with diameter 10mm, and 300 turn
- ferrite P- core, with cross surface, ca 150 $mm^2$ and 200 turns
- ferrite bar-core, with cross surface, ca 12 $mm^2$ and 200 turns

To maintain stable and repeatable magnetizations conditions, during examination of each detection sensor, the magnetization yoke with 400 turn of windings was used.

The investigations were performed on the two samples, for two magnetization frequencies. The first one was laboratory specimen used to tensile stress test, plasticity deformed and the second was a piece of hot rolled 5 mm steel sheet, prepared with using semi-industrial two high rolling mills. Both samples were made from the same grade, S235JGR2 of steel although obtained from different factory batches.

In first case the measurement were done in the same middle point of sample and in second case, the measurements were done in nine points, organized in matrix 3×3 with 50 mm distance between them. In both case any additional surface preparation were not applied to the samples, especially to hot rolled sheet to keep as raw conditions as in real industrial process.

## III. RESULTS

Comparison of the exemplary obtained results, allows to state, that observed differences were quantitative rather than qualitative, as expected. Figure 1 shown the variation of $BN_{RMS}$ with magnetization current $I_m$ in the first sample, measured by three of tested sensors. The course of each curve is similar but the P-core detection coil has the most sensitivity. The analogical result can be observed in Figure 2, for envelope plots of BN recorded in one of the selected measurement point on the investigated steel sheet. Despite of more sensitivity of P-core sensor, the significant deformation of envelope were not noticed.

Thus, should be developed universal calibration standard and procedure to measurement sensitivity of Barkhausen sensors, which let to compare results of scientific studies or industrial measurements.

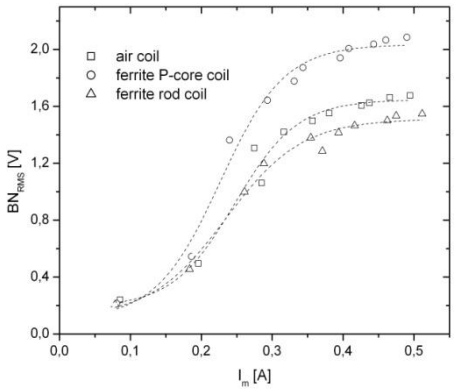


*Fig.1. Variation of $BN_{RMS}$ with $I_m$*

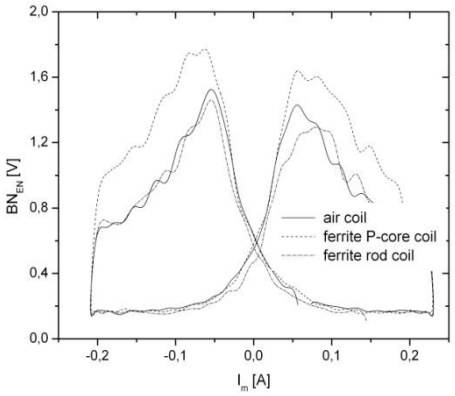


*Fig.2. Plots of BN envelope*

## IV. ACKNOWLEDGMENTS

This study was carried out under principal research project No. BS/PB-201-301/2013

## REFERENCES

[1] Augustyniak B, Magnetomechanical effects and their applications at nondestructive evaluation of materials, *Publisher Gdańsk University of Technology*, Gdańsk, 2003.

[2] Grum J., Pecnik B., Calibration of various sensor units by using different parameters of the magnetic Barkhausen noise, *Proceedings of 4th International Conference on Barkhausen Noise and Micromagnetic Testing*, Brescia, Italy, 2003, pp. 211-218

[3] Garstka T, Jagieła K, Dobrakowski R., Influence of the measuring heads' construction on Barkhausen noise voltage measurements characterizing changes of microstructure, *Proceedings of 5th International Scientific Conference on New Technologies and Achievements in Metallurgy and Materials Engineering*, Częstochowa, Poland, 2004, pp. 260-265

[4] Garstka T., The complex system for residual stress determination based on Barkhausen noise measurement, *Proceedings of 5th International Conference in Barkhausen Noise and Micromagnetic Testing*, Petten, The Netherlands, 2005, pp.219-228

# MAGNETIC FIELD STRENGTH SENSOR

D. Gaworska-Koniarek[1], J. Bajorek[2] and W. Wilczynski[3]

[1] Electrotechnical Institute, Division of Electrotechnology
and Materials Science, Curie-Sklodowskiej 55/61, Wroclaw, gaworska@iel.wroc.pl
[2] R&J Measurement, Lipowa 48, Borowa, bajorek@rjmeasurement.com.pl
[3] Electrotechnical Institute, Pozaryskiego 28, Warsaw, w.wilczynski@iel.waw.pl

***Abstract.*** *The paper presents a new kind of sensor for magnetic field strength measurement in soft materials by direct method. The sensor consists of induction coil and ferromagnetic electrodes. Its construction makes possible to measure the magnetic field strength directly at the sample surface. The principle of operation and construction of sensor were provided. Also, preliminary experimental study of the sensor was presented. The values of strength of magnetic field measured by the sensor were compared with the values obtained by means of Epstein frame. The obtained results showed that designed magnetic field strength sensor is adequate to test electrical steel.*

## I. INTRODUCTION

For assessment of magnetic properties of an object, measurement and appropriate assignment of basic magnetic quantities are necessary. The quantities include induction and strength of magnetic field. A way of magnetizing a tested sample should enable determining magnetic properties of the material not the object. This enforces using uniform distribution of a tangent component of magnetic field strength in the measurement region of the tested object.

Meeting this requirement is very hard, even in the case of normalised test circuits, despite a closed magnetic circuit with a uniform and accessible cross-section.

However, in case of measurements of magnetic field strength by direct method, due to the field strength gradient over the surface of the tested object, the tangential component sensors should be place as close as possible to the sample. On the other hand, design issues cause that the distance from the surface of the tested object is equal to a few millimetres, which introduces a significant field measuring error $H_T$. Because of that, gradient sensors are used and the magnetic field strength value on the surface of the tested object is determined using the linear extrapolation method. This method is used both in case of measuring the field strength component with a flat coil [1, 2], as well as with Hall effect sensors [3, 4]. Serious doubts arise due to averaging measurement of the field using induction sensors and uncertainty of assessment of their distance from the surface of the tested object.

In this paper a new kind of sensor for magnetic field strength measurement in soft materials by direct method has been presented. Its essential property is significant limitation or even complete elimination of typical shortcomings of methods commonly used for measurement of magnetic field strength.

## II. MAGNETIC FIELD STRENGTH SENSOR

A principle of operation of the sensor is presented in Fig.1. In case of a multilayer coil, the magnetic flux associated with its winding can be expressed as

$$\psi_c = A_c N \frac{n}{l} \mu_0 u_\mu, \tag{1}$$

where: $A_c$ – cross section area of inductive coil, N – number of layers in the coil, n – number of turns in a single layer of the coil, $l_c$ – distance between faces of the coil, $\mu_0$ – permittivity of free space, $u_\mu$ – difference of magnetic potentials or magnetic voltage between the faces of the coil, $l_p$ – distance between the faces of the inductive coil.

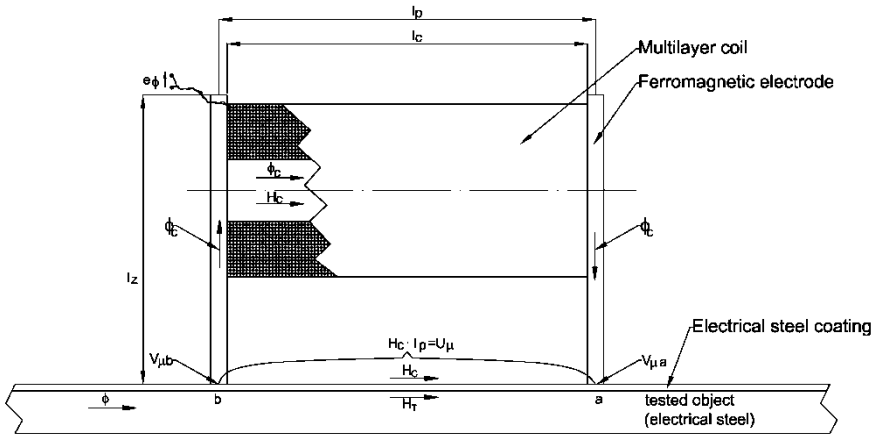


*Fig.1. Scheme of sensor operation*

It seems that ensuring constant magnetic potentials on both faces of the coil is a necessary and sufficient condition for the output signal of passive inductive coil to be proportional to the difference of magnetic potentials or magnetic voltage drop. The fact has been used for designing a magnetic field strength sensor with ferromagnetic electrodes in which an inductive coil has been used.

Equipotential faces of the coil were achieved by using rectangular stripes of a ferromagnetic material with high initial magnetic permeability, closely adjacent to the coil faces. The shorter side of the stripes was not smaller than the outer diameter of the coil and the longer one served to transferring magnetic potential from the tested object to the faces of the induction coil.

Assuming that there is no magnetic voltage drop on the air gaps of a sensor circuit and its electrodes, magnetic voltage in points a and b in Fig. 1 and on the surface of tested object is transferred without losses on the coil faces, as

$$u_{\mu_{ab}} = H_T l_p = H_c l_c, \tag{2}$$

where: $H_T l_p$ - magnetic voltage between points a and b and on the surface of tested object, $H_c l_c$ magnetic voltage between the faces of coil of the sensor.

## REFERENCES

[1] Nakata T., Kawase Y., Nakano M., Miuira M., Analysis and Improvement of Measuring Method of Magnetic Fields in Single Sheet Testers, *vol. TJMJ-1*, 7, 1986, 873–874

[2] Tumanski S., A multi-coil sensor for tangential magnetic field investigations, *J. Magn. Magn. Mater.*, vol. 242–245, 2002, 1153–1156

[3] Stupakov O., Wood R., Melikhov Y., Jiles D., Measurement of Electrical Steels With Direct Field Determination, *IEEE Trans. Magn.*, 46, 2, 2010, 298–301

[4] Perevertov O., Measurement of the surface field on open magnetic samples by the extrapolation method, *Rev. Sci. Instrum.*, 76, 10, 2005, 104701

# INVESTIGATION OF CRITICAL BEHAVIOR IN $Gd_{75}Ge_{15}Si_5Ce_5$ ALLOY

P. Gębara[1] and M. Hasiak[2]

[1] Institute of Physics, Częstochowa Universtity of Technology, Armii Krajowej 19, 42-200 Częstochowa, Poland, pgebara@wip.pcz.pl

[2] Department of Mechanics and Materials Science, Wrocław University of Science and Technology, Smoluchowskiego 25, 50-370 Wrocław, Poland, Mariusz.Hasiak@pwr.edu.pl

The main goal of present work was to study critical behavior of the as-quenched $Gd_{75}Ge_{15}Si_5Ce_5$ (wt. %) in the vicinity of the critical temperature $T_C$. Sample was prepared by arc-melting of high purity constituent elements under Ar atmosphere. The magnetization as a function of magnetic field was measured in temperature range from 150 K to 340 K (with step 5 K). These data were used to construct the Arrott plots (Fig.1). Positive slope of the Arrott plots suggests second order phase transition from ferro- to paramagnetic state [1].

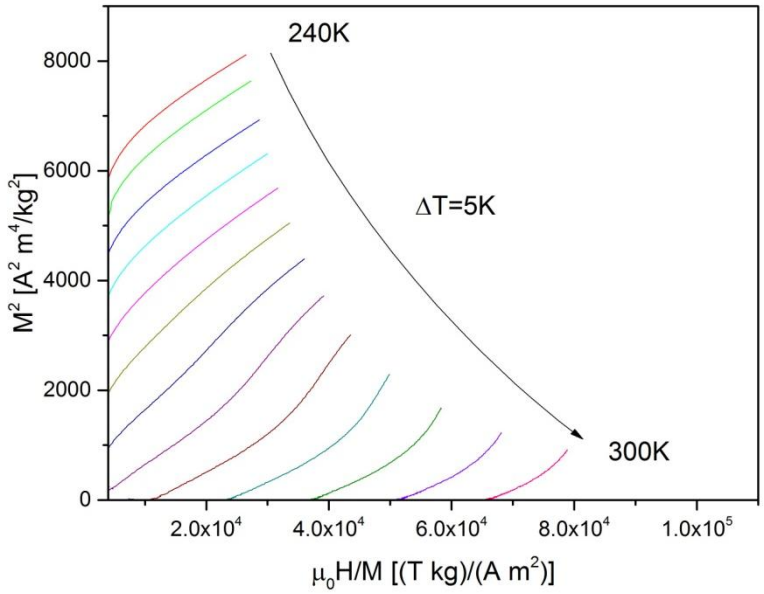


*Fig.1. The Arrott plots constructed for the as-quenched $Gd_{75}Ge_{15}Si_5Ce_5$ alloy using mean field values of critical exponents*

Detailed studies of the phase transformation nature were carried out using free energy relation expanded into a power series in the vicinity of Curie point. This relation is written in following way [2]:

$$F(M,T) = \frac{c_1}{2}M^2 + \frac{c_2}{4}M^4 + \frac{c_3}{6}M^6 + \ldots - \mu_0 HM \quad , \tag{1}$$

where: F(M,T) - magnetic free energy, $c_1$(T), $c_2$(T) and $c_3$(T) - Landau coefficients, M - magnetization, T - temperature, $\mu_0$ - magnetic permeability of vacuum, H - magnetic field.
The calculation of Landau coefficients is possible after reconstruction of equation (1) in following form [2]:

$$\mu_0 H = c_1(T)M + c_2(T)M^3 + c_3(T)M^5 \quad . \tag{2}$$

The temperature dependences of Landau coefficient $c_1$ revealed minimum at $T_C$, which is typical for this coefficient. In case of $c_2$, it changes its sign at Curie point and this behavior suggests occurrence of second order phase transition in investigated alloy.

In order to investigate critical behavior, the Kouvel-Fisher method and magnetization isotherm at Curie temperature were applied [3,4]. Based on the Kouvel-Fisher plot (Fig.2) and Widom scaling relation ($\delta=1+\gamma/\beta$) [5], the values of critical exponents $\beta=0.376$, $\gamma=1.032$ and $\delta=3.745$ were obtained.

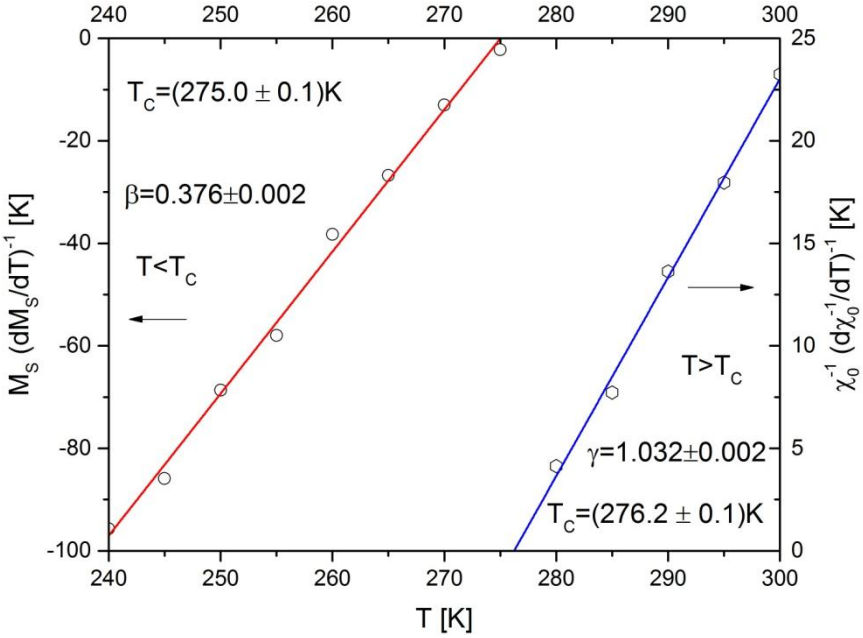


*Fig.2. The Kouvel-Fisher plot for $M_S(T)$ and $\chi_0^{-1}(T)$, solid lines are the linear fitting of the data.*

## REFERENCES


[1] Banerjee S.K., On a generalised approach to first and second order magnetic transitions, *Phys. Lett.* 12, 16 (1964)

[2] Shimizu M., Itinerant electron metamagnetism, *Rep. Prog. Phys.* 44 329 (1981)

[3] Fisher M.E., The theory of equilibrium critical phenomena, *Rep. Prog. Phys.* 30, 615 (1967)

[4] Kouvel J.S., Fisher M.E., Detailed magnetic behavior of nickel near its Curie point, *Phys. Rev.* 136, A1626 (1964)

[5] Widom B., Equation of state in the neighborhood of the critical point, *J. Chem. Phys.* 43, 3898 (1965)

# CONSOLIDATION OF NANOCRYSTALLINE Nd-Fe-B POWDER OF HYDROSTATIC EXTRUSION AT HIGH TEMPERATURE

T. Gizynski[1], W. Kaszuwara[1], M. Kulczyk[2] and M. Leonowicz[1]

[1] Warsaw University of Technology, Faculty of Materials Science and Engineering, Woloska 141, 02-507 Warsaw, Poland; tomasz.gizynski@inmat.pw.edu.pl
[2] Institute of High Pressure Physics, Polish Academy of Sciences, Sokolowska 29/37, 01-142 Warsaw, Poland

Hydrostatic extrusion (HE) is a modern method of shaping materials microstructure and properties. HE can also be successfully used for consolidation of hard magnetic powders. The effect of extrusion temperature, within the range of 700 - 800 °C, on the magnetic properties of the bulk, final product was studied. A commercial MQU-F42 powder, dedicated to hot pressing, was placed in copper capsules and initially cold compacted up to 60% of the theoretical density. Subsequently, the billet was heated in an oven to temperatures 700 and 800 °C, respectively and subjected to hydrostatic extrusion. The extruded product had a form of a copper rod, with the Nd-Fe-B core, having 96% of theoretical density (true strain 1.85 after extrusion at 800 °C). The extrusion process led to deterioration of the coercivity, for which coarsening of the $Nd_2Fe_{14}B$ grains was blamed. In order to prove this hypothesis, the starting powder was annealed in a temperature range of 500-800 °C for various time. The crystallite size, measured after annealing, by the X-ray diffraction method, showed that with extension of time and elevation of the temperature the crystallite size increases, however the dominating parameter is the temperature. Correlation of the crystallite size with temperature indicates that when the crystallites are larger than 80 nm the magnetic properties dramatically decrease. Additionally, after HE at 800 °C micrometric size Nd-reach phase appear in the microstructure. The Nd is squeezed from the grain boundary of the $Nd_2Fe_{14}B$ phase leading to non-isolated grains, which also contributes to the deterioration of the coercivity.

# MAGNETIC PROPERTIES AND FLUX DISTRIBUTION IN THE LaFeCoSi/FeCoV HYBRID STRUCTURES

R. Gozdur[1] and M. Lebioda[2]

[1] Lodz University of Technology, Department of Semiconductors and Optoelectronic Devices,
211/215 Wolczanska St., 90-924 Lodz, gozdur@p.lodz.pl
[2] Lodz University of Technology, Institute of Electrical Engineering Systems
18/22 Stefanowskiego St., 90-924 Lodz, marcleb@p.lodz.pl

***Abstract.*** *The present study contains a description of magnetic properties of FeCoV/LaFeCoSi/FeCoV structure. The hybrid structure consists magnetocaloric LaFeCoSi core laminated with high-induction ferromagnetic layers. Resultant, magnetizing field inside the magnetic structure is gained by fringing field from FeCoV laminations. Experimental investigations of improved magnetic properties of LaFeCoSi/FeCoV were presented in the paper.*

## I. INTRODUCTION

The discovery of the giant magnetocaloric effect in 1995 resulted in the growth of interest in magnetocaloric materials. It stems from the fact that the magnetocaloric effect (MCE) can be used for heat transfer. Theoretically, the efficiency of cooling system based on MCE is significantly higher than that of conventional compressor refrigerators. Unfortunately, magnetocaloric cooling in room temperature requires the usage of expensive materials containing rare earth elements. Apart from that, strong magnetocaloric effect is activated by the magnetic field with the value over 1T. The intense development in material engineering has led to the commercial availability of the magnetocaloric materials, such as Calorivac C and Calorivac H. The magnetic entropy change in the room temperature approaches the level of 33 $kJm^{-3}K^{-1}$ and 89 $kJm^{-3}K^{-1}$ respectively. The above mentioned entropy changes can be registered in the magnetic field of 1.0T [1, 2]. Therefore, the most significant technological barrier in the design of magnetocaloric cooling systems is the requirement of strong magnetizing field for the excitation of the MCE [3]. Present-day magnetic systems are based on hard magnets, Halbach matrices, electromagnets or inductors with superconducting coils.

This work presents research on the field distribution and magnetic properties of the LaFeCoSi magnetocaloric material (MCM) with FeCoV laminations (FM). Locally combined field of external source and fringing field from FeCoV layers boosts the effective field. The magnetic properties and field distribution have been investigated in a ring type sample asa FM/MCM/FM hybrid structure.

## II. HYBRID STRUCTURE

Investigated structure has been made as a toroidal cartridge laminated with ferromagnetic rings. The cartridge has been filled with sintered LaFeCoSi (Calorivac C 300H) powder with defined Curie temperature of 300K. The magnetocaloric toroidal sample was laminated with FeCoV (Vacoflux 50) rings with a thickness of 100μm. The sheets of Vacoflux were annealed in order to boost magnetic saturation up to 2.4T with estimated maximum MCM/FM permeability ratio of 1:7. The layout of the ring type tested sample is depicted in the figures 1a-c.

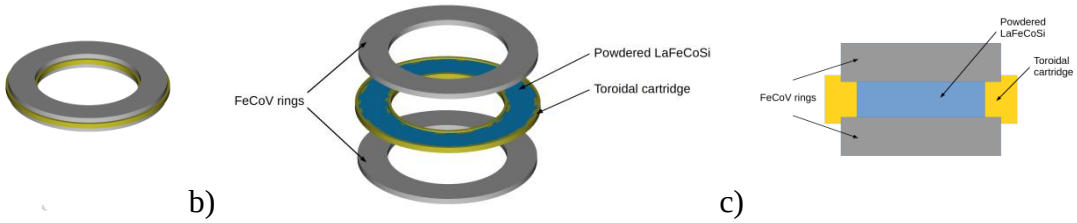


a) b) c)

*Fig.1a-c. The diagrams of the FM/MCM/FM hybrid structure*

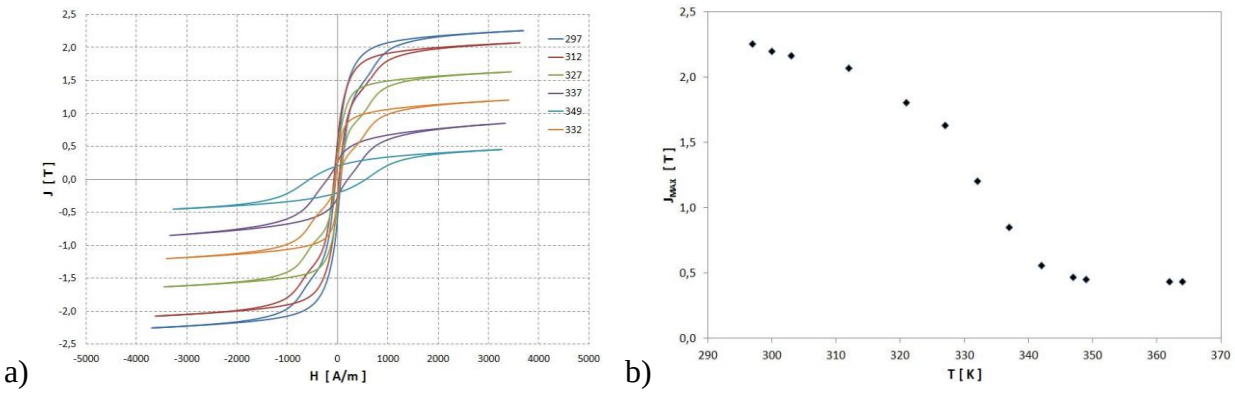


a) b)

*Fig.2. Magnetic properties of the FM/MCM/FM hybrid structure*
*a) Temperature dependencies of magnetic hysteresis loops with frequency 1Hz*
*b) Influence of temperature on peak magnetic polarization density*

The most significant measurements of magnetic properties of FeCoV/ LaFeCoSi /FeCoV structure were presented in the figures 2a-b. The average magnetic polarization density in the toroidal structure was measured with pickup coils and Hall sensors. The influence of temperature on the structure was investigated in the temperature range from 297K to 365K. Achieved peak polarization density in the ferromagnetic state exceeds 2.2T and stabilizes on the level of 0.4T in the paramagnetic state of LaFeCoSi. The observed strong depreciation of the ferromagnetic properties is related to the phase transition in LaFeCoSi because FeCoV has a Curie temperature of more than 1200K [4].

## III. SUMMARY

The work presents magnetic properties of FeCoV/ LaFeCoSi /FeCoV structure. The laminated FeCoV rings in the structure improve the efficiency of the magnetization and the structure remains in ferromagnetic state even temperature exceed Curie point in LaFeCoSi. Strong magnetic coupling between ferromagnetic rings and magnetocaloric core provides opportunities for further improvement of efficiency of magnetocaloric effect and thermo-magnetic process.

## REFERENCES

[1] Bjørk R., Bahl C.R.H., Katter M., Magnetocaloric properties of $LaFe_{13-x-y}Co_xSiy$ and commercial grade Gd, *J. Magn. Magn. Mater.*, vol. 322, no. 24, pp. 2010, 3882–3888
[2] Magnetocaloric materials CALORIVAC, Tech. Note Vacuumschmelze, Edition 2015
[3] Balli M., Sari O., Zamni L., Mahmed C., Forchelet J., Implementation of La(Fe, Co) 13-xSix materials in magnetic refrigerators: Practical aspects, *Mater. Sci. Eng. B Solid-State Mater. Adv. Technol.*, vol. 177, no. 8, 2012, 629–634
[4] Gozdur R., Lebioda M., Bernacki Ł., Power losses in $LaFe_xCo_ySi_{1.1}$ intermetallics near the magnetic phase transition, Acta Phys. Pol. A. 128 (2015), 98–103

# INTERCOMPARISON OF MEASUREMENTS OF MAGNETIC POWER LOSSES

R. Gozdur[1], P. Szczurek[2] and A. Majocha[1]

[1] Lodz University of Technology, Department of Semiconductors and Optoelectronic Devices, 211/215 Wolczanska St., 90-924 Lodz, gozdur@p.lodz.pl, andrzej.majocha@p.lodz.pl
[2] Stalprodukt S.A., 69 Wygoda St., 32-700 Bochnia, pawel.szczurek@stalprodukt.pl

***Abstract.*** *The paper presents recent achievements in the accurate measurements of power losses in soft magnetic materials. Intercomparison and validation have been developed on the basis of measured power losses in the grain-oriented SiFe electrical steel in the Epstein frame. The measurements were performed in the laboratories of PTB, Stalprodukt and Lodz University of Technology.*

## I. INTRODUCTION

Progress in magnetic materials and components is associated with improved energy efficiency and growing technological demands. An important part of this process is the development of methods and instrumentation for accurate measurements of magnetic parameters. In terms of power losses, the total loss density is a fundamental magnetic parameter measured and used for the evaluation of quality of electrical steels. The methods of measurement and metrological recommendations are specified in the IEC standards [1]. In spite of widely discussed disadvantages [2,3,4], Epstein frame is still an highly approved standard in the industrial and laboratory tests. In addition, easy recreation of a tested magnetic circuit in the frame and relatively good reproducibility of tests provide an opportunity of comparison and mutual verification [5-9]. Therefore, for the tests a set of strips was prepared. The measurements were performed in the following places PTB (Physikalisch-Technische Bundesanstalt), Magnetic Measurement Laboratory Stalprodukt and Magnetic Laboratory Lodz University of Technology (LUT). Based on the total loss density data and uncertainty of measurements, the intercomparison and verification of convergence have been performed.

## II. STANDARD SAMPLE AND MEASUREMENT SYSTEMS

For the purpose of interlaboratory measurements a set of 28 strips had been prepared. Technical parameters of the package are presented in table 1.

*Table 1. Technical specification of the tested package*

| | | |
|---|---|---|
| Manufacturer assignment: | \| | 5223400 – 1 – 28 |
| Electrical steel grade: | \| | ET-117 30 |
| Length: | \| | 305.0mm |
| Width: | \| | 30.0mm |
| Thickness: | \| | 0.2828 mm |
| Density: | \| | 7650 kg/m$^3$ |
| Total mass of the strips: | \| | 554.26 g |

The package was annealed in order to remove mechanical stresses. Additionally, the sequence of the packaging has been placed.

The PTB and LUT laboratories employed their own systems with precisely defined range of uncertainty of measurements of power losses, magnetic field strength and magnetic polarization. Stalprodukt laboratory used a commercial system Brockhaus 200D.

## III. PRESENTATION OF MEASUREMENT SCATTER

Experimental work considered four magnetic polarization densities such as 1.0T, 1.3T, 1.5T and 1.7T with the frequency of 50Hz. In each case the magnetic field strength, form factor and demagnetization were controlled.

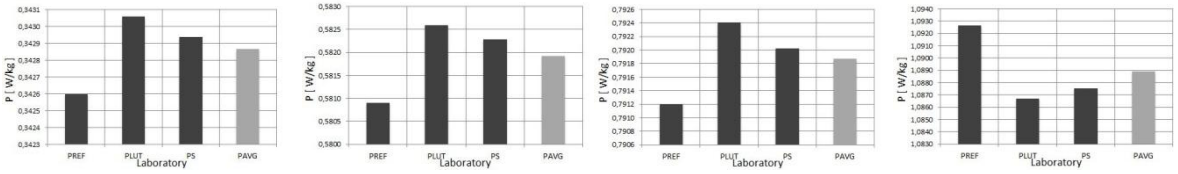


*Fig.1. Comparison of the measurements of the total loss density for the maximum magnetic polarization a) 1.0T, b) 1.3T, c) 1.5T, d) 1.7T*

The scatter of each measurement has not been higher than 6mW/kg and 0.36%. The paper is going to contain all the measurements and the detailed evaluation of uncertainty.

## IV. SUMMARY

Considering the ranges of uncertainties of the measurements, one can state that all the measurements are in the common range of uncertainty. This approach constitutes validation of used measurement systems. The tested package can be successfully used for the verification of other systems and measurements.

## REFERENCES


[1] IEC 60404-2:1996 + A1:2008, Magnetic materials - Part 2: Methods of measurement of the magnetic properties of electrical steel strip and sheet by means of an Epstein frame

[2] Fiorillo F., Characterization and measurement of magnetic materials, *Elsevier*, Netherlands 2004

[3] Ahlers H., Ludke J., The uncertainties of magnetic properties measurements of electrical sheet steel, *J. Magn. Magn. Mater.*, vol. 215–216, 2000, pp. 711–713

[4] Antonelli E., Cardelli E., Faba A., Epstein frame: How and when it can be really representative about the magnetic behavior of laminated magnetic steels, *IEEE Trans. Magn.*, vol. 41, no. 5, 2005, pp. 1516–1519

[5] Cheng Z., Takahashi N., Forghani B., Moses A.J., Anderson P.I., Fan Y., Liu T., Wang X., Zhao Z., Liu L., Modeling of magnetic properties of GO electrical steel based on Epstein combination and loss data weighted processing, *IEEE Trans. Magn.*, vol. 50, no. 1, 2014

[6] De Wulf M., Makaveev D., Houbaert Y., Melkebeek J., Design and calibration aspects of small size single sheet testers, *J. Magn. Magn. Mater.*, vol. 254–255, 2003, pp. 70–72

[7] Freitag C., Joost C., Leibfried T., Modified Epstein frame for measuring electrical steel under transformer like conditions, *ICHVE 2014 - 2014 Int. Conf. High Volt. Eng. Appl.*, 2015, pp. 2–5

[8] Manyage M.J. Pillay P., New Epstein frame for core loss measurements at high frequencies and high flux densities, *Conf. Rec. - IAS Annu. Meet. (IEEE Ind. Appl. Soc.*, vol. 22, no. 3, 2008, pp. 614–620

[9] Sievert J., The measurement of magnetic properties of electrical sheet steel – survey on methods and situation of standards, *J. Magn. Magn. Mater.*, vol. 215–216, 2000, pp. 647–651

# SOFT MAGNETIC PROPERTIES AND MAGNETOCALORIC EFFECT OF IRRADIATED Fe-Mo-Cu-B ALLOY

M. Hasiak

Wrocław University of Science and Technology, Department of Mechanics and Materials Science, Smoluchowskiego 25, 50-370 Wrocław, Poland, Mariusz.Hasiak@pwr.edu.pl

***Abstract.*** *Thermomagnetic characteristics and magnetocaloric properties of the $Fe_{81}Mo_9Cu_1B_9$ alloy after ion irradiation by nitrogen ions with the fluencies from $5 \times 10^{15}$ $N^+/cm^2$ to $2.5 \times 10^{17} N^+/cm^2$ are studied.*

## I. INTRODUCTION

Fe-based soft magnetic materials are very interesting because present unique combination of magnetic properties [1].The parameters such as low coercivity, high magnetization and nearly zero magnetostriction lead thatmetallic glasses can be effectively utilized in variety of practical application [2]. Among others, magnetic shielding, transformer cores or sensors belong to the most widely employed [1, 3]. Moreover, Fe-based metallic glasses are suggested as candidates for magnetic cores of accelerator RF-cavities [4].

In this paper, the impact of irradiation with $N^+$ ions upon magnetic parameters as well as magnetocaloric effect of the $Fe_{81}Mo_9Cu_1B_9$ alloy alloy is studied.

## II. EXPERIMENTAL PROCEDURE

As-quenched$^{57}$Fe rich ribbon with a nominal composition of $Fe_{81}Mo_9Cu_1B_9$ (at. %) about 1 mm wide and 20 μm thick was prepared by rapid quenching method on a single Cu water cooled wheel. All samples of investigated alloy were irradiated using 130 keV nitrogen ions with the fluencies from $5 \times 10^{15}$ $N^+/cm^2$ to $2.5 \times 10^{17}$ $N^+/cm^2$. DC thermomagnetic characteristics recorded in zero field and field cooled mode were measured by VersaLab system (Quantum Design). Magnetization as a function of external magnetic field was recorded in a temperature range 50 K - 400 K.Magnetocaloric effect of irradiated materials was studied as magnetic entropy change according to the Maxwell thermodynamic relation[5] and calculated from set of isothermal magnetization curves. Moreover, Arrott plots [6] were also constructed from obtained data.

## III. RESULTS AND DISCUSSION

Magnetic field dependence of magnetization recorded in the temperature range from 150 K to 330 K together with Arrott plots constructed at constant temperature from these curves according to formula $M^2 = f(\mu_0 H/M)$is presented in Fig. 1. It is seen from Arrott plots that investigated sample does not show clear transformation from ferromagnetic to paramagnetic state. This behavior is connected with microstructure and structural changes which occurred during production of the investigates materials. Fig. 2 shows magnetocaloric effect as magnetic entropy change ($-\Delta S_M$) for the $Fe_{81}Mo_9Cu_1B_9$ alloy after irradiation with $2.5 \times 10^{17}$ ions/cm$^2$. The maximum value of $-\Delta S_M$ in the investigated alloy is observed in the temperature from 240-260 K.

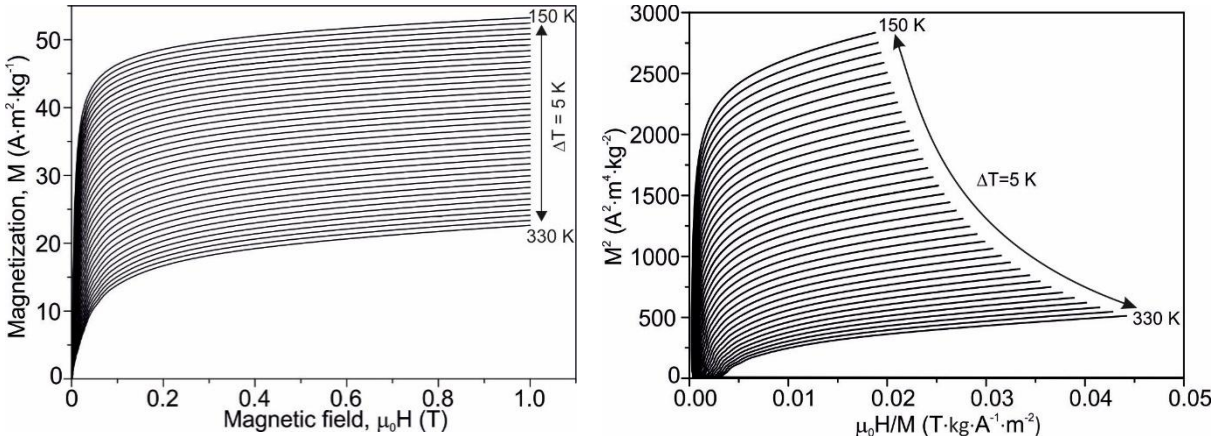


*Fig. 1. Sets of isothermal magnetization curves in the temperature range 150-330 K (left side) and Arrott plots (right side) of the $Fe_{81}Mo_9Cu_1B_9$ alloy after irradiation with 2.5 × $10^{17}$ ions/$cm^2$*

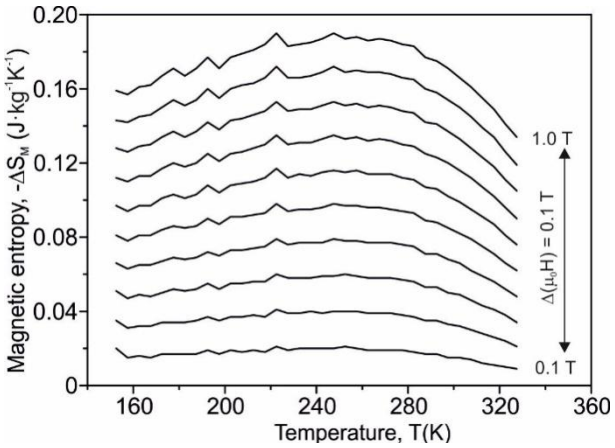


*Fig.2. Magnetic entropy change versus temperature for the $Fe_{81}Mo_9Cu_1B_9$ alloy after irradiation with 2.5 × $10^{17}N^+/cm^2$*

## REFERENCES


[1] McHenry M.E., Willard M.A., Laughlin D.E., Amorphous and nanocrystalline materials for applications as soft magnets, *Progress Mat. Sci.* **44** (1999) 291-433, DOI: 10.1016/S0079-6425(99)00002-X

[2] Willard M. A., Daniil M., Nanocrystalline soft magnetic alloys two decades of progress, Chapter Four, *Handbook of Magnetic Materials*, vol.**21** (2013), Elsevier B.V., ISSN 1567-2719, DOI:10.1016/B978-0-444-59593-5.00004-0

[3] Hasiak M., Miglierini M., Łukiewski M., Kaleta J., Microstructure, Magnetic Properties, and Applications of Co-Rich HITPERM-Type Amorphous Alloys. *IEEE Trans. Magn*. **48** (2012) 1665-1668, DOI: 10.1109/TMAG.2011.2172590

[4] Saito K., Hirota J.I., Noda F., FINEMET-core loaded untuned RF cavity, *Nuclear Instruments and Methods in Physics Research Section A: Accelerators, Spectrometers, Detectors and Associated Equipment*402 (1998) 1-13, DOI:10.1016/S0168-9002(97)01062-0

[5] Pecharsky V.K., Gschneidner K.A. Jr, Magnetocaloric effect and magnetic refrigeration, *J. Magn. Magn. Mater.* **200** (1999) 44-56, DOI: 10.1016/S0304-8853(99)00397-2

[6] Arrott A., Criterion for Ferromagnetism from Observations of Magnetic Isotherias, *Phys. Rev.***108** (1957) 1394-1396

# FIRST ORDER REVERSAL CURVE ANALYSIS OF ANNEALED Fe-Co-Si-B-Mo-P METALLIC GLASS

M. Hasiak[1] and M. Miglierini[2,3]

[1]Wrocław University of Science and Technology, Department of Mechanics and Materials Science, Smoluchowskiego 25, 50-370 Wrocław, Poland
[2]Slovak University of Technology in Bratislava, Faculty of Electrical Engineering and Information Technology, Institute of Nuclear and Physical Engineering, Ilkovičova 3, 812 19 Bratislava, Slovakia
[3]Czech Technical University in Prague, Faculty of Nuclear Science and Physical Engineering, Department of Nuclear Reactors, V Holešovičkách 2, 180 00 Prague, CzechRepublic

***Abstract.*** *The paper presents characterization of magnetic particle interactions in the $Fe_{51}Co_{12}Si_{16}B_8Mo_5P_8$ metallic glass after annealing at 798 K for 1 h. The first order reversal curves (FORC) method was utilized to analyze hysteresis curves which provide more precise estimation of the strength of interactions.*

## I. INTRODUCTION

Recently, Fe-Si-B-P-Cu soft magnetic material (NANOMET) [1-2] as well as alloys containing Co atoms [3] are intensively studied. They exhibit interesting soft magnetic characteristics, *i.e.* high magnetic saturation, high magnetic permeability, and extremely low coercivity which are required for magnetic cores. One of the most important parameter in creation of nanocrystalline structure in Fe-Si-B-P-Cu alloys is the heating rate [4]. The heat treatment with high heating leads to formation of ultrafine structure whereas the low heating rate produces non-uniform structure and deterioration of magnetic properties. The aim of this work is to study magnetic interactions among particles in the $Fe_{51}Co_{12}Si_{16}B_8Mo_5P_8$ metallic glass after annealing in a vicinity of the crystallization temperature by using first order reversal curves (FORC) method [5].

## II. EXPERIMENTAL PROCEDURE

Amorphous ribbons with a nominal composition of $Fe_{51}Co_{12}Si_{16}B_8Mo_5P_8$ (at. %) about 0.02 mm thick and about 6 mm wide were prepared using a rapid solidification method on a copper quenching wheel. Amorphicity and degree of crystallinity of the as-quenched and annealed materials were examined at room temperature by X-ray diffractometry. Magnetic characteristics were measured with the help of VersaLab system (Quantum Desing). Magnetization ($M$) as a function of external magnetic field ($H$) and/or temperature was recorded in a wide temperature range below the Curie point. Hysteresis loops as well as first order reversal curves were measured as a set of $M$ ($H$) curves. Evaluation of the obtained results was performed by the VARIFORC software [6]. All measurements were performed upon as-quenched samples and after their annealing at 798 K for 1 h.

## III. FORC DIAGRAM

Magnetic characterization of one-phase magnets *i.e.* magnetic interactions in materials with high value of coercivity is usually performed by investigations of hysteresis loops. A problem appears when complex magnetic interactions are present in a multi phase material. The first order reversal curves analysis is one of the methods which can provide information about interaction field between multiphase magnetic particles/phases such as $\alpha$-Fe/NdFeB, present in magnetic composite Nd-Fe-B alloys. The information from analysis of the distribution of coercivity can be used in creation of new hard magnetic materials with high energy density.

Set of first order reversal curves for the annealed $Fe_{51}Co_{12}Si_{16}B_8Mo_5P_8$metallic glass and the obtained FORC distribution are presented in Fig. 1. The latter is defined as the second derivative [5]:

$$\rho(H_a, H_b) \equiv -\frac{\partial^2 M(H_a, H_b)}{\partial H_a \partial H_b}$$

where $H_a$ and $H_b$ are reversal field and magnetization field, respectively, converted according to: $H_c = (H_b - H_a)/2$ and $H_u = (H_b + H_a)/2$. It is seen that in the investigated sample measured at 50 K with maximum external magnetic field of 500 Oe only one kind of magnetic interactions among the particles can be distinguished. Moreover, the value of $H_c$ is almost the same as coercive field for the $Fe_{51}Co_{12}Si_{16}B_8Mo_5P_8$ alloy under the same magnetic field. The use of higher magnetic field leads to visualization of high field magnetic interactions among particles created during heat treatment.

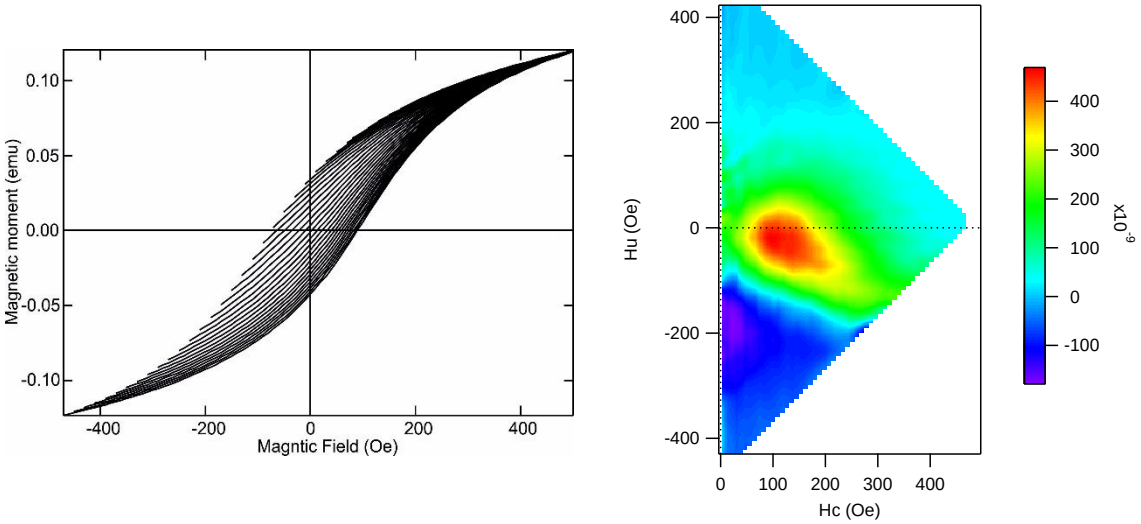


*Fig.1. Set of first order reversal curves (left side) and FORC diagram (right side) for the $Fe_{51}Co_{12}Si_{16}B_8Mo_5P_8$ metallic glass after annealing at 798 K for 1 h measured at temperature of 50 K with maximum external magnetic field of 500 Oe.*

## ACKNOWLEDGEMENTS

Financial support of the grants GACR 14-12449S and VEGA 1/0182/16 is acknowledged.

## REFERENCES

[1] M. Chiba, A. Urata, H. Matsumoto, S. Yoshida, A. Makino, Characteristics of Fe-Si-B-P-Cu nanocrystalline soft magnetic alloy powders with high $B_s$, *IEEE Transaction on Magnetics*, **47** (10) (2011) 2845-2847

[2] A. Makino, Nanocrystalline soft magnetic Fe-Si_B-P-Cu alloys with high B of 1.8-1.9 T contributable to energy saving, *IEEE Transaction on Magnetics*, **48** (4) (2012) 1331-1335

[3] K. Takenaka, A.D. Setyawan, Y. Zhang, P. Sharma, N. Nishiyama, A. Makino, Production of nanocrystalline (Fe, Co)-Si-B-P-Cu alloy with excellent soft magnetic properties for commercial applications, *Materials Transaction*, **56** (3) (2015) 372-376

[4] P.Sharma, X. Zhang, Y. Zhang, A. Makino, Competition driven nanocrystallization in high $B_s$ and low coreloss Fe-Si-B-P-Cu soft magnetic alloys, **95** (2015) 3-6

[5] Ch.R. Pike, A.P. Roberts, K.L. Verosub, Characterizing interactions in fine magnetic particle systems using first order reversal curves, *J. Appl. Phys.*, **85** (9) (1999) 6660-6667

[6] R. Egli, VARIFORC: An optimized protocol for calculating non-regular first order reversal curve (FORC) diagrams, *Global and Planetary Change*, **110** (2013) 302-320

# CHARACTERIZATION OF SOFTMAGNETIC MATERIALS IN AC MAGNETIC FIELDS BY DIGITAL METHODS

R. Hiergeist, K. Wagner and G. Ross

Magnet-Physik Dr. Steingroever GmbH, Emil-Hoffmann-Straße 3, 50996 Köln, Germany,
robert.hiergeist@magnet-physik.de, klaus.wagner@magnet-physik.de, gunnar.ross@magnet-physik.de

Nowadays, for the characterization of soft magnetic materials in AC magnetic fields digital methods are used. Magnet-Physik offers a family of computer controlled measuring instruments. These allow the measurement of AC hysteresis loops under various conditions [1].

The models of these instruments are carefully adapted to the different specimen and material classes of soft-magnetic material. They cover frequency ranges up to 10 kHz, 20 kHz or 500 kHz, depending on the selected components. For the measurement of grain-oriented and non-grain-oriented electrical steel, a standard Epstein frame (25 cm) can be used together with a high output power supply, offering a maximum output power of 1100 VA. Therefore, this instrument allows measurements following the standards IEC 60404-2 [2], ASTM A343/A343M [3] and ASTM A889/A889M [4]. The standard Epstein frame is optimized for power line frequencies (50 Hz, 60 Hz) and can be used from 10 Hz up to approximately 200 Hz. For the frequency range from 100 Hz up to 10 kHz a special high frequency Epstein frame according to the standard ASTM A348/A348M [5] was built.

Besides the application of this apparatus to Epstein samples, all models are able to measure ring specimen (solid ring cores, sintered cores, tape-wound cores with round or rectangular shape, sheet stampings (single samples or stacks)) with a primary winding connected to the AC power amplifier and a secondary winding connected to the pick-up circuit.

For the measurement of ring cores of crystalline Ni-Fe-alloys and compounds, lower rated versions of the instrument, providing a maximum output power of 50 VA, 100 VA or 200 VA in the frequency range from 10 Hz up to 10 kHz were made.

The 200 VA models and the high power version feature a digital waveform control to maintain a sinusoidal secondary induced voltage (or flux density), even at relatively high excitation.

Tape wound cores of amorphous magnetic materials or of nanocrystalline magnetic materials, as well as rings of soft magnetic ferrites can be measured either with the 200 VA rated instrument or with a special version with an output rating of 180 VA and the ability to measure even in a frequency range from 10 Hz up to 500 kHz.

For the characterization of amorphous or nanocrystalline soft magnetic materials in the shape of thin ribbons or strips [6] a special single strip tester unit (AM-SST) [7] can be used in connection with a low power system.

The software of the instruments is continuously expanded and updated. A recent version allows, for instance, – after automated measuring of the hysteresis loops at different magnetization frequencies – the separation of the magnetic power losses into hysteretic losses, eddy current losses and anomalous losses within this software and provides therefore fast and sophisticated measurement reports.

## REFERENCES

[1] Steingroever E., Ross G., Magnetic Measuring Techniques, 2008, 68

[2] IEC 60404-2, Methods of Measurement of the Magnetic Properties of Electrical Strip and Sheet by means of an Epstein Frame, *IEC*, Geneva, 2009

[3] ASTM A343/A343M, Standard Test Method for Alternating-Current Magnetic Properties of Materials at Power Frequencies Using Wattmeter-Ammeter-Voltmeter Method and 25-cm Epstein Test Frame, *Annual Book of ASTM*, 03.04 Magnetic Properties, 2012, 38-53

[4] ASTM A889/A889M, Standard Test Method for Alternating-Current Magnetic Properties of Materials at Low Magnetic Flux Density Using the Voltmeter-Ammeter-Wattmeter-Varmeter-Method and 25-cm Epstein Frame, *Annual Book of ASTM*, 03.04 Magnetic Properties, 2012, 211-215
[5] ASTM A348/A348M, Standard Test Method for Alternating Current Magnetic Properties of Materials Using the Wattmeter-Ammeter-Voltmeter Method, 100 to 10000 Hz and 25-cm Epstein Frame, *Annual Book of ASTM*, 03.04 Magnetic Properties, 2012, 58-67
[6] Hilzinger R., Rodewald W., Magnetic Materials, *Publicis Publishing*, ISBN 978-89578-352-4, 2013, 280
[7] Watanabe R., Takahashi Y., Fujiwara K., Ishihara Y., Azuma D., Investigation into measurement method of Fe-based amorphous strip for IEC standardization and its application to electrical steel sheet, *7th International Conference On Magnetism And Metallurgy*, Rome, Italy 2016 (Preprint)

# TWO METHODS OF MAGNETOELASTIC EFFECT UTILIZATION TO EVALUATE MECHANICAL STRAIN IN THE TRUSS STRUCTURES

D. Jackiewicz[1], A. Juś[2], R. Szewczyk[1] and A. Bieńkowski[1]

[1] Institute of Metrology and Biomedical Engineering, Andrzeja Boboli 8, 02-525 Warsaw, Poland, d.jackiewicz@mchtr.pw.edu.pl, szewczyk@mchtr.pw.edu.pl
[2] Industrial Research Institute for Automation and Measurements PIAP, Aleje Jerozolimskie 202, 02-486 Warsaw, Poland, ajus@piap.pl

***Abstract.*** *The article presents the possibility of using the magnetoelastic effects to monitor mechanical strain in trusses. Test stand enabling loading of the special truss structure was designed, which allowed for installation of sample members. Study was carried out on two different configurations of the truss. The first configuration consists of three separate sample members. The magnetoelastic characteristics were measured for each member separately. The second configuration consists of three measuring members combined in a single magnetic circuit. Measurements of the hysteresis loops of the sample members was carried out under varying mechanical load, which allowed to obtain magnetoelastic characteristics. The obtained results confirmed the possibility of using the magnetoelastic effects to monitor stresses in the truss structures.*

## I. INTRODUCTION

Truss constructions increasingly require monitoring of the stresses due to the growing security requirements. Current methods for assessment of stresses, such as a strain gauge or the magnetostrictive method, have serious limitations. There is therefore a need to develop methodology for allowing the execution of such measurements. The development of magnetic measurements allows the use of them in different scientific fields. A phenomenon that can be used to monitor stresses in the constructions is the magnetoelastic effects [1].

## II. EXPERIMENTAL

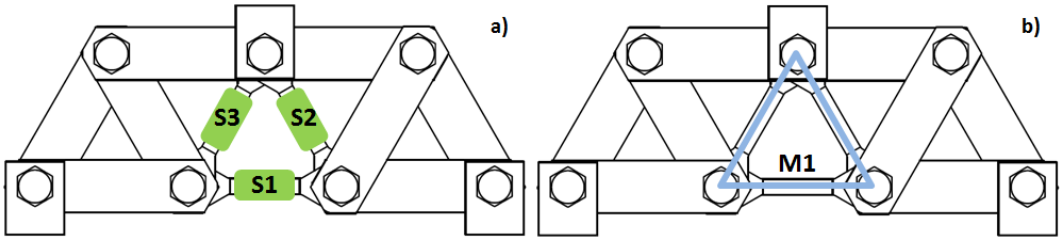


*Fig.1. Schematic diagram of the truss structures: a) first configuration, b) second configuration*

The test stand enabling loading of the special truss structure was designed, which allowed for installation of sample members. The hysteresis loops measurements are done on the hysteresisgraph. The truss was supported on the bottom edge nodes. The mechanical load was exerted vertically by the oil hydraulic press on the upper central node of the truss. Measurements of magnetoelastic characteristics were made for two different configurations of the truss.

In the first configuration (figure 1a) has been used for sample members shown in figure 2a. The measuring elements are designed to be appropriate for individual windings. In the columns of sample members uniform stress distribution was assumed. The magnetoelastic characteristics were measured for each sample member separately.

In the second configuration (figure 1b), the magnetic circuit is closed by means of three sample members. Used samples (figure 2b) have a reduced cross-sectional area, so as to not damage the rest of the truss during tests. The magnetoelastic characteristics were measured for magnetic core enclosed on three elements.

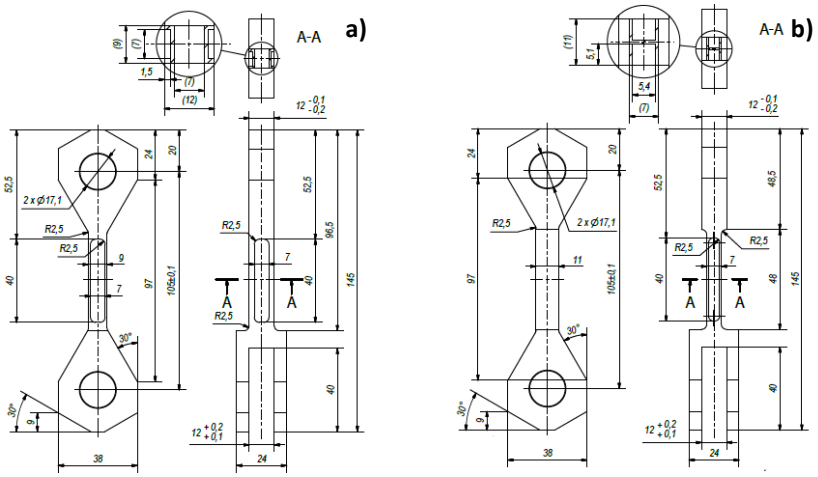


*Fig.2. Schematic diagram of the sample members*

## III. RESULTS AND DISCUSSION

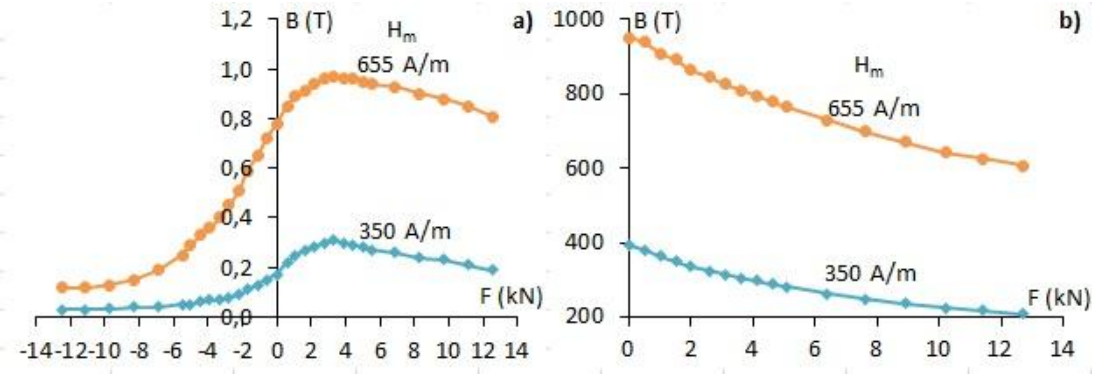


*Fig.3. Magnetoelastic characteristics for: a) first configuration, b) second configuration*

Figure 3a shows the measurement results for first configuration. The magnetoelastic characteristics consists of two parts: the negative force value shows the results for compressed component and the positive values of force for the tensed member. The value of flux density at first increases, and after crossing Villari point, decreases.

Figure 3b shows the measurement results for second configuration. The magnetoelastic characteristics were determined for the three sample members combined in a single magnetic circuit. The value of flux density decreases under external force.

## III. CONCLUSIONS

Test stand enabling loading of the special truss structure, which allowed for installation of sample members was developed. The measurements were carried out for two different configurations of the truss. The results confirmed the possibility of using magnetoelastic effects to monitor stresses in the truss structures. The advantages of the second configuration over the first are simpler sample construction and monotonous, unequivocal characteristic.

## REFERENCES

[1] Bozorth R.M., Ferromagnetism, *Van Nostrand*, New York, 1951

# MEASUREMENTS OF PROPERTIES OF POLYMER-METALLIC COMPOSITES

A. Jakubas, P. Gębara, A. Gnatowski and K. Chwastek,

Częstochowa University of Technology, J. H. Dąbrowskiego 69, 42-201 Częstochowa, Poland
adam.jakubas@gmail.com, pgebara@wip.pcz.pl, krzysztof.chwastek@gmail.com

***Abstract.*** *In the paper the results of measurements carried out on polymer-metallic composites are presented. The samples under investigation are made from 99% pure iron powder and suspense polyvinyl chloride PVC-S. Relevant magnetic and electric properties are determined for samples differing in polyvinyl content.*

## I. INTRODUCTION

Engineering community has noticed the advantages resulting from the application of powder metallurgy in the design of electromagnetic converters and electric machines [1-5]. Soft magnetic composites (SMCs) reveal interesting physical and chemical properties, which may be easily optimized and fine-tuned to specific applications by an appropriate material processing [1, 3, 6, 7].

Quite a lot of research is devoted to the optimization of circuits made of commercially available SMC powders [7-9]. In the present paper we focus on the possibility to develop ”home-made” SMC cores. The paper considers the effect of varying polymer content on the magnetic properties of self-assembled SMC cores.

## II. MEASUREMENTS

Samples have been prepared from iron (99% pure Fe, granulation>150μm) powder and suspense polyvinyl chloride PVC-S (granulation 15−100μm). Fine structure of both components allowed us to obtain highly homogeneous mixtures. Polyvinyl chloride used as the binder has good mechanical properties. Moreover it is resistant against the action of many solvents and is a good electrical insulator. From the obtained mixtures cylinder-shaped samples were formed using a hydraulic press with a self-assembled form and a band with a thermocouple for controlling heat treatment conditions, cf. Fig. 1.


*Fig.1. The material under study at different stages of preparation: a) raw Fe powder, b) PVC-S, c) the hydraulic press with a heating band used during material processing, d) the ready-made core, e) the assembled core with windings*

The first stage of research was the determination of optimal PVC content to make up stable samples, that are able to maintain reasonably good magnetic properties. The tests were started at 20% polymer content, yet for further studies four samples with appropriately higher Fe content

were chosen. The raw materials were mixed using weight proportions. The PVC contents in the final samples were equal to 0.5, 1.0, 1.5 and 2.0 %, respectively. The cylinder shaped shapes were next subject to reticulation for 30 minutes at 165°C and at pressure 200 MPa. The magnetic properties were determined using two windings wound around the developed cores and recorded with a digital oscilloscope.

An exemplary measured dependence of magnetic permeability on polymer content is presented in Fig. 2. The dependence has been obtained for $B_m$ = 1.0 T and $f$ = 50 Hz. It can be stated that permeability may be correlated with PVC content. It is decreased as the PVC content is increased. The observed trend is in accordance with the results reported by other scientists [1,8].

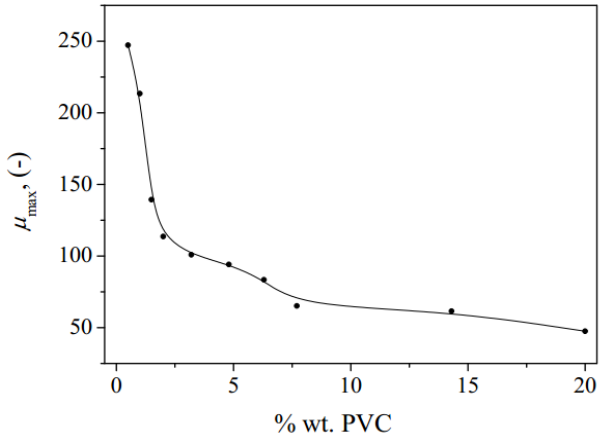


*Fig.2. The dependence of relative permeability on polymer content*

## REFERENCES


[1] Shokrollahi H., Janghorban K., Soft magnetic composite materials (SMCs), *J. Mater. Process. Technol.*, 2007, vol. 189, pp. 1-12

[2] Cvetkovski G., Petkovska L., Performance Improvement of PM Synchronous Motor by Using Soft Magnetic Composite Material, *IEEE Trans. Magn.*, 2008, vol. 44, pp. 3812-3815

[3] Actis Grande M., Bidulský R., Cavagnino A., Ferraris L., Ferraris P., Investigations on different processing conditions on Soft Magnetic Composite material behavior at low frequency, *IEEE Trans. Ind. Appl.*, 2012, vol. 48, pp. 1335-1342

[4] Wojciechowski R., Jędryczka C., Łukaszewicz P., Kapelski D., Analysis of high speed permanent magnet motor with powder core material, *COMPEL*, 2012, vol. 31, pp. 1528-1540

[5] Xiaobei Li, Jing Zhao, Zhen Chen, Application of Soft Magnetic Composite Material in the field of electrical machines, *Appl. Mech. Mater.* , 2013, vol. 380-384, pp. 4299-4302

[6] Gilbert I., Bull S., Evans T., Jack A., Stephenson D., de Sa A., Effects of processing upon the properties of soft magnetic composites for low loss applications, *J. Mater. Sci.*, 2004, vol. 39, pp. 457-461

[7] Ślusarek B., Szczygłowski J., Chwastek K., Jankowski B., A correlation of magnetic properties with material density for soft magnetic composite cores, *COMPEL*, 2015, vol. 34, 637, pp. 1-11

[8] Kollár P., Füzer J., Bureš R., Fáberová M., AC Magnetic Properties of Fe-Based Composite Materials, *IEEE Trans. Magn.* , 2010, vol. 46, pp. 467-470

[9] Jankowski B., Ślusarek B., Szczygłowski J., Chwastek K., Modelling hysteresis loops in Fe-based soft magnetic composites using Takács description, *Acta Phys. Pol. A.*, 2015, vol. 128, pp. 116-119

# USING THE PHASED ANTENNA ARRAY TO INCREASE GEOMETRIC SIZE OF THE INTERROGATION ZONE IN UHF RFID SYSTEM

P. Jankowski -Mihułowicz, D. Kawalec and M. Węglarski

Rzeszow University of Technology, Faculty of Electrical and Computer Engineering,
Department of Electronic and Communications Systems, W. Pola 2, 35-959 Rzeszow,
pjanko@prz.edu.pl, http://pjanko.sd.prz.edu.pl, damkaw@prz.edu.pl,
wmar@prz.edu.pl, http://wmar.sd.prz.edu.pl

***Abstract.****The problem to increase geometric size of theinterrogation zone in UHF RFID systems with phased antenna array is presented in the paper. The perceived issues have been effectively dealt with and the solution has been proposed on the basic of the elaborated model. Conducted studies have been used to develop the software tool in the Mathcad environment. The research results are analyzed in details for different system configurations and can be implemented in practical projects to be developed in cooperation with companies.*

## I. INTRODUCTION

The typical RFID system consists of a read/write device (RWD), its antenna and at least one transponder that is intended for marking an object [1]. Communication in this system can be provided with one or simultaneously with multiple transponders (single or anti-collision system respectively) that can also be found in static or dynamic state (moving objects).

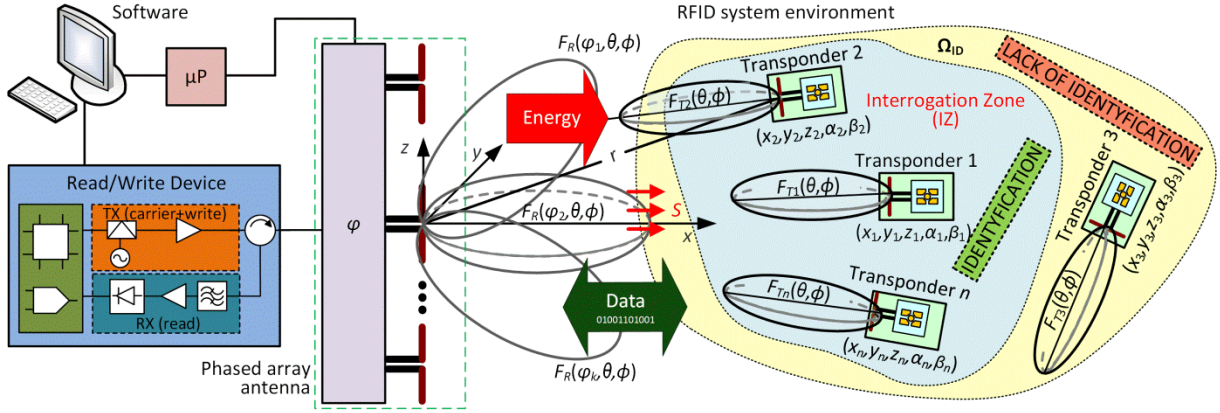


*Fig.1. Anti-collision UHF RFID system with phased antenna array*

The main parameter of RFID systems is interrogation zone (IZ) – figure 1. It is defined as the space within which it is possible to conduct the radio transmission between RWD and transponders intended for marking objects. The shape and size of the interrogation zone strongly depends on many factors, e.g. RFID system band (HF/UHF), the transponder type (passive/semi-passive) and its parameters (e.g. sensitivity), type, orientation and location of the marked object in operation space. In each of these cases, for the correct exchange of data with a predetermined communication protocol, a key factor is to provide energy electromagnetic field with RWD antenna to chip transponders [1, 2].

The IZ should be estimated in any direction of 3D space ($\mathbf{\Omega_{ID}}$) taking into account the variable localizations of activated transponder(s). It should be noted that a lot of issues in this regard remain unresolved at the current stage of the contemporary knowledge.These problems are due to the fact that many parameters and phenomena describing RFID systems have to be considered in a different way than it is in the classical theory valid for typical radio communication systems. For this reason,

the authors were paid particular attention to the problem of energy transfer in RFID systems with phased antenna array.

## II. MODEL

The problem to solve is the arrangement of phasedantenna array connected to the one RWD. The antennas have to be switched while marked objects are being identified in the inside of a cube of side *b* (Fig. 2). The process of energy transfer from RWD to RFID transponders is subjected to the analysis in the study to be carried out. The radiated electromagnetic wave of power density*S* is an energy medium supplying transponders(Fig. 1). The developed solution is the basis for IZ determination using the Monte Carlo method.

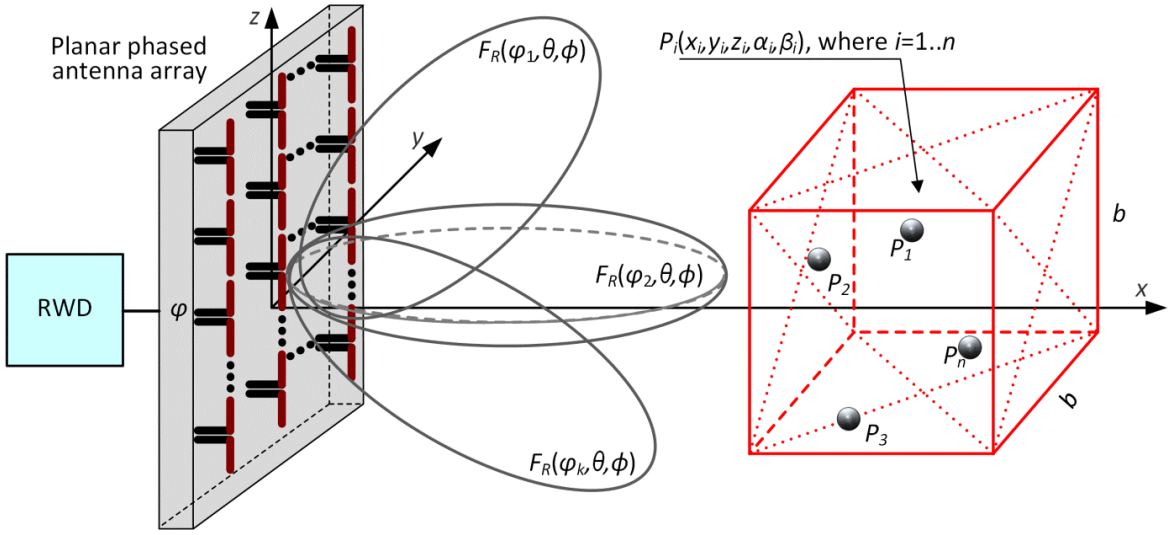


*Fig. 2. Problem of objects identification in the UHF RFID systems with RWDplanar phased antenna array*

The proposed concept of increase geometric size IZ so it can be described using the features, which includes the location of the *k*-th position of the main beam in relation to the *n*-th transponders space $\mathbf{\Omega_{ID}}$:

$$IZ(\mathbf{\Omega_{ID}}) = f(F_R(\varphi_k,\theta,\phi), F_{Tn}(\theta,\phi), \tau_n, \chi_n, P_{RWD}, P_{Tmin}) \quad (1)$$

where: $F_R(\varphi_k,\theta,\phi)$ means the radiation pattern of RWD phased antenna array, $F_{Tn}(\theta,\phi)$ – the transponder radiation pattern, whereas $\varphi$ – the angle of phase shift in the course of feeding the individual array antenna, $P_{RWD}$- the power supplied to terminals of the impedance-matched RWD antenna, $P_{Tmin}$ – the minimal power, that ensures proper operation transponder, $\chi_n$ – the polarization matching factor for given arrangement of radio communication antennas, $\tau_n$ – the coefficient of power transfer from antenna to the chip.

## ACKNOWLEDGMENTS

This work was supported in part by the NCBR under Grant No. PBS1/A3/3/2012. The work was developed by using the equipment purchased under Grants No. POPW.01.03.00-18-012/09-00 and UDA-RPPK.01.03.00-18-003/10-00.

## REFERENCES

[1] Finkenzeller K., RFID Handbook, 3rd Ed., *Wiley*, 2010
[2] De Vita G., Iannaccone G., Design criteria for the RF section of UHF and microwave passive RFID transponders, *IEEE Trans. Microw. Theory Tech.*, Vol. 53, No. 9, 2005, pp. 2978-2990

# A COMPARISON OF DIFFERENT ESTIMATION METHODS FOR HYSTERESIS MODELLING

R. Jastrzębski[1], K. Chwastek[1], I. Biondić[2] and K. Miličević[2]

[1] Faculty of Electrical Engineering, Częstochowa University of Technology, ul. A.K. 17, 42-201 Częstochowa, Poland, e-mail: krzysztof.chwastek@gmail.com

[2]Faculty of Electrical Engineering, J. J. Strossmayer University of Osijek, 31000 Osijek, Croatia

***Abstract.*** *The paper focuses on the estimation of parameters for a low dimensional hysteresis model. Four artificial intelligence based methods are compared in terms of their capabilities and robustness.*

## I. INTRODUCTION

An important stage of hysteresis modeling is the identification of model parameters. For this purpose different optimization techniques, including those based on artificial intelligence methods and soft-computing, are applied [1-3]. Improper choice of values for model parameters may result in excessive prediction errors if other phenomena (e.g. eddy currents) are accounted [4]. On the other hand different sets of model parameters may yield identified hysteresis loops that are quite similar in shape [5]. The present paper is aimed at development of a methodology to choose an optimum procedure to estimate the parameters of a low dimensional hysteresis model, described in Refs. [6-8].

## II. MODEL DESCRIPTION

The description advanced by Jiles and Atherton [9] has attracted a lot attention of the scientific community in the last thirty years. In the present paper we focus on its modification proposed by the Brazilian team GRUCAD [6,7], which has addressed a number of problems with the original description. As pointed out in Ref. [10], in the original Jiles-Atherton model the loop branches are obtained by introducing offsets along the *M*-axis. On the contrary, the GRUCAD proposal is based on introducing offsets along the *H*-axis from the so-called anhysteretic (truly reversible) curve. Therefore the latter model yields an improved description of reversible magnetization processes in the sense of thermodynamics, for example there is no need to introduce artificial "switching off" of the irreversible magnetization component after sudden field reversals. Another practical advantage of the GRUCAD description is its formulation directly as *B*-input model, what is in compliance with international standards concerning magnetic measurements.

The model equations are:

$$H_{\mathrm{an}} = B/\mu_0 - M_{\mathrm{s}}\left(\coth\lambda - 1/\lambda\right) \tag{1}$$

$$\lambda = \frac{1}{a}\left[\left(-\alpha\right)H_{\mathrm{an}} + \alpha\frac{B}{\mu_0}\right] \tag{2}$$

$$H_{\mathrm{h}} = H_{\mathrm{HS}}\left(\coth\lambda_{\mathrm{H}} - 1/\lambda_{\mathrm{H}}\right) \tag{3}$$

$$\lambda_{\mathrm{H}} = \frac{H_{\mathrm{h}} + \delta H_{\mathrm{HS}}}{\gamma},\ \text{where}\ \delta = \pm 1\ \text{is the sign of}\ \mathrm{d}B/\mathrm{d}t \tag{4}$$

$$H = H_{\mathrm{an}} + H_{\mathrm{h}} \tag{5}$$

The model parameters are $\alpha, a, \gamma, H_{\mathrm{HS}}$ and $M_{\mathrm{s}}$.

## III. COMPARISON OF DIFFERENT ESTIMATION TECHNIQUES

In order to compare the efficiency of different estimation techniques we propose the following procedure:

1. estimation of model parameters using a generated loop with *a priori* preset parameters,
2. the same as in previous point, but an artificially generated noise is added to the values for the reference point to simulate inevitable measurement errors,
3. estimation of model parameters for a real life sample.

For comparison we choose the following methods: Particle Swarm Optimization, Nonlinear Simplex + Simulated Annealing, Shuffled Complex Evolution Approach and Genetic Algorithms. The first three algorithms have been implemented by B. Donckels [11] and the codes have been tested using chosen benchmark functions in Ref. [12]. The fourth method has been implemented as a freeware Matlab toolbox by Houck *et al.* [13].

## REFERENCES


[1] Riganti Fulginei F., Salvini A., Softcomputing for the identification of the Jiles-Atherton model parameters, *IEEE Trans. Magn.* 41 (2005) 1100-1108

[2] Chwastek K., Szczygłowski J., Estimation methods for the Jiles-Atherton model parameters - a review, *Przegl. Elektrotechn.* 12 (2008) 145-148

[3] Naghizadeh R.-A., Vahidi B., Hosseinian S.H., Parameter identification of Jiles-Atherton model using SFLA, *COMPEL* 31 (2012) 1293-1309

[4] Steentjes S., Petrun M., Dolinar D., Hameyer K., Effect of parameter identification procedure of the static hysteresis model on dynamic hysteresis loop shapes, IEEE Trans. Magn. (2016) doi:10.1109/TMAG.2015.2511800

[5] Lozito G.M., Salvini A., An empirical investigation on the static Jiles-Atherton model identification by using different set of measurements, Published in: AEIT Annual Conference - From Research to Industry: The Need for a More Effective Technology Transfer (AEIT), 2014, 18-19 Sept. 2014, Trieste, Italy, pp. 1-6, doi:10.1109/AEIT.2014.7002045

[6] Koltermann P.I., Righi L.A., Bastos J.P.A., Carlson R., Sadowski N., Batistela N.J., A modified Jiles method for hysteresis computation including minor loops, *Physica B* 275 (2000) 233-237

[7] Righi L.A., Sadowski N., Carlson R., Bastos J.P.A., Batistela N.J., A new approach for iron losses calculation in voltage fed time stepping finite elements, *IEEE Trans. Magn.* 37 (2001) 3353-3356

[8] Steentjes S., Chwastek K., Petrun M., Dolinar D., Hameyer K., Sensitivity analysis and modeling of symmetric minor hysteresis loops using the GRUCAD description, *IEEE Trans. Magn.* 50 (2014) doi: 10.1109/TMAG.2014.2323250

[9] Jiles D.C., Atherton D.L., Theory of ferromagnetic hysteresis, *J. Magn. Magn. Mater.* 61 (1986) 48-60

[10] Zirka S.E., Moroz Yu.I., Harrison R.G., Chwastek K., On physical aspects of the Jiles-Atherton hysteresis models, *J. Appl. Phys.* 112 (2012) 043916 (7 pp.)

[11] Oldenhuis R., 2009. GODLIKE Matlab toolbox. Available from: https://www.mathworks.com/matlabcentral/fileexchange/24838-godlike-a-robust-single---multi-objective-optimizer?requestedDomain=www.mathworks.com

# STUDY ON RAYLEIGH HYSTERESIS MODEL AND ITS APLICABILITY IN MODELLING MAGNETIC HYSTERESIS PHENOMENON IN FERROMAGNETIC MATERIALS

M. Kachniarz and R. Szewczyk

Institute of Metrology and Biomedical Engineering, Warsaw University of Technology, sw. Andrzeja Boboli 8, 02-525 Warsaw, Poland; m.kachniarz@mchtr.pw.edu.pl

***Abstract.*** *The following paper presents the basis of Rayleigh magnetic hysteresis model and its application for modeling magnetic characteristics of different ferromagnetic materials. Moreover, the range of magnetizing field where Rayleigh model can be applied in these materials was investigated based on correlation coefficient between experimental results and modeling.*

## I. INTRODUCTION

Modeling magnetic properties of ferromagnetic materials is very important matter in modern physical science as well as in technical applications of magnetic materials. There are several approaches to the subject of modeling magnetic hysteresis phenomenon, one of the most popular being Jiles-Atherton model and Preisach model [1]. However, there is still a need to developed more simplified models, which would allow to easily simulate magnetic properties of the materials for technical purposes. One of the possible solutions to this problem is so-called Rayleigh hysteresis model basing on second order polynomial equations.

## II. RYLEIGH HYSTERESIS MODEL

Rayleigh model utilizes parabolic curves and second order polynomials to approximate hysteresis loop [2]. This model is very simple, but partially considers physical phenomenon occurring during magnetization process. Model is based on the second order equation describing initial magnetization curve (known as Rayleigh law of magnetization) [3]:

$$B(H) = \mu_0 \mu_i H + \mu_0 \alpha_R H^2 \tag{1}$$

where $B$ is magnetic flux density, $H$ is magnetizing field and $\mu_0$ is magnetic permeability of free space. There are also two material constants: Rayleigh coefficient $\alpha_R$ and initial relative magnetic permeability $\mu_i$, being coefficients of the equation. In Rayleigh's approach hysteresis loop is described by the system of two second order equations:

$$B(H) = \mu_0[(\mu_i + \alpha_R H_m)H \pm \frac{\alpha_R}{2}(H_m^2 - H^2)] \tag{2}$$

where $H_m$ is amplitude of magnetizing field. On the basis of presented equations there is a possibility to calculate values of basic magnetic parameters of the material like coercive field, magnetic remanence and power losses in certain volume of the material.

While for high magnetizing field Rayleigh model is not satisfactory because of low correlation between hysteresis loop and parabolic curves, this model is a very good approximation of hysteresis loop obtained for low magnetizing fields, lower than saturation coercive field. For such fields, hysteresis loop exhibits lenticular shape, which could be well approximated with two intersecting parabolic curves.

## III. EXPERIMENTAL RESULTS AND MODELING

One of the investigated materials was 13CrMo4-5 constructional steel characterized by saturation magnetic flux density $B_m$ = 1.5 T, coercive field $H_c$ = 670 A/m and initial relative magnetic permeability $\mu$ = 250. The material was investigated for the range of magnetizing field amplitude $H_m$ from 100 A/m to 700 A/m. Experimental results compared with modeling data for three selected values of $H_m$ are presented in Fig. 1a.

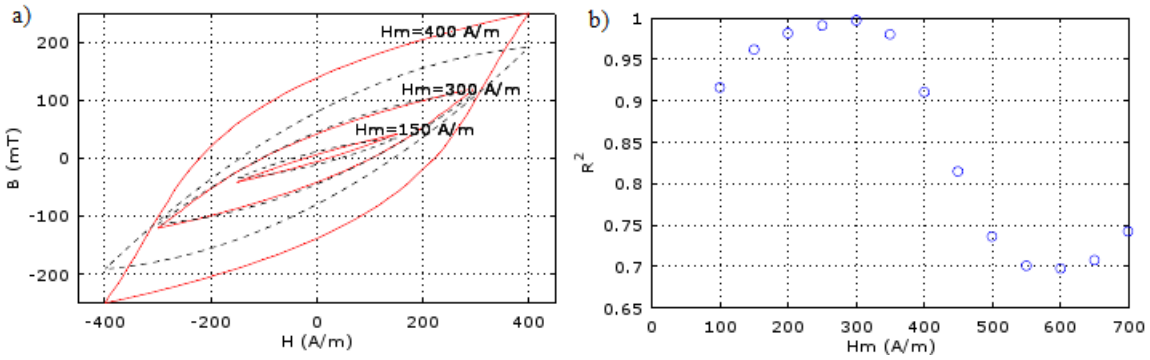


*Fig.1. a) Selected hysteresis loops for 13CrMo4-5 steel: red line – measurement data, black line – model*
*b) Dependence of coreleation coefficient $R^2$ between experimental data and model on the value of magnetizing filed amplitude*

For low magnetizing fields, results of modeling and measurement are consistent, which is confirmed by high determination coefficient $R^2$ between measurement and modeling results presented in Fig. 1b. For higher fields, over 400 A/m, model is no longer consistent with measurement data, because for such fields dependence between magnetic flux density and magnetizing field starts to lose its initial parabolic character.

## IV. CONCLUSION

During performed investigation possibility of application of Rayleigh hysteresis model was tested for several different ferromagnetic materials, one being 13CrMo4-5 constructional steel. Obtained results indicate that model is correct for initial range of magnetizing field of values lower than saturation coercive field $H_c$ for the material. In the case of investigated steel the limit of magnetizing field, where the model is correct (determination coefficient $R^2$ between measurement and modeling results is higher than 0.9), is 410 A/m, which is about 0.7 value of the saturation coercive field $H_c$ = 670 A/m for the material. For higher fields, the nature of dependence between magnetic flux density and magnetizing field differs too much from its initial parabolic character to be still described with Rayleigh model.

It should be indicated that Rayleigh model is simple enough to be utilized in technical applications, especially for modeling parameters of ferromagnetic cores of inductive components in electronic devices, which are usually working with relatively low magnetizing fields.

## REFERENCES


[1] Liorzou, F., Phelps B., Atherton D.L., Macroscopic Models of Magnetization, *IEEE Transactions on Magnetics*, vol. 36, no. 2, 2000, 418-428

[2] Jiles D.C., Introduction to Magnetism and Magnetic Materials, *CHAPMAN&HALL/CRC*, London, 1998

[3] Lord Rayleigh, On the behavior of iron and steel under the operation of feeble magnetic forces, *Philosophical Magazine and Journal of Science*, vol. 23, no. 142, 1887, 225-245

# MR CLUTCH WORK CONTROL IN HIL LOOP USING A DSP PROCESSOR

P. Kielan and Z. Pilch

Faculty of Electrical Engineering, Mechatronic Department, Silesian University of Technology,
44100 Gliwice, Poland, pawel.kielan@polsl.pl, zbigniew.pilch@polsl.pl

***Abstract.*** *The paper presents concept of the HiL loop building with DSP processor. This system is dedicated for MR clutch control work. Temperature determined changes electric, magnetic and rheological properties for MR clutch. These changes have an influence on the value of engaging torque clutch.*

## I. INTRODUCTION

Varying viscosity fluids (magnetorheological, electrorheological) belong to one of the groups of smart materials. This type of fluid in magnetic field works in three different mode (flow mode, compressing mode and clutch mode) [5]. In the present case, we will be interested in the flow-type clutch mode.

Magnetorheological fluid properties are determined by the shear stress τ [6] as functions of flux density B – curve in Fig.1.

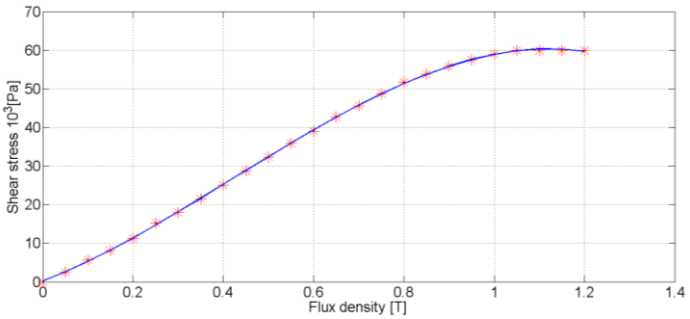


*Fig.1. The shear stress τ as a functions of flux density B curve for MRF-140CG fluid*

Other parameters of the liquid MRF-140CG [6]: density 3,54-3,74[g/cm$^3$], working temperature -40 do 130[$^O$C], flash-point >150[$^0$C].

According to the Bingham model, which describes the change in the tension of the magnetic fluid [1]:

$$\tau = \operatorname{sgn}\left(\frac{d\gamma}{dt}\right)\tau_0(B) + \mu\frac{d\gamma}{dt} \tag{1}$$

where: τ - shear stress in the liquid, $\tau_0(B)$ - limiting shear stress-dependent induction of B, μ - dynamic viscosity of a liquid (non-magnetic induction B), γ - shear deformation of the liquid.

The value of torque transmitted through the clutch depends on the shear stress τ. The full expression for the torque transmitted by the clutch, take into account the velocity shear in the liquid takes the form:

$$T = \frac{4\pi}{3}\cdot i_{tcz}\cdot\left(R_2^3 - R_1^3\right)\cdot\left(\tau_0(B) + \mu\frac{d\gamma}{dt}\right) \tag{2}$$

where: $i_{tcz}$ - number of clutch discs, $R_2$, $R_1$ - outer and the inner radius of clutch discs.

In use, the coupling heat is produced. It is the result of mechanical losses. Losses are incurred by slipping between the clutch discs in the liquid [2], [3]. They are also due to friction in the bearings [3]. These losses converted into heat increase the temperature of the liquid and all components of the coupling.

## II. CONCEPTION OF THE HIL LOOP

The temperature increase causes the:

- increase the resistance of the power supply circuit clutch coil (using a constant voltage source - decline in current),
- decline in the value of current to decrease the magnetic induction in the magnetic circuit coupling,
- decrease the viscosity of the MR fluid [4] which affect the component of stress (or torque) in a state of slip.

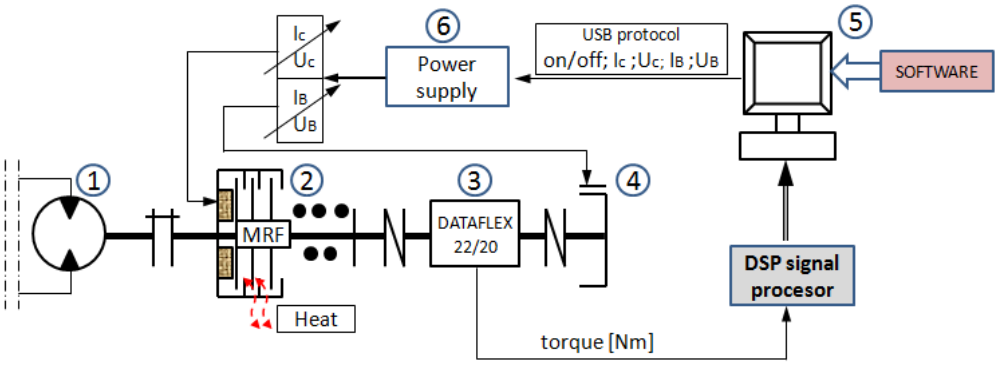


*Fig.2. The concept of the HiL loop building with DSP processor*

## III. SUMMARY

In the paper presented concept of the HiL LOOP with DSP processor. The system adjusts the parameters of the power coupling in order to maintain a constant torque coupling.

## REFERENCES


[1] Claracq J., Sarrazin J., Montfort J.p., Viscoelastic properties of magnetorheological fluids. *Rheol Acta* (2004) 43: 38–49 DOI 10.1007/s00397-003-0318-7.

[2] Hou You Fu Tian Zu Zhi Wang Nan Nan, The Steady-state and Transient Temperature Field of a Magnetorheological Fluid Transmission Device. International Conference on Computer, Mechatronics, *Control and Electronic Engineering (CMCE)*, pp. 149-153, 2010.

[3] Pilch Z., Analysis of Established Thermal Conditions for Magnetorheological Clutch for Different Loading Conditions., ISBN-13: Analysis and Simulation of Electrical and Computer Systems. *Springer International Publishing*. 2015/1/1. p. 197-213, ISBN-13: 978-3-319-11247-3.

[4] Potoczny M.: Ciśnienie krytyczne i opory ruchu w uszczelnieniach z cieczą magnetoreologiczną. *Rozprawa doktorska.* Akademia Górniczo-Hutnicza, Kraków 2012r.

[5] Szeląg W.: Electromagnetic converters with magnetorheological fluid (in polish), *Publishing House of Poznan University of Technology*, Poznań, 2010.

[6] Information materials LORD Corporation: *www.rheonetic.com*

# STRUCTURAL AND MAGNETIC STUDIES OF THE Fe-Co-Zr-Mo-W-B AMORPHOUS ALLOY

K. Kotynia[1], P. Pawlik[1], M. Hasiak[2], M. Pruba[1] and K. Pawlik[1]

[1]Institute of Physics, Częstochowa University of Technology, Czestochowa, Poland,
kkotynia@wip.pcz.pl, pawlik@wip.pcz.pl, mpruba@wip.pcz.pl, kpawlik@wip.pcz.pl
[2]Department of Mechanics and Materials Science, Wrocław University of Science and Technology, Wrocław, Poland,
mariusz.hasiak@pwr.edu.pl

***Abstract.*** *The paper presents characterization of microstructure by X-ray diffraction, Mössbauer spectroscopy and isothermal magnetic entropy changes in the bulk amorphous $Fe_{58}Co_{10}Zr_{10}Mo_5W_2B_{15}$ alloy in the as-quenched state. Ingot samples were obtained by arc-melting under the low pressure of Ar atmosphere. The magnetic measurements at various temperatures allowed to study the Curie temperature $T_C$, magnetic entropy changes $|\Delta S_M|$ and relative cooling power (RCP). XRD analysis and Mössbauer spectroscopy revealed fully amorphous structure of the ribbon samples. Those results indicate its good glass forming ability (GFA).*

## I. INTRODUCTION

Iron based metallic glasses have attracted great attention of researchers, due to their good magnetic and mechanical properties as well as possibility of utilizing of the magnetocaloric effect. There are three main factors alloying to estimate potential of magnetocaloric materials: the magnetic entropy change $|\Delta S_M|$, the adiabatic temperature change $|\Delta T_{ad}|$ and refrigerant capacity (RC). An ideal magnetic refrigerant has to possess large values of both $|\Delta S_M|$ and $|\Delta T_{ad}|$ as well as the and RCP around room temperature at low magnetic field. The magnetocaloric effect (MCE) is significant mostly at around the phase transition temperature. In most materials it is the Curie temperature ($T_C$). The search for new magnetocaloric material for commercial applications has concentrated mainly on tunable $T_C$ and reasonable MCE. A promising iron based alloy with good GFA is $Fe_{58}Co_{10}Zr_{10}Mo_5W_2B_{15}$. By changing the Fe and Co ratio it is possible to modify $T_C$ for this type of materials to get its value around room temperature [1].

The Fe-Co-Zr-Mo-W-B sample used in this work was obtained by arc-melting of the mixture of high purity (99,98 %) constituent elements Fe, Co, Zr, Mo, W with the addition of pre-alloyed Fe-B. Ingot was re-molten at least seven times to guarantee the homogeneity of the alloy.

The ribbon was prepared by melt-spinning technique at surface velocity of the copper roll of 40 m/s. All the arc-meting and melt-spinning were performed under Ar atmosphere to avoid oxygenation.

The phase structure was investigated by X-ray diffractometry (XRD) using Bruker D8 Advance with CuKα radiation and the LynxEye semiconductor detector. The data were recorded using the step-scanning method in 2Θ range from 30 to 120 degrees. Mössbauer spectrum was measured at room temperature using Polon Mössbauer spectrometer with a $^{57}$Co(Rh) source of the activity of 50 mCi in transmission geometry. It was subsequently analyzed using WiNormos for Ingot software.

Magnetic measurements M(H) in the temperature range 225-325 K were performed and the magnetocaloric effect (MCE) was estinated by calculation of the field dependences of magnetic entropy change $|-\Delta S_M|$. Its reaches maximum value of 0.495 $Jkg^{-1}K^{-1}$ for the maximum change of external magnetic field of 2 T. The magnetic entropy change $|-\Delta S_M|$ was calculated using the formula:

$$\Delta S_M = \int_0^H \left(\frac{\partial M}{\partial T}\right) dH.$$

The investigation of the $|-\Delta S_M|$ is one of the methods which allows to obtain information about the magnetic phase transition in these materials.

## REFERENCES

[1] Pawlik P., Rola składu chemicznego i procesu wytwarzania w kształtowaniu właściwości magnetycznych masywnych amorficznych i nanokrystalicznych stopów żelaza, *Prace naukowe Wydziału Inżynierii Procesowej, Materiałowej i Fizyki Stosowanej, Politechnika Częstochowska*, Monografia 12, Częstochowa 2011

# UNCERTAINTY OF THE MAGNETIC FLUX LINKAGES MEASUREMENTS PERFORMED WITH THE USE OF THE MODIFIED CURRENT DECAY TEST

Z. Kowalik

Department of Mechatronics, Faculty of Electrical Engineering, Silesian University of Technology, Akademicka 10A, 44-100 Gliwice, zygmunt.kowalik@polsl.pl

***Abstract.*** *The paper presents methodology of estimation of the uncertainties of the magnetic flux linkage measurements, when the flux linkages waves, rather than a single values, are measured and computed. The computed uncertainties are then used to estimate the quality of the approximation of current-flux characteristic in the mathematical model of an electrical machine when the approximation is based on measurements results.*

## I. INTRODUCTION

Mathematical models of electrical machines require the determination of the relation between currents in the windings of the machine and flux linkages in these windings. In the models that take into account the nonlinearities of the magnetization curve, the most convenient way to do it is to approximate the current-flux characteristic, i.e. the vector function, that for a given vector of phase currents assigns a corresponding vector of flux linkages. Such an approach is used in the Hamiltonian model of an electrical actuator [1].

In the Hamiltonian model the current-flux characteristic can be approximated using simplicial approximation [2]. It requires corresponding sets of points in the spaces of flux and currents and the division (triangulation) of both spaces based on those points. The sets of points can be obtained for a fixed rotor angular position using a measuring procedure that is a modification of the current decay test.

In the paper an estimation of uncertainties of the approximation of the current-flux characteristic, based on sets obtained with the use of measurement results, is presented. First, the measuring method is briefly described, followed by the estimation of the uncertainties of physical quantities that are computed using its results. The results of the measurements and computations, done for the prototype Synchronous Reluctance Machine (SynRM) are presented. In the extended paper the impact of these uncertainties on the quality of the approximation of the flux-current characteristic and its influence on the mathematical model of the electrical machine will be discussed.

## II. METHOD OF MEASUREMENT

The measurements of the flux linkages in the windings of the machine are performed with the fixed angular position of the rotor. For a three-phase machine with phase windings in a wye configuration, the electrical state of the machine is given by two phase currents values and two corresponding generalized flux linkage values. The measuring procedure for obtaining these values consists of setting the specified currents values in the machine windings, followed by short-circuit of them and registration of the decaying current waves. Corresponding flux linkage waves are obtained by integration of the current waves multiplied by phase resistances. The result of a single measurement, done with the use of this method, is a pair of corresponding trajectories, one in the space of fluxes and one in the space of currents. From this pair of trajectories several points can be chosen to be included into the sets required by the simplicial approximation. The selection of points is based on the magnetic field coenergy calculations. The method of measurement and selection of points building the required sets of points is described in literature [3]. The laboratory stand that was used during the measurements is described in [4].

## III. UNCERTAINTIES OF CURRENT AND FLUX LINKAGES MEASUREMENTS

In the calculation of uncertainties of current measurements standard procedures [5] uncertainties were used to obtain the uncertainty of every sample of the measured wave. That way the uncertainty designates the area of the space of currents, where the measured trajectory should be located. This uncertainty affects the uncertainty of the calculated flux linkages and designates analogous area in the space of fluxes. The uncertainty of flux linkages are calculated by an integration of the current uncertainties and thus are bigger for big values of fluxes due to bigger integration interval. During the calculation great emphasis should also be put on designating the time, after which the current and flux linkages waves are assumed to be 0. In the paper this time was the time after which, for the particular pair of trajectories, the calculated coenergy value diminished to 0.25% of its initial value.

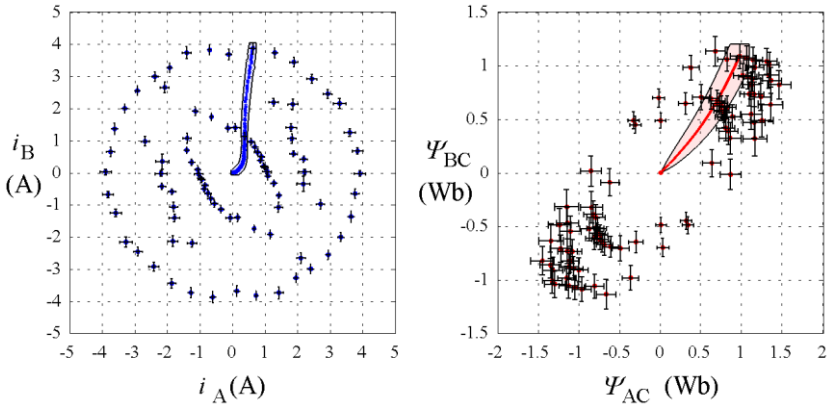


*Fig.1. Points chosen to approximate the current-flux characteristic and an exemplary pair of corresponding trajectories*

From the measured trajectories several points were chosen to construct sets for the approximation of the current-flux characteristic. The chosen points with error bars are presented in the figure 1, along an exemplary pair of corresponding trajectories in both spaces and the areas of these spaces determined by the calculated uncertainties. The uncertainties of the flux and current values in the chosen points are determined similarly. Final average relative uncertainties of flux linkages values is approximately equal to 15%. The influence of these uncertainties on the flux-current characteristic approximation quality will be discussed in the extended paper.

## REFERENCES


[1] Burlikowski W., Hamiltonian model of electromechanical actuator in natural reference frame, Part 1&2, *Archives of Electrical Engineering*, vol. 60(3), 2011, pp. 317-348

[2] Agoston M. K., Computer Graphics and Geometric Modeling - Mathematics, *Springer*, 2005

[3] Kowalik Z., Measurement Results Based Approximation of the Nonlinear Flux-Current Characteristic of an Electromechanical Actuator, *Measurement Automation Monitoring*, vol. 02/2016, 2016, pp. 49-54

[4] Burlikowski W., Kohlbrenner L., The Measurement Test for the Identification of Current – Flux Linkage Characteristics in Synchronous Reluctance Motors, *Measurement Automation Monitoring*, vol. 01/2016, 2016, pp. 33-36

[5] Expression of the Uncertainty of Measurement in Calibration, *Główny Urząd Miar*, Warszawa, 2001

# EQUIVALENT-CIRCUIT APPROACH TO MR MULTI-DISC CLUTCH DESIGNING AGAINST THE BACKGROUND OF MAGNETIC FIELD CALCULATION

P. Kowol and K. Kluszczyński

Silesian University of Technology, Faculty of Electrical Engineering, Department of Mechatronics,
ul. Akademicka 10A, 44100 Gliwice, Poland,
pawel.kowol@polsl.pl, krzysztof.kluszczynski@polsl.pl

***Abstract.*** *In the paper clutches with magnetorheological fluid (MR clutches) are presented and the design methodology of MR clutch is depicted. Two methods of magnetic calculations (equivalent-circuit and FEM) which are a leading part of design process are described and compared.*

## I. INTRODUCTION

Magnetorheological fluids (MR fluids) belong to the group of Smart Materials [3]. The feature of the MR fluids which can be controlled with the help of external magnetic field (generated by excitation winding or permanent magnet) is viscosity: the stronger magnetic field, the greater viscosity. Because of this property MR fluids have found different applications in dampers and brakes [1]. Very promising application seems to be MR clutches in which process of engaging two mechanical parts is brought to applying electrical or magnetic signal. As regards the structure of MR clutches, they can be divided in to two basic types: cylindrical structure or disc structure [1,2]. Disc structure can include one disc (number of discs $N$=1) or more discs (multi-disc construction with $N$>1) [2,5]. The authors focus their attention on multi-disc constructional solution. The example of 3-disc MR clutch is presented in Fig.1a (because of symmetry there is sufficient to consider only half of cross-section).

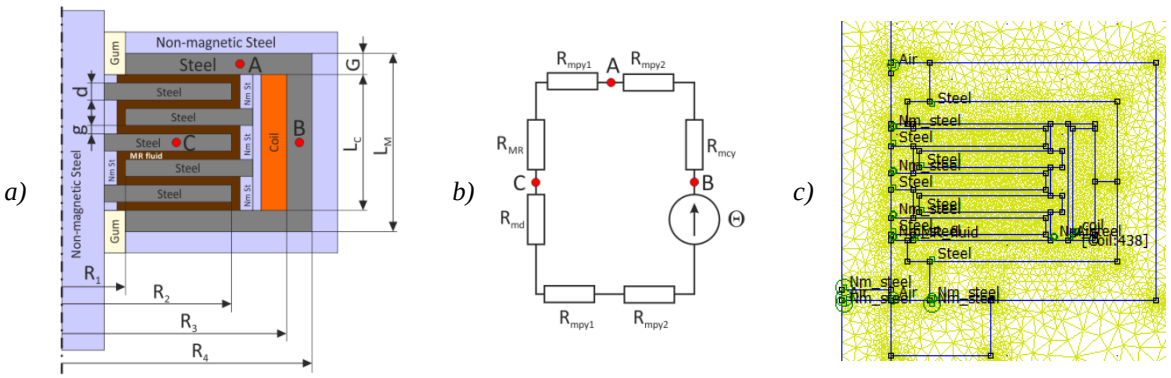


*Fig.1. For the MR multi-disc clutch: a) axisymetric cross-section with characteristic points of magnetic circuit (A, B, C) and geometric parameters, b) equivalent magnetic circuit with characteristic points of magnetic circuit, c) magnetic field model made in FEM software*

## II. MAGNETIC CALCULATIONS IN MR CLUTCH DESIGN PROCESS

The design methodology of the MR clutch have to take into account calculations of different nature: magnetic calculations, mechanical calculations and fluid-dynamic calculations. Of course, magnetic calculations play leading role because clutching torque $T_C$ (developed by the MR clutch) depends mainly on magnetic field distribution.

The shape of MR clutch is characterized by the following constructional data: $R_1$, $R_2$, $R_3$, $R_4$, $L_M$, $L_C$, G, $d$, g marked in Fig.1a. The number of discs $N$ and thickness of single disc $d$ are

concerned as constructional variables. Magnetic calculations are aimed at finding optimal number of discs *N* and their thickness *d*.

## III. CALULATIONS OF MAGNETIC FIELD AND CLUTCHING TORQUE

Magnetic calculations can be performed according to two methods: equivalent-circuit approach (E-C method) [2,5] and field approach (FEM method) [1,2]. As regards E-C method, calculations (based on algebraic equations) are carried out under the following assumptions: B-H curve is linear and cross-sectional distribution of magnetic field along the selected parts of a core is homogenous. Advantages of such an approach are simple algorithm and direct dependencies between constructional variables and geometrical/material data. As far as FEM field calculation are concerned, nonlinearity of magnetic circuit is taken into account and knowledge about real magnetic field distribution allows to find location of the most saturated points of magnetic core (as a result, the designer can avoid saturation in each part of magnetic circuit).

The clutching torque $T_C$ can be determined according to the equation $T_C = \int_S r\tau_0(B)dS$ on the basis of magnetic field calculations (value of magnetic flux density *B* in point C denoted in Fig.1a), yield stress of the MR fluid $\tau_0$ (depending on *B*) [4] and geometrical clutch data (disc radius *r* and facing area of the disc *S*).

The results of calculations on magnetic field in the MR clutch (magnetic flux density *B* in point C) and clutching torque $T_C$ for the selected number of discs *N* and different thickness of the single disc *d* are put together in Tab.1. Table 1 enables to compare results of calculations performed according to the E-C method (B-H curve is linear) and FEM method (B-H curve is nonlinear). Calculations according to E-C method and FEM method lead to the results differing no more than 27%. It means that the introductory values of *N* and *d* can be determined on the basis of the simplified E-C algorithm and then (after choosing the optimal variant) additional calculations employing FEM method have to be carried out again in order to determine exact value of clutching torque $T_C$. Good compatibility of the both considered method is the reason that the authors decided to elaborate the design algorithm basing on E-C approach which in their opinion will be very useful in quick finding range of optimal solutions.

*Table 1. Results of calculations of magnetic field B and clutching torque $T_C$ for multi-disc MR clutch*

| | | | Equivalent circuit | | FEM | |
|---|---|---|---|---|---|---|
| *N* | *d* | *Θ* | *B* | $T_C$ | *B* | $T_C$ |
| | mm | A | T | N·m | T | N·m |
| 2 | 4 | 226 | 0.354 | 4.47 | 0.324 | 3.41 |
| 3 | 3 | 307 | 0.342 | 6.25 | 0.332 | 5.23 |
| 4 | 2 | 323 | 0.284 | 5.57 | 0.306 | 5.85 |
| 5 | 2 | 419 | 0.3 | 7.85 | 0.321 | 8.04 |

## REFERENCES


[1] Jędryczka C., Sujka P., Szeląg W., The influence of magnetic hysteresis on magnetorheological fluid clutch operation, *COMPEL*, Vol. 28, No. 3, 2009, pp. 711-721

[2] Karakoc K., Park E.J., Suleman A., Design considerations for an automotive magnetorheological brake, *Mechatronics*, Vol. 18, No. 8, 2008, pp. 434–447

[3] Kim K.J., Lee C. W., Koo J.H., Design and modeling of semi-active squeeze film dampers using magneto-rheological fluids, *Smart Materials and Structures*, Vol. 17, No. 3, 2008, 12 pp.

[4] Lord Corporation, Product Bulletins: www.lord.com

[5] Shafer A.S., Kermani M.R., On the feasibility and suitability of MR fluid clutches in human-friendly manipulators, *IEEE/ASME Transactions on Mechatronics*, Vol. 16 , No. 6, 2011, pp. 1073–1082

# PREPARATION AND MAGNETIC CHARACTERISTICS OF $Co_{1-\delta}Zn_{\delta}Fe_2O_4$ FERRITE NANOPOWDERS

M. Kubisztal, I. Herok, M. Karolus, K. Prusik and G. Haneczok

Institute of Materials Science, University of Silesia, ul. 75 Pułku Piechoty 1A, 41-500 Chorzów,
Marian.Kubisztal@us.edu.pl

## I. INTRODUCTION

Magnetic nanoparticles are of significant interest in fundamental research and find many industrial applications. One can mention about their high catalytic activity and applications in drug delivery systems or as contrasts in MRI technology. Especially interesting are magnetic oxide nanoparticles (MNp) with mixed spinel type structure and chemical composition $(M_{1-\delta}Fe_{1-\delta})^{A}[M_{1-\delta}\ Fe_{1-\delta}]^{B}O_4$ where M denotes Co, Zn, Mn, Cu etc. and the brackets A and B stand for tetrahedral and octahedral sites, respectively. In that case unique properties are consequence of exceptional combination of crystalline structure and nanosized dimensions of a singular particle [1-5]. Nevertheless, functional characteristics of magnetic oxide nanoparticles can be controlled by technological parameters applied in process of production. In our work we have synthesized $Co_{1-\delta}Zn_{\delta}Fe_2O_4$ ferrite nanopowder ($0 \leq \delta \leq 1$) by applying standard chemical technique based on co-precipitation of nanoparticles in water solutions at given temperature $T_R$, flow rate $v_{FR}$ and nanopowder concentration $c = V_p/(V_R + V_p)\cdot 100$ % (where $V_p$ and $V_R$ denote the volume of co-precipitated nanopowder and water, respectively), we have used: $T_R$ = 50 $^0$C, 70 $^0$C and 90 $^0$C, $v_{FR}$ = 1 cm$^3$/min. and 120 cm$^3$/min. and $c$ = 0.1 % and 0.3 %. The applied technique allows obtaining ferrite particles with mean particle size (dependently on applied technological parameters) in nanometer scale. Note that controlling of nanoparticle size is important problem in nanotechnology as in nanoscale the properties of the final material strongly depend on size. Magnetic measurements were performed by applying VSM Quantum Design apparatus operating in temperature range 2 – 400 K and at magnetic field up to 7 T.

## II. RESULTS

Fig. 1a presents the relation of magnetization $M$ *vs.* magnetic field $\mu_0 H$ obtained for $Co_{1-\delta}Zn_{\delta}Fe_2O_4$ ferrite nanopowders. It can be seen that the registered hysteresis characterize high symmetry with coercive field ranging from 0.05 T to 0.9 T dependently of Zn content. However, even in high magnetic field (up to 7 T) saturation in magnetization is not reached. Fig. 1b presents the relation of $M_{7T}$ *vs.* Zn content $\delta$ obtained for ferrite nanopowders synthesized with $v_{FR}$= 120 cm$^3$/min., $c$ = 0.3 % and at different reaction temperature $T_R$. In that case, for $T_R$ = 70 $^0$C and 90 $^0$C we observe a broad peak with maximum located at $\delta$ = 0.2 and with value $M_{7T}$ c.a. 80 emu/g. However, for $T_R$ = 50 $^0$C the maximum is shifted to higher values of $\delta$ (i.e. 0.6) and reaches significantly lower $M_{7T}$ i.e. 60 emu/g. Such result suggests that magnetic characteristics of ferrite $Co_{1-\delta}Zn_{\delta}Fe_2O_4$ nanopowder may be tailored by proper placing of $Co^{2+}$, $Zn^{2+}$ and $Fe^{3+}$ ions in A and B sites of the spinel structure, where according to the Néel theory of materials with two magnetic sublattices the resultant magnetic moment $\mu_R$ of the sample is equal to $\mu_B$-$\mu_A$. Fig 1c shows the squareness of the loop defined as $S = M_r/M_{7T}$ ($M_r$ - magnetic remanence) plotted versus Zn content $\delta$. Increase in $\delta$ results in strong decrease in $S$, which means that addition of nonmagnetic ions of zinc influences the magnetization processes related with applied external magnetic field $\mu_0 H$. Note that the observed change in $S$ reaches 80 %. Fig. 1d presents the relations of Néel temperature $T_N$ *vs.* Zn content $\delta$ obtained for $Co_{1-\delta}Zn_{\delta}Fe_2O_4$ nanopowder synthesized at different $T_R$. Here, increase in $\delta$ results in strong decrease in $T_N$ and the observed change is from 780 K ($\delta$ = 0) to 465

K ($\delta$ = 1). In the case of $Co_{1-\delta}Zn_\delta Fe_2O_4$ ferrite nanopowder with $\delta > 0.6$ measured $T_N$ almost does not depend on applied reaction temperature $T_R$.

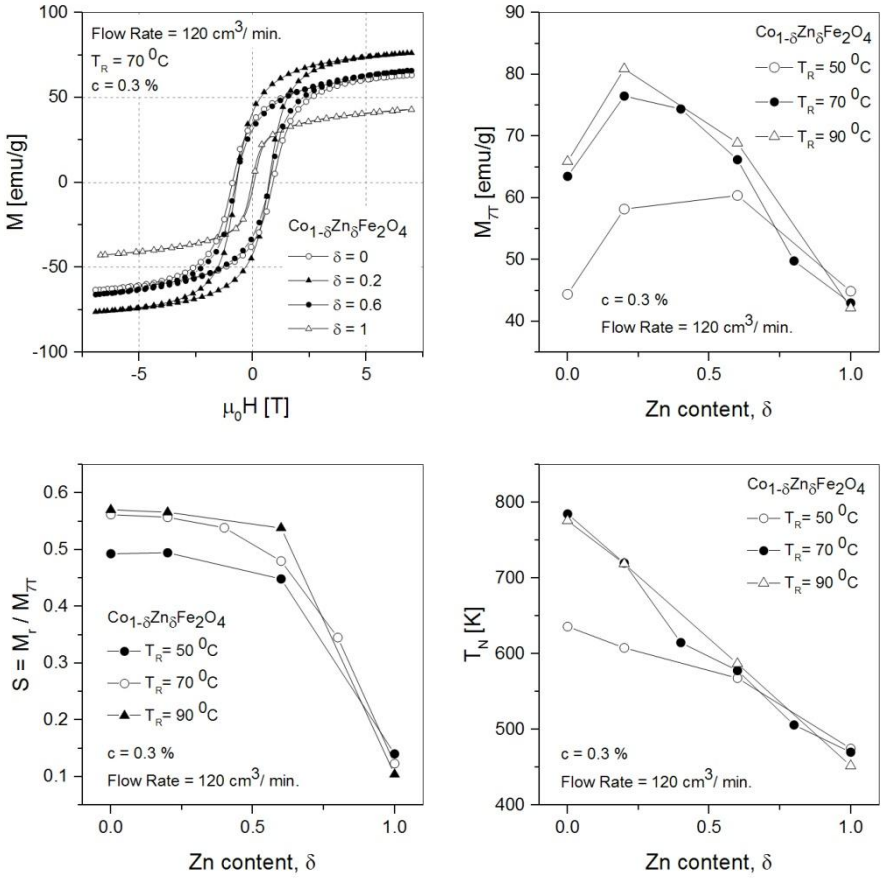


*Fig.1. Magnetic characteristics of $Co_{1-\delta}Zn_\delta Fe_2O_4$ nanopowders a) magnetization M vs. magnetic field $\mu_0 H$ (5 K), b) magnetization $M_{7T}$ determined in magnetic field $\mu_0 H$ = 7 T (5 K) vs. Zn content $\delta$, c) squareness ratio $S = M_r/M_{7T}$ (5 K) vs. Zn content $\delta$ and d) Néel temperature $T_N$ vs. Zn content $\delta$; $T_R$ - temperature of chemical reaction, c - nanopowder concentration in reactant solution.*

## REFERENCES


[1] Sozeri H., Durmus Z., Baykal A., Structural and magnetic properties of triethylene glycol stabilized $Zn_xCo_{1-x}Fe_2O_4$ nanoparticles, *Materials Research Bulletin*, 47, 2012, 2442-2448

[2] Raut A.V., Barkule R.S., Shengule D.R., Jadhav K.M., Synthesis, structural investigation and magnetic properties of $Zn^{2+}$ substituted cobalt ferrite nanoparticles prepared by the sol–gel auto-combustion technique, *Journal of Magnetism and Magnetic Materials*, 358-359, 2014, 87-92

[3] Raeisi Shahraki R., Ebrahimi M., Seyyed Ebrahimi S.A., Masoudpanah S.M., Structural characterization and magnetic properties of superparamagnetic zinc ferrite nanoparticles synthesized by the coprecipitation method, *Journal of Magnetism and Magnetic Materials*, 324, 2012, 3762-3765

[4] Deraz N.M., Alarifi A., Structural, morphological and magnetic properties of nano-crystalline zinc substituted cobalt ferrite system, *Journal of Analytical and Applied Pyrolysis*, 94, 2012, 41-47

[5] Upadhyay R.V., Parmar H., Acharya P., Banerjee A., Progressive freezing of finite cluster in locally canted spin $Co_{0.3}Zn_{0.7}Fe_2O_4$ spinel ferrite system, *Solid State Communications*, 163, 2013, 50-54

# INVESTIGATION OF THERMO-MECHANICAL BEHAVIOR IN SHAPE MEMORY ALLOY ACTUATOR

M. Kurzawa and D. Stachowiak

Poznan University of Technology, Piotrowo 3a, 60-965 Poznań, Poland,
milena.kurzawa@put.poznan.pl, dorota.stachowiak@put.poznan.pl

***Abstract.*** *In the paper, the thermo-mechanical behavior of shape memory alloy wire actuator has been studied. The cycle of heating and cooling has been performed under a constant load. The selected results and conclusions have been presented. The proposal of a concept of the linear actuator using the shape memory alloy wire has been given.*

## I. INTRODUCTION

The shape memory alloys (SMAs) are functional materials, which can be applied in many applications like the linear actuators due to their large strain recovery, high stiffness and strength [1,2]. The SMA materials have the ability to change of their shape in depending on the transformation temperatures. In this type of materials two crystalline structures can be distinguished (a) mertensite (M) which is the thermodynamically stable at lower temperature and (b) austenite (A), which is the parent phase stable for higher temperature. The SMA materials in the martensite phase have the crystal structure with simply symmetry, such as tetragonal, rhombohedral, orthorhombic, monoclinic or triclinic depending on the composition of the alloy, whereas in the austenite phase has a higher symmetry usually based on a cubic lattice [1,2]. SMAs are characterized by the four temperatures, i.e. the start and finish transformation temperatures: $M_s$, $M_f$ (martensite start and finish) and $A_s$, $A_f$ (austenite start and finish).

The paper deals with the thermo-mechanical behavior of a linear actuator, in which as active element has been applied the SMA wire from the Nitinol (Ni-Ti). The goals of the paper are the discussion of the thermo-mechanical properties of Nitinol material and the proposal of a concept of the linear actuator using the Nitinol wire. The SMA wire is the most commonly applied form for these actuators because of its ease of use and convenient electrical activation.

## II. THE ELABORATED EXPERIMENTAL SETUP

The application of SMA wire as active element of actuator is only possible if the characterizations under various operating conditions are known. Therefore, the Authors elaborated the special experimental setup for the investigation of the SMA wire properties. The view and schematic block diagram of the used experimental setup have been shown in Figure 1. The changes of wire length have been measured by the Potentiometric Linear Transducer (PLT) displacement sensor, which has been placed series to SMA wire.

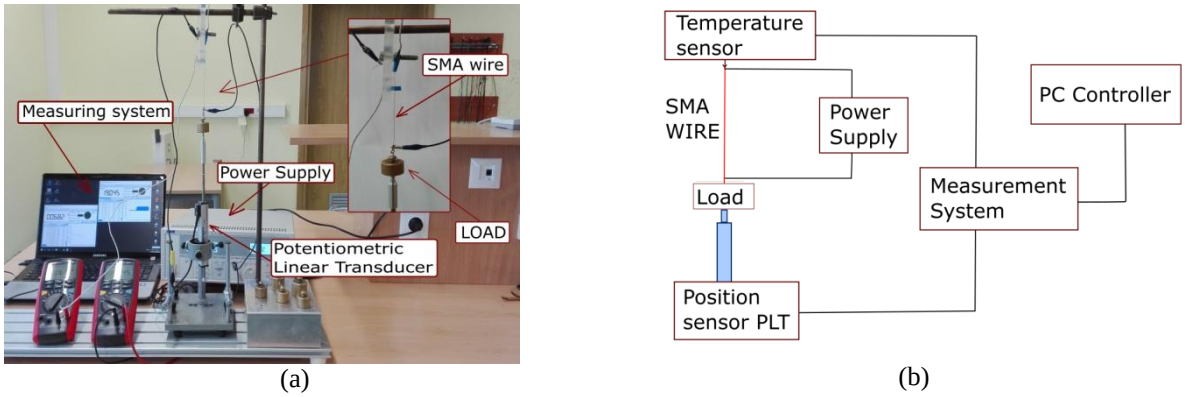


(a) (b)

*Fig.1. The experimental setup: a) view, b) block diagram*

## III. RESULTS AND CONCLUSIONS

In order to obtain the thermo-mechanical properties and parameters of SMA wire, the experimental setup has been carried out. The SMA wire of type 'Flexinol LT' has been considered, for which the diameter was 0.25 mm and length was 135 mm.

The power supply QPX600DP (80 V, 50 A) was chosen to the linear SMA actuator. It allows for stabilization of the value of current (*I*) as well as voltage (*U*). The Joule-heating of the wire and its subsequent contraction are produced by current that flows through the wire. Both values of *U* and *I* are measurable in real-time therefore, electrical resistance $R = U/I$ can also be computed in real-time. Three thermocouples (*K* type) have been used to measurement the wire temperature.

Figure 2 shows the obtained displacement – temperature hysteresis for the considered material under constant load. The temperature and displacement of the SMA wire registered during the heating and cooling cycle have been given in Figure 3. The displacement curve shows that wire is shortening by 2.35 mm (1.75 %) from initial length of 135 mm. The SMA wire elongation and shortening are induced both mechanically and thermally.

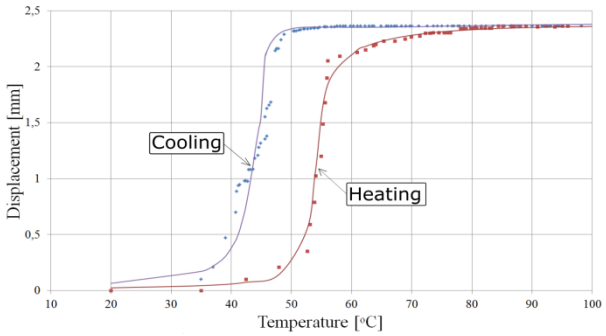


*Fig.2. Displacement - temperature hysteresis at applied load (Q = 0.1 kg)*

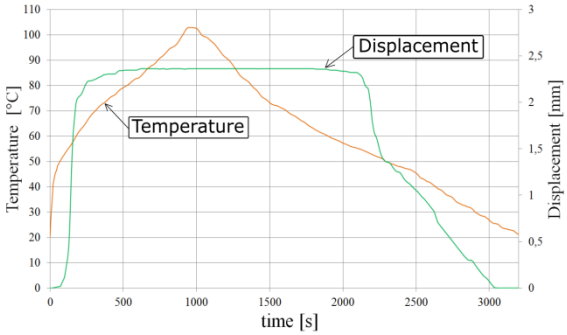


*Fig.3. The temperature and displacement of the SMA wire registered during the heating and cooling cycle*

Based on the obtained results and the thermo-mechanical properties of the shape memory alloy the project of thermal circuit switch of SMA wire actuator has been elaborated and built (Fig. 4). The special control system of the current value as a function of the resistance and temperature of SMA wire has been designed and elaborated.

The more details about the obtained characteristics and results for the considered SMA material will be presented in the extended version of the paper.

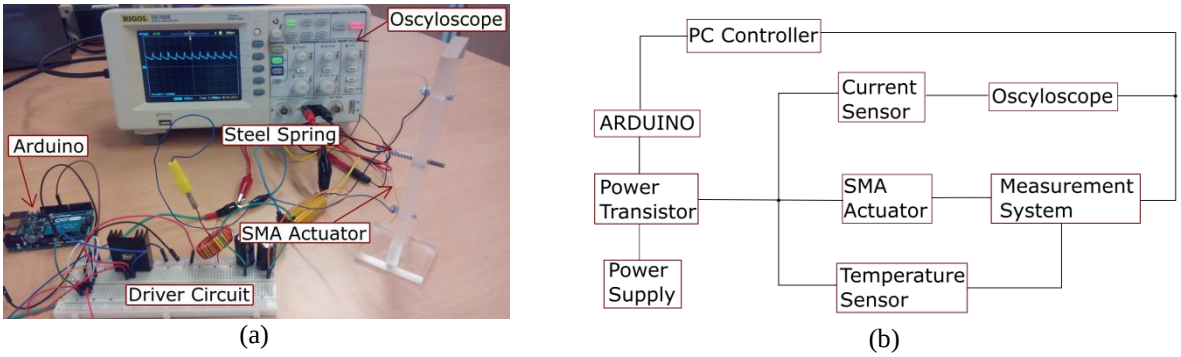


(a) (b)

*Fig.4. Example of the SMA wire use: a) view of the setup, b) driver diagram*

## REFERENCES


[1] Lagoudas D.C., Shape Memory Alloys: Modeling and Engineering Applications. *Springer*, 2008

[2] Barbarino S., Saavedra Flores E.I., Ajaj R.M., Dayyani I. and Friswell M.I., A review on shape memory alloys with applications to morphing aircraft. *Smart Materials and Structures* 23, 063001 (19pp), 2014

# MAGNETIC PROPERTIES OF Co-Fe-Si-B MICRO-WIRES

P. Kwapuliński[1], J. Gieraltowski[2], C. Dolabdjian[3], Z. Stokłosa[1] and G. Haneczok[1]

[1] University of Silesia, Institute of Materials Science, Chorzów, 75 PułkuPiechoty 1A, piotr.kwapulinski@us.edu.pl
[2] LDO/IUEM UMR CNRS 6538, UEB, Université de Bretagne Occidentale, Place Copernic, Technopôle Brest-Iroise, 29280 Plouzané, France.
[3] Normandie Univ., France; UCBN, GREYC, CNRS, UMR 6072, F-14032 Caen, France

## I. INTRODUCTION

Cobalt based amorphous micro-wires belong to new magnetic materialsshowing agiant magneto-impedance effect. One of the most promising applications of these materials are magnetic sensors of very high sensitivity [1-6].In the present paper magnetic properties i.e. magnetization curves, observation of domain structure (magneto-optic Kerr effect), contact and non-contactmagneto-impedanceeffects for the $Co_{68.15}Fe_{4.35}Si_{12.55}B_{15}$micro-wire (diameter of about 100 μm) have been examined. The relative changes of material impedance $Z$(measured at alternating field$H_{ac}$) due to application of external static magnetic field $H_{dc}$are defined as [4]:

$$\Delta Z/Z = [|Z(H_{dc})| - |Z(H_{dc\,max})|]/|Z(H_{dc\,max})| \cdot 100\% \quad (1)$$

where$|Z(H_{dc})|$is the impedance determined at field $H_{dc}$ and$|Z(H_{dc\,max})|$is the impedance determined at the maximum of the applied field$H_{dc}$. The sensitivity of magneto-impedance effect to the changes of magnetic field $H_{dc}$ − $\xi$is defined as [5]:

$$\xi = 2\,(\Delta Z/Z)_{max}/\Delta H_{dc} \quad (2)$$

where $\Delta H_{dc}$is the half width of the maximum $\Delta Z/Z$ plotted vs. $H_{dc}$.

## II. RESULTS AND DISCUSSION

Magneto-impedance measurements were carried out by applying precision RLC meter (Agilent E4980A). Fig. 1 presents $\Delta Z/Z$determinedby applying contact ($(\Delta Z/Z)_C$ ) and non-contact ($(\Delta Z/Z)_{NC}$ ) methodplotted versus frequency$f$ (1 kHz ≤$f$≤ 2 MHz) of magnetic field $H_{ac}$ and the applied field $H_{dc}$.Fig. 2 shows the ratio $(\Delta Z/Z)_{NC}/(\Delta Z/Z)_C$of magneto-impedance effect. According to these figures the$(\Delta Z/Z)_{NC}$effect in the region $H_{dc}$≤200 A/m is at least 7 times higher than $(\Delta Z/Z)_C$. Magneto-impedance sensitivity $\xi$ versus frequency for contact and non-contact measurements is presented in Fig. 3. Note, in both cases $\xi$shows a maximum located at about 200 kHz and 300 kHz for non-contact and contact geometry, respectively. At this maximum $\xi_{NC}$is about 50 times higher than $\xi_C$. These facts suggest that application of non-contact method of measurements allows improving sensitivity of magneto-impedance sensor especially at relatively low magnetic fields.

In conclusion, one can state that the examined $Co_{68.15}Fe_{4.35}Si_{12.55}B_{15}$ micro-wire with diameter of about 100 μm can be used as high sensitive magneto-impedance sensor in non-contact geometry especially at low magnetic fields.

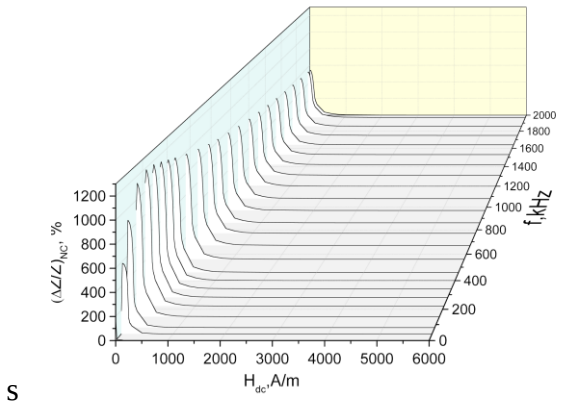


S

*Fig.1 Magneto-impedance effect $\Delta Z/Z$ vs. frequency f and the applied magnetic field $H_{dc}$; left - contact measurements $(\Delta Z/Z)_C$ and right - non-contact measurements $(\Delta Z/Z)_{NC}$.*

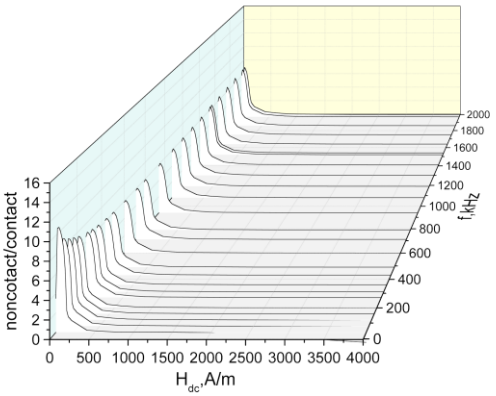


*Fig.2 Ratio$(\Delta Z/Z)_{NC}/(\Delta Z/Z)_C$ of non-contact/contactmagneto-impedance effect*

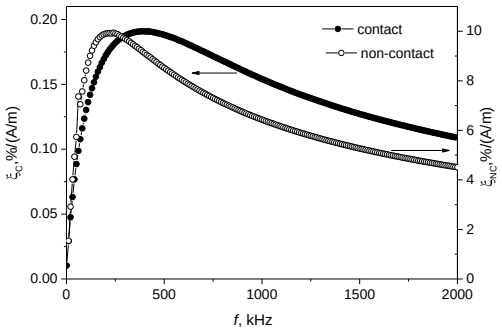


*Fig.3 Magneto-impedance sensitivity $\xi$versus frequency for contact and non-contact measurements*

## REFERENCES


[1] Beato-López J.J., de la Cruz Blas C.A., Mitra A., Gómez-Polo C., Electrical model of giant magnetoimpedance sensors based on continued fractions, *Sensors and Actuators A* 242 (2016) 73–78

[2] Valenzuela R., Fessant A., Gieraltowski J., Tannous C., Effect of the metal-to-wire ratio on the high-frequency magnetoimpedance of glass-coated CoFeBSi amorphous microwires , *Sensors and Actuators A* 142 (2008) 533–537

[3] Dufay B., Saez S., Dolabdjian C., Yelon A., Menard D., Physical properties and giant magnetoimpedance sensitivity of rapidly solidified magnetic microwires, *Journal of Magnetism and Magnetic M*aterials 324 (2012) 2091–2099

[4] Zhukov A., Ipatov M., Zhukova V. in: Handbook of Magnetic Materials, Volume 24, Chapter 2, *Elsevier* 2015

[5] Amirabadizadeh A., Lotfollahi Z., Zelati A., Giant magnetoimpedanceeffectofCo68.15 Fe4.35 Si12.5 B15 amorphous wire in the presence of magnetite ferrofluid, *Journal of Magnetism and Magnetic Materials* 415 (2016) 102–105

# EFFECTS OF DOPING ON THE STRUCTURAL DISTORTION OF $La_{0.7}Dy_{0.3}Mn_{1-x}Zn_xO_3$

J.F. López[1], M. Rios[1,2] and G.A. Mendoza[1]

[1] Magnetic materials and nanostructures Group, Faculty of science, National University of Colombia
[2] Basic Science Department, ECCI University, Bogotá, Colombia

***Abstract.*** *$MnO_6$ octahedra are the basic units in perovskite manganese oxides. This paper presents results on structural distortions by Zn substitution in $La_{0.7}Dy_{0.3}Mn_{1-x}Zn_xO_3$ ($0 < x < 0.4$). The polycrystalline samples were produced by the solid state reaction method. The octahedral distortion was analyzed by the Rietveld refinement method to fit the XRD data. As the cell distortion parameters were obtained, the Mn-O bond length on the Mn-O plane and along the c –axis. Also the Mn-O-Mn angle was obtained along the c-axis and on the plane. In these samples three simultaneous phases were observed: two orthorhombic Pbnm and Pnma phases as well as a trigonal phase R-3C. The presence of each phase into the samples depend on the doping.*

## I. INTRODUCTION

Structural distortions such as octahedral rotation, tilting or deformation have been attributed to the strong hybridization between 3d orbitals and the $O_{2p}$ orbitals [1]. D. Fuchs *et al* correlated the structural distortions to magnetic and electronic properties of perovskite cobaltates. Ten years ago, S. Tan *et al* [2] showed that Zn doping on B sites in an $ABO_3$ compound indicate paramagnetic–ferromagnetic transitions without an insulator–metal transition. Furthermore, they discussed the origin of the insulating behavior in ferromagnetic (FM) state as consequence of two types of $MnO_6$ octahedra in the same system. In order to correlate the strong hybridization model with the type of octahedra it requires measurements of local distortions at the Mn site (EPR), and global distortions like Mn-O-Mn bonds angle and Mn-O bond lengths by XRD analysis.

## II. RESULTS

The $La_{0.7}Dy_{0.3}Mn_{1-x}Zn_xO_3$ polycrystalline samples in the doping range $0 < x < 0{,}4$ were prepared by solid state reaction method. In this process, stoichiometric amounts of the precursor reagent $La_20_3$, $Dy0_3$, $Mn_2O_3$ $ZnO_2$+OH were homogenized and calcined at 1.237 K for 24 hours. X-ray powder diffraction patterns were taken at room temperature using a Philips PW1710 diffractometer with cooper target. The Rietveld refinements were performed using the FullProf software [3]. The observed and calculated diffraction profile obtained from the Rietveld analysis for the samples with $x = 0.2$ is shown in the figure 1.a. All the observed peaks were indexed in three phases: two orthorhombic phases (Pbnm and Pnma) and one trigonal phase (R-3C).

Some results obtained by Rietveld refinement are listed in table 1. For Zn doping, there occurs the transition from Trigonal R-3C phase to orthorhombic Pbnm phase. The above-mentioned transition was observed by measuring the fraction of the phases in the samples, i.e. the fraction of the Orthorhombic Phase Pbnm increases by doping increasing while the other phases decrease by doping.

The octahedrons contorted by the Zn doping were characterized by the $Mn\text{-}O_{1,2}\text{-}Mn$ angles. Table 1 shows an angle reduction, which means a greated contortion of the octahedrons.

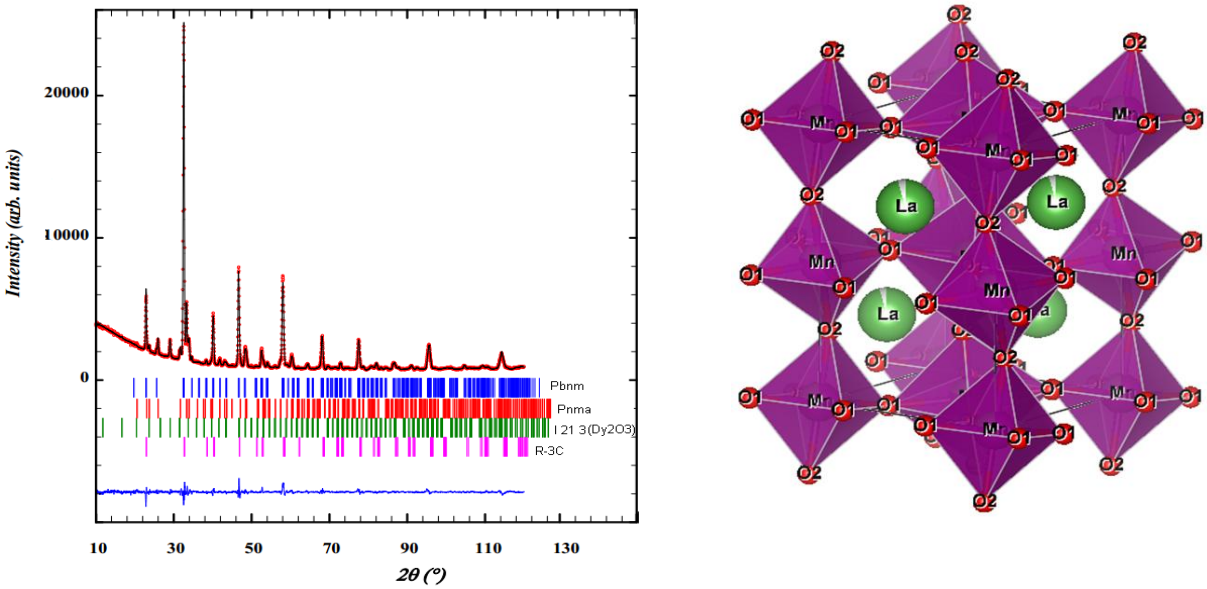


*Fig.1. (a) XDR Rietveld refinement results for sample $La_{0.7}Dy_{0.3}Mn_{0.8}Zn_{0.2}O_3$. The bars down the pattern correspond to picks for Pbnm, Pnma, and R-3C. The line on the bottom, corresponds to the difference between measured and calculated pattern. (b) The structure of $La_{0.7}Dy_{0.3}Mn_{0.8}Zn_{0.2}O_3$. The Mn ions are in the octahedral coordination. The $O_1$ atoms are in Mn planes while the $O_2$ atoms are along the c –axes.*

The distortion of the octahedra is discussed from the ratio O1-Mn / O2-Mn. In non-distorted octahedra we expect the ratio to be 1. The distortion it is used to evaluated the Jean –Teller interaction.

*Table 1. The Mn-$O_{1,2}$-Mn angles and Mn-O bond length in $La_{0,7}Dy_{0,3}Mn_{(1-x)}Zn_xO_3$*

| Zn doping | $x = 0$ | $x = 0,1$ | $x = 0,2$ | $x = 0,3$ | $x = 0,4$ |
|---|---|---|---|---|---|
| Mn-$O_1$-Mn angle (degree) | 159,81 | 159,35 | 156,62 | 156,64 | 153,89 |
| Mn-$O_2$-Mn angle (degree) | 155,12 | 151,36 | 148,52 | 146,52 | 147,03 |
| $O_1$-Mn length ( $\overset{o}{A}$ ) | 2,1820 | 2,1301 | 2,0529 | 2,1492 | 2,1687 |
| $O_2$-Mn length ( $\overset{o}{A}$ ) | 1,9526 | 1,9693 | 2,0263 | 2,0422 | 2,0391 |
| Fraction of Trigonal Phase R-3C | 0,4208 | 0,1436 | 0,2168 | 0,2219 | 0,2603 |
| Fraction of Orthorhombic Phase Pbnm | 0,2928 | 0,5618 | 0,5111 | 0,4998 | 0,4781 |
| Fraction of Orthorhombic Phase Pnma | 0,2341 | 0,251 | 0,2272 | 0,243 | 0,1969 |

## REFERENCES


[1] Fuchs D., Merz M., Nagel P., Schneider R., Schuppler S., and von Löhneysen H., Double Exchange via $t_{2g}$ Orbitals and the Jahn-Teller Effect in Ferromagnetic $La_{0.7}Sr_{0.3}CoO_3$ Probed by Epitaxial Strain, *Physical Review Letters*, 111(2013) 157203-1

[2] Shun Tan, Song Yue, Yuheng Zhang, Jahn, Teller distortion induced by Mg/Zn substitution on Mn sites in the perovskite manganites, *Physics Letters A*, 319(2003) 530-538

[3] Rodríguez-Carvajal J., Recent advances in magnetic structure determination by neutron powder diffraction + FullProf, *Physica B*, 192 (1993)55

[4] Rodríguez-Carvajal J., Recent developments of the program FULLPROF, Commission on powder diffraction (IUCr), *Newsletter*, (2001)

# WIEGAND SENSOR AS AN EFFECTIVE ENERGY SOURCE FOR SUPPLYING ULTRA LOW POWER ELECTRONICS

A. Majocha and R. Gozdur

Lodz University of Technology; Department of Semiconductor and Optoelectronics Devices
90-924 Lodz, Wolczanska Str. 211/215, Poland; Tel. +(48) 42 631 25 10; Fax: +(48) 42 636 80 24
e-mail: andrzej.majocha@p.lodz.pl, gozdur@p.lodz.pl

***Abstract.*** *The Wiegand sensors are used as position detectors and linear or rotary motion sensors. They are generative sensors and can therefore be used to supply electronic circuits with ultra low power consumption such as pulse counters, comparators, operational amplifiers, microcontrollers. The paper presents the results of measurements of the maximum energy of a single pulse in matching conditions. Based on energy value the maximum power obtainable from a commercial Wiegand sensor was calculated. The value of this power is approx. 0,6mW and provides proper supply of an electronic circuit with very low power consumption (e.g. 3V/0,2mA). The results of measurements of the harvested energy using specialized system are presented in this paper.*

## I. INTRODUCTION

The development of integrated circuits such as logic, analog circuits, microcontrollers makes less and less power consumption to power them. These systems are applicable to devices powered from the battery for several years. Another device is powered with renewable energy sources such as solar or wind power. They also develop modern systems named energy harvesters for converting electricity power from kinetic, thermal energy based on electromagnetic, piezoelectric or thermoelectric phenomena [1, 2]. The Wiegand sensor belongs to the group of kinetic harvesters [2]. Conversion process can be done by the direct conversion of kinetic energy into electrical one. The magnetic field in this case is the energy carrier. The type of conversion depends on the way of inducing the Wiegand effect. Avalanche process of magnetization in the Wiegand sensors can be excited by bidirectional changes of magnetic field from permanent magnets or AC/DC current. Commonly applied and developed solutions based on rotated permanent magnets.

## II. EXPERIMENTS

The industrial Wiegand sensor WG112 was used as the object under test. Bi-directional magnetic field acting on the sensor prepared in two ways. In the first case, the field was generated by a set of two magnets mounted on the shaft (Fig. 1), or one magnet rotating around the center of the sensor. In the second case, the field was obtained by the magnetization the sensor by coil fed from AC generator with adjustable frequency and output current (Fig. 2). The magnetic field and the electrical signals were measured and recorded by the measuring system consisting of gaussmeter Lakeshore DSP475 with transverse Hall probe and digital signal analyzer NI-4462.

At the beginning of the tests the impedance matching was determined. The value of energy harvested from the Wiegand sensor was determined in two cases. The first was to load the sensor by the resistor providing impedance matching. The second, was to use a specific integrated harvesting circuit, which produces a voltage of a predetermined value.

During the tests of the excitation by the magnet, gap width, frequency and load ($R_{load}$) were determined. The harvested energy value for a single cycle of excitation was calculated. Because of the random nature of the avalanche of changes magnetic polarity, the average waveforms of EMF pulses was used to calculate the energy efficiency.

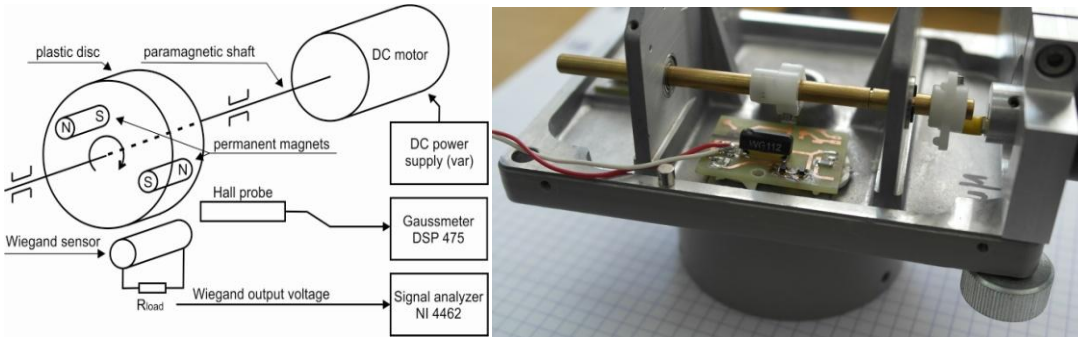


*Fig.1. Diagram and view of experimental setup for investigation the Wiegand sensor*

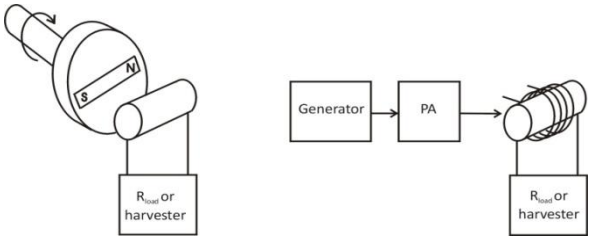


*Fig.2. Methods of excitation of the Wiegand sensor*

The Wiegand sensor actuated by the alternating magnetic field provides electromotive force EMF which is the sum of two phenomena. The first phenomena is $EMF_W$ due to the Wiegand effect. The energy of a single pulse is independent of the frequency of the magnetic field. The second phenomena is the $EMF_C$ in the pickup coil of Wiegand sensor due to changes of the magnetic flux. In this case, the additional energy is directly proportional to the frequency of the magnetic field. Based on measurements of the energy from the Wiegand sensor the frequency dependence of the energy from both phenomena was determined.

## III. CONCLUSIONS

Typical Wiegand sensors working in energy harvesting mode provide approximately energy of 32nJ per pulse. Energy efficiency's peak is achieved in range of $R_{LOAD}$ from 2000 to 5000 Ohms. Taking rotation frequency into consideration (up to approx. 30kHz), available electrical power riches the level of 600μW.

## REFERENCES

[1] Gilbert J. M., Balouchi F., Comparison of Energy Harvesting Systems for Wireless Sensor Networks, *International Journal of Automation and Computing*, 05(4), October 2008, pp. 334-347

[2] Ongaro F., Saggini S., Corradini L., Low-Power Energy Harvester for Wiegand Transducers, *IEEE Proceedings of Applied Power Electronics Conference and Exposition (APEC), 2013 Twenty-Eighth Annual IEEE* , March 2013, pp. 453-459

# ANALYSIS OF THERMAL STRATIFIED STORAGE TANK

D. Mazur[1], R. Smusz[2] and P. Kielan[3]

[1] Rzeszów University of Technology, The Faculty of Electrical and Computer Engineering
ul. W. Pola 2, B206, 35-959 Rzeszów, Poland, mazur@prz.edu.pl
[2] Rzeszów University of Technology, Department of Thermodynamics and Fluid Mechanics,
ul. Powstańców Warszawy 12, 35-959 Rzeszów, Poland, e-mail: robsmusz@prz.rzeszow.pl
[3] Faculty of Electrical Engineering, Department of Mechatronics
Bolesława Krzywoustego 2, 44-100 Gliwice, Poland, e-mail: pawel.kielan@polsl.pl

***Abstract.*** *The paper presents the temperature stratification system in an accumulation tank. The range of the research concerns the shape and dimensions of stratification system for an accumulation tank. Thermal stratification is a process that comprises in maintaining temperature stratification at different levels of accumulation tank that is reducing to minimum the process of temperature equalization. It results from the fact that thermal stratification in a tank increases in a significant way the installation efficiency and improves the process of energy storing.*

## I. INTRODUCTION

Providing vertical stratification of temperature in a tank is extremely important from the perspective of process energy effectiveness of the process of utilising waste energy. It is connected with proper location of inlet and outlet ports, sizes, shape, the method of distributing hot water within a tank, as well as the placement of elements that potentially interfere with temperature stratification, such as heat exchangers, booster heaters etc. It requires proper configuration of stratification system elements so as to reduce mixing of cold and hot water in a tank. The application of stratification system enables 'direct' transfer of heated water to upper parts of a tank, without mixing with cold water, which increases effectiveness of the heat recovery system.

Fig. 1 presents three cases of the accumulation of the same value of thermal energy, but with different levels of stratification. The first case corresponds to the highest level of temperature stratification and is the most beneficial one. It is determined by the fact, that the share of the zone of the highest and homogenous temperatures in an accumulation tank is the greatest. Together with the increase of mixing level the zone of thermocline expands until full mixing of the coefficient.

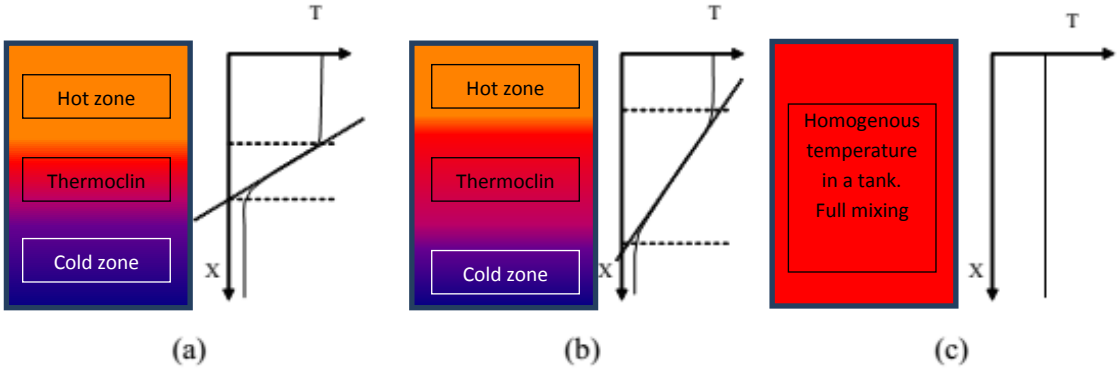


*Fig.1. Different levels/layers of temperature stratification by the same amount of the accumulated thermal energy*

Providing vertical stratification of temperature in a tank is important and its quality is connected with sizes, shape of a tank, method of distributing hot water in a tank, as well as the arrangement of elements that may potentially interfere with temperature stratification. It requires proper configuration of stratification system elements so as to reduce mixing of cold and hot water in a tank. Heat, mass and momentum exchange are the basic instrumental processes that influence the processes taking place inside an accumulative tank.

The main factors destabilizing thermal stratification are:

- forced convection inside a tank, caused by supplying cold water and reception of warm water by the external hydraulic system. The streams of supplying and received water while filling the tank induce mixing of water in a tank;
- free convection which is a result of the density difference between cold and warm zones in an accumulative tank;
- heat conductance between levels of water with different temperatures.

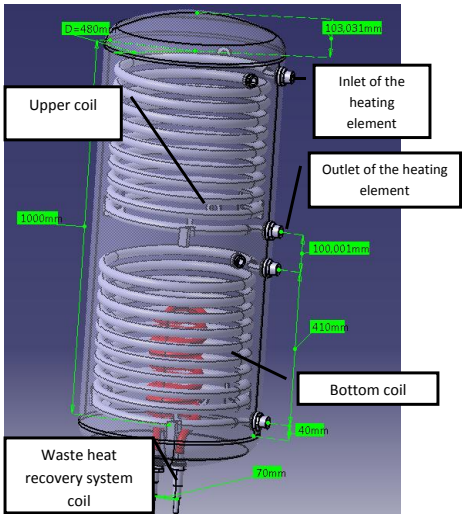


*Fig.2. 3D visualization of an accumulation tank*

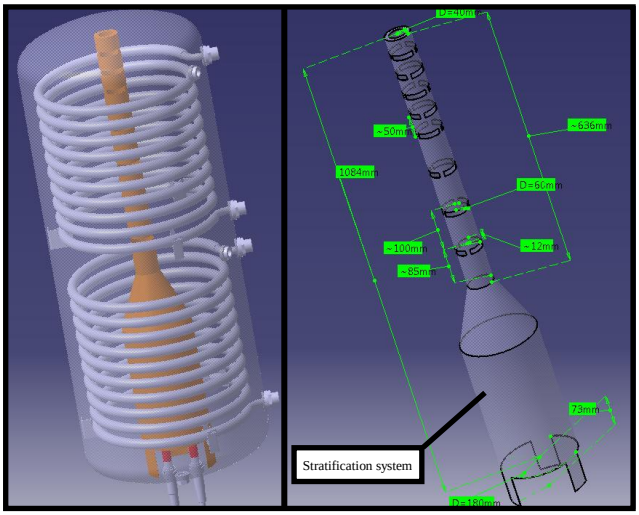


*Fig. 3. 3D visualization of an accumulation tank with stratification system*

## II. RESULTS

In the analysed issue we concentrated on defining level-distribution of heat in a tank during heat recovery system coil operation and its interaction with other elements, as well as defining proper geometrical dimensions/sizes of stratification system in order to minimize the process of cold and hot water mixing. In the first variant calculations were made for an operating coil of waste heat recovery system without stratification unit. In the second variant the influence of different geometric variants was analysed, and stratification unit of the temperature stratification in an accumulation tank.

Numerical simulations were made by using COMSOL Multiphysics commercial software. For the model with stratification system, 1774510 finite elements were applied (152951 three-node triangular elements, 245000 four-node square elements and 53690 and 1888 boundary and apex elements) [3].

## REFERENCES


[1] Seok-Ki Choi, Tae-Ho Lee, Yeong-Il Kim, Dohee Hahn, Numerical analysis of thermal stratification in the upper plenum of the monju fast reactor, *Nuclear Engineering and Technology*, 2013, vol. 45, issue 2, p. 191–202

[2] He Zhang, Fenglei Niu, Yu Yu, Shuming Zhang, Han Wang, Zhi Gang, Modeling and experimental studies on mixing and stratification during natural convection in containments, *Annals of Nuclear Energy*, 2015, vol. 85, pp. 317–325

[3] Hua Li, W. Villanueva, P. Kudinov, Approach and Development of Effective Models for Simulation of Thermal Stratification and Mixing Induced by Steam Injection into a Large Pool of Water, *Science and Technology of Nuclear Installations*, 2014

# PHENOMENOLOGICAL MODELLING OF HYSTERESIS: APPLICATIONS AND LIMITATIONS

Y. Melikhov[1,2]

[1] Institute of Physics, Polish Academy of Sciences, Al. Lotnikow 32/46, 02-668 Warsaw, Poland
[2] Wolfson Centre for Magnetics, School of Engineering, Cardiff University, Cardiff, CF24 3AA, U.K.
melikhov@ifpan.edu.pl , melikhov@cardiff.ac.uk

***Abstract.*** *Hysteretic behavior observed in magnetization under changing magnetic field in ferromagnetic materials is the simplest example of hysteresis. Phenomenological models to describe such behavior have been known and used for years but, in order to be physically sound, these models must originate from energetic considerations. The most famous examples of such models are the Jiles-Atherton model and the Preisach model and, with the theory available behind those models, extension to more complicated cases of hysteresis can be achieved. This paper reviews recent extensions of these models together with examples of their applications to describe: (1) temperature effects (observed in magnetoelastic cation substituted cobalt ferrite compound), (2) two-magnetic-phase materials behavior (observed in CGO electrical steel under compressive stresses), (3) hysteresis in systems exhibiting magnetic-structural first order phase transition (observed in magnetocaloric $Gd_5(Si_xGe_{1-x})_4$), and (4) hysteresis of magnetotransport properties (observed in half-metallic ferromagnets).*

## I. INTRODUCTION

Hysteretic behavior observed in magnetization under changing magnetic field in ferromagnetic materials is the simplest example of hysteresis. Successful phenomenological models must originate from energetic considerations and the most famous examples of such models are the Jiles-Atherton model [1] and the Preisach model [2]. This paper presents recent extensions of these models to describe more complicated cases of hysteresis.

## II. EXTENSIONS AND EXAMPLES

### *A. Hysteresis with temperature effects and Hysteresis of two-magnetic-phase systems*

The Jiles-Atherton model [1] is based on the assumption that the total magnetization, $M$, of a ferromagnetic material can be expressed as the sum of contributions of irreversible, $M_{irr}$, (i.e. due to lossy processes such as domain wall pinning) and reversible, $M_{rev}$, (due to lossless processes such as domain wall bowing) magnetisation components. Five parameters of the Jiles-Atherton model are assumed to be constant: spontaneous magnetisation, $M_S$, pinning factor, $k$, domain density, $a$, domain coupling, $\alpha$, and reversibility factor, $c$.

If variation of the parameters of the Jiles-Atherton model, for example, with temperature is allowed the temperature effects in hysteretic behavior [3] can be described (see Fig. 1(a)). Variation of the parameters with external field and change from one set of parameters into the other set at some specific exchange/coupling magnetic field could lead to description of hysteretic behavior exhibiting behavior of two-magnetic-phase systems [4] (see Fig. 1(b)).

### *B. Hysteresis in systems exhibiting magnetic-structural first order phase transition*

First order phase transitions may occur in several magnetic systems, with two structural phases having different magnetic properties each and a structural transition between them. In order to model such systems magnetization is represented by the volumetric amounts of ferromagnetic (described by extended Jiles-Atherton theory) and paramagnetic (described by the Curie-Weiss law) in respective phases [5]. Accompanied with an identification procedure to extract material parameters from experimental data, the model successfully describes hysteresis in systems exhibiting magneto-structural first order phase transition (see Fig. 1(c)).

*C. Hysteresis of magnetotransport properties*

The Preisach model assumes that a system is represented by a set of bistable units (called hysterons), allowing each unit to be in only one of the two possible states m=±Δm (i.e., magnetization "up" or "down"), with an energy barrier between the states [2]. The Gibbs energy determines the stability of the unit with the free energy of the unit and the coupling of the unit to the external magnetic field $k(m;H)$. Magnetization of the system is then calculated by double integral over the known probability of the bistable units.

Taking ordinary magnetic hysteron as a base and having physical understanding of the magnetotransport properties in half-metallic ferromagnets, one can easily introduce a conductivity hysteron between two neighboring magnetic hysterons [6]. Considering the system as three-dimensional random resistor network where the intrinsic thermodynamic percolation effects are not only due to magnetic field variation but also due to temperature changes as well, we can connect Preisach magnetic distribution function with Preisach conductivity distribution function, and successfully model $M(H,T)$ and $R(H,T)$ (see Fig. 1(d)).

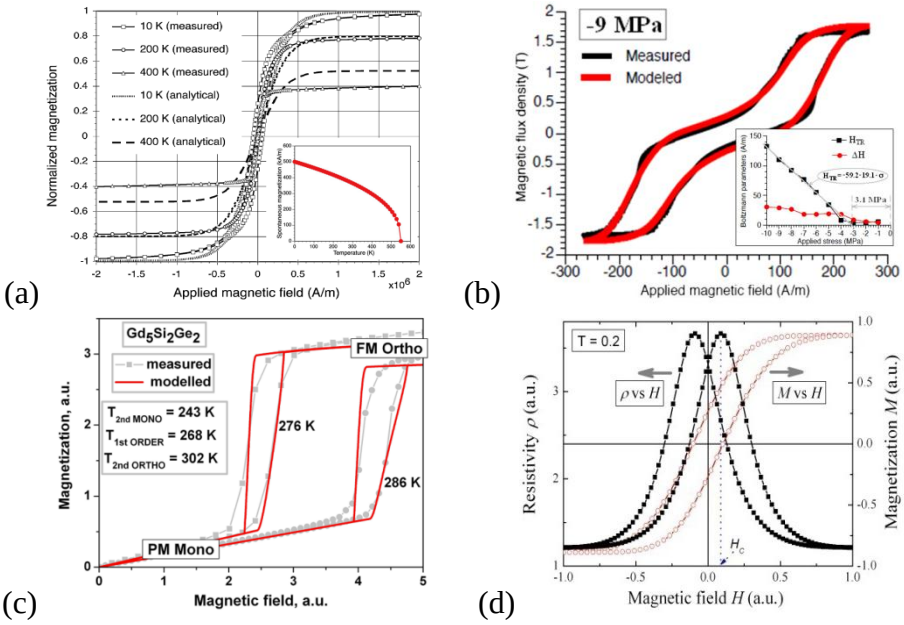


*Fig.1. Measured and modelled (a) major hysteresis loops at different temperatures for $Co_{1.4}Ge_{0.4}Fe_{1.2}O_4$ with Curie temperature $T_C \approx 550$ K [3]; (b) magnetization curves of CGO electrical steel under 9 MPa compressive stress showing two-magnetic-phase behavior [4]. Inset shows dependence of Boltzmann parameters on applied stress; (c) magnetization curves showing the induced magnetic-structural (MS) first order phase transition (FOPT) in $Gd_5Si_2Ge_2$ [5]; (d) major hysteresis curves of magnetization and resistance as a function of applied field at certain temperature observed in half-metallic ferromagnets [6]*

## REFERENCES


[1] Bertotti G., Hysteresis in Magnetism, *Academic Press*, 1998

[2] Jiles D.C., Atherton D.L., Theory of ferromagnetic hysteresis, *Journal of Magnetism and Magnetic Materials*, 61, 1986, pp. 48-60

[3] Raghunathan A. et al., Modeling the Temperature Dependence of Hysteresis Based on Jiles–Atherton Theory, *IEEE Transactions on Magnetics*, 45, 2009, pp. 3954-3957

[4] Raghunathan A. et al., Application of Jiles-Atherton Model to Stress Induced Magnetic Two-Phase Hysteresis, *IEEE Transactions on Magnetics*, 49, 2013, pp. 3187-3190

[5] Melikhov Y. et al., Phenomenological modelling of first order phase transitions in magnetic systems, *Journal of Applied Physics*, 115, 2014, 183902

[6] Krivoruchko V.N. et al., Relationship between hysteretic behavior of magnetization and magnetoresistance in half-metallic ferromagnets, *Physical Review B*, 77, 2008, 180406(R)

# NONEQUILIBRIUM PATTERNS IN SPINODAL GRANULAR MATTER

A. Mendoza[1, 2], J.F. López[1, 2] and O. Guzmán[2]

[1] Physics Department, National University of Colombia, Colombia
[2] Magnetic materials and nanostructures Group, Faculty of science, National University of Colombia

***Abstract.*** *This study is focused on metastabile systems where the Ginzburg-Landau Ansatz turn out to be useful. The model begins with a functional suitable to describe first order phase transitions [1]. The order parameter is the concentration of one of the two species. The bifurcation is discussed for the equations obtained by minimization of the functional. The study is restricted to the one-dimensional stationary case.*

## I. INTRODUCTION

A molten binary alloy when quenched shows a sudden appearance of a fine grained structure which is known as spinodal decomposition. The decomposition is characterized by two phases, one rich in one component and the other rich in the other component.

Spinodal decomposition is a non-equilibrium segregation process that when interrupted before the end lead to a continuous quasiperiodic distribution of solute in a matrix. To this spinodal granular matter belong the magnetic granular alloys studied in reference [1]. The authors from this reference show a spinodal decomposition in Cu-Co ribbons which are composed of a periodic distribution of Co within Cu. They observed lamellar profiles associated with giant magneto-resistance although in the profiles no well-defined interfaces are formed. The observed distribution of Co concentrations over the sample has been analyzed by a simulation based on Cahn –Hilliard equations [2].

In higher space dimensions, the complexity of the equations obtained from the functional makes the treatment of the bifurcation problem difficult. Thus, here the bifurcation problem for the family of equations derived from the Gizburg-Landau functional is discussed in one dimension.

## II. TECHNICAL INSTRUCTIONS

The starting point of the model is the functional:

$$E[\vec{\varphi}] = \int d\vec{r}\left\{const + \frac{1}{2} r_o \vec{\varphi}^2 + \frac{\mu_o}{4}\vec{\varphi}^4 + \frac{1}{2} A(\nabla\vec{\varphi})^2 + \frac{1}{4}(\nabla\vec{\varphi})^4\right\} \tag{1}$$

Which represent a double expansion in powers of $\vec{\varphi}$ and $(\Delta\vec{\varphi}).\vec{\varphi}$ represent a n-component order parameter. By minimization of the functional $E[\vec{\varphi}]$ and taking into account the structure of the coefficient $A$ one can obtain a family of equations for the order parameter:

$$\Delta\vec{\varphi} - \lambda F(\vec{\varphi}) = 0 \tag{2}$$

$$-\Delta(\Delta\vec{\varphi}) - \lambda F(\vec{\varphi}) = 0 \tag{3}$$

$\lambda$ is the eigenvalue associated to the interaction of the system.

The first equation is known as the Allen-Cahn equation, and the second ones is the Cahn – Hilliard equation. Properties of the bifurcating branches in the first equation such as monotonicity, asymptotic behavior of these branches as $\lambda \to \infty$, or in which the stationary solutions are solution of the second one, can helps us to study the patterns formation in the Cahn-Hilliard equation. The one dimensional analysis may be brings us near to results in two and three dimensions [3].

## REFERENCES


[1] Hohenberg P.C., Krekhov A.P., An introduction to the Ginzburg–Landau theory of phase transitions and nonequilibrium patterns, *Physics Reports*, 572, (2015) pp. 1-42

[2] Miranda M.G.M., da Rosa A.T., Hinrichs R., Golla-Schindler U., Antunes A.B., Martínez G., Estévez-Rams E., Baibich M.N., Spinodal decomposition and giant magnetoresistance, *Physica B*, 384 (2006) pp.175-178

[3] Binder K., Materials science and technology in Phase transformations in materials, vol 5, *Wiley-VCH Verlag GmbH*, Weinheim, Germany, 1991

[4] Chaffee N., Infante E.F., A bifurcation problem for a nonlinear partial differential equation of parabolic type, *Applicable anal* 4 (1974/75) pp. 17-37

# SCALING-BASED MODELLING OF POWER LOSSES IN AMORPHOUS AND NANOCRYSTALLINE ALLOYS

M. Najgebauer

Częstochowa University of Technology, Faculty of Electrical Engineering
al. Armii Krajowej 17, 42-200 Częstochowa, Poland, najgebauer@el.pcz.czest.pl

***Abstract.*** *The paper presents the scaling-based approach to modelling of power losses in Fe-based amorphous and nanocrystalline magnetic alloys. The modelling results are satisfactory due to relatively low discrepancies between measured and modelled losses curves.*

## I. INTRODUCTION

Power losses in soft magnetic materials are generated by hysteresis phenomenon and eddy currents, flowing in different scales as in whole material bulk, around moving domain walls or micro-currents related to Barkhausen jumps. Some authors propose to consider all types of power losses separately, while others suggest that these should be considered as total.

Modelling of power losses is still an interesting issue both for scientists and researchers. There are many approaches to modelling of power losses. The most popular model has been proposed by Bertotti [1-2]. It is composed of three power law components of frequency and magnetic induction, related to hysteresis, classical and excess losses. This model also assumes that power losses are scale-invariant phenomena. On the other hand, some authors proposed simpler models composed of two or even one losses component.

Referring to multi-scale aspects of power losses, Sokalski *et al.* has proposed a new approach to the losses analysis, which was based on the Widom scaling procedure [3-4]. It leads to a two-component description of power losses, given in new coordinates – scaled losses and scaled frequency. However this model has some limitations, because exponents of the scaled frequency can be only integers. Recently, a modified approach to scaling analysis of power losses was postulated, in which scaling exponents can be fractional numbers [5]. The fractional scaling gave the power law describing scaled power losses in the following form:

$$P_{\mathrm{tot}}/B_{\mathrm{m}}^{\beta} = p\left(f/B_{\mathrm{m}}^{\alpha}\right)^{x}, \tag{1}$$

where: $P_{\mathrm{tot}}/B_{\mathrm{m}}^{\beta}$ – scaled losses, $f/B_{\mathrm{m}}^{\alpha}$ – scaled frequency, $\alpha$, $\beta$ and $p$ – scaling parameters, $x$ – fractional exponent. The expression (1) provided promising results of power losses modelling for 3% Si-Fe grain-oriented steel [5] and magnetocaloric alloys [6]. In the present study, the expression (1) is examined in modelling of power losses in Fe-based alloys with amorphous and nanocrystalline internal structures.

## II. MATERIALS AND MEASUREMENTS

In the study, samples of commercially produced Fe-based amorphous and nanocrystalline alloys are analyzed. The amorphous sample is made of Metglas and the nanocrystalline is made of Finemet. Both samples have cylindrical shapes with dimensions (outer radius, inner radius and height) 27.2 x 13.5 x 10.5 mm and 12.5 x 8.0 x 10.0 mm, respectively for amorphous and nanocrystalline ones.

Power losses of these samples were measured using the computer-aided measurement system MAG-RJJ-2.0, according to the IEC international standard and with the B-type uncertainties lower than 1.5%. The measurement ranges were: 50 to 400Hz for frequency and 0.1 to 1.2T for magnetic induction. The measurements provided a set of power losses curves for each sample.

## III. RESULTS

In the proposed approach to modelling of power losses, the expression (1) is used after it rescaling to the form that describes power losses directly:

$$P_{\mathrm{tot}} = pf^{x}B_{\mathrm{m}}^{\beta-\alpha x}. \tag{2}$$

The model parameters are estimated from the set of losses measurements, using the least squares method. The parameter values should be estimated in such a way that allows collapsing all measured losses curves onto the single one. Therefore, the parameter values are universal in the whole measured range. Selected results of the power losses modelling for the Fe-based amorphous alloy are presented in Figure 1. Maximum percentage error of the scaling-based losses modelling does not exceed 8%, what is a satisfactory result.

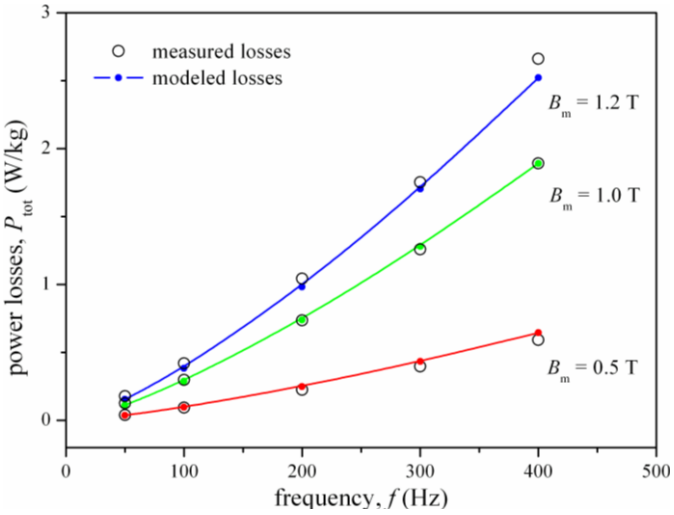


*Fig.1. Scaling-based modelling of power losses for Metglas 2605TCA amorphous alloy: solid line – modelled losses, circles – measurements.*

## IV. CONCLUSIONS

In the present study, the scaling-based approach to power losses modelling is examined for Fe-based amorphous and nanocrystalline alloys. Measured curves of power losses are collapsed onto a single curve, what allows estimating the model parameters. The obtained data collapses reveal also scaling behaviour of power losses in amorphous and nanocrystalline alloys. Results of the scaling-based modelling of power losses are satisfactory due to relatively low discrepancies between measured and modelled losses curves.

## REFERENCES


[1] Bertotti G., A general statistical approach to the problem of eddy current, *Journal of Magnetism and Magnetic Materials*, vol. 41, pp. 253-260, 1984

[2] Bertotti G., General properties of power losses in soft ferromagnetic materials, *IEEE Transaction on Magnetics*, vol. 24, no. 1, pp. 621-630, Jan 1988

[3] Sokalski K., Szczyglowski J., Najgebauer M., Wilczynski W., Losses scaling in soft magnetic materials, *COMPEL*, vol. 26, 2007, pp. 640-649

[4] Najgebauer M., Scaling theory and its chosen applications in electromagnetism, *Przegląd Elektrotechiczny*, vol. 84, issue 12, 2008, pp. 213-216

[5] Najgebauer M., Application of fractional scaling in modelling of magnetic power losses, *Acta Physica Polonica A*, vol. 128, 2015, pp. 107-110

[6] Gozdur R., Najgebauer M., Measurements and scaling analysis of power losses in La-containing alloys, *Journal of Electrical Engineering*, vol. 66, no. 7/s, 2015, pp. 37-40

# FEM-BASED FORWARD EDDY CURRENT TOMOGRAPHY TRANSFORMATION FOR AUTOMOTIVE INDUSTRY

P. Nowak[1], M. Nowicki[2] and R. Szewczyk[1]

[1] Institute of Metrology and Biomedical Engineering, Warsaw University of Technology, sw. Andrzeja Boboli 8, 02-525 Warsaw, Poland; p.nowak@mchtr.pw.edu.pl, r.szewczyk@mchtr.pw.edu.pl
[2] Industrial Research Institute for Automation and Measurements, al. Jerozolimskie 202, 02-486 Warsaw, Poland; mnowicki@piap.pl

***Abstract.*** *The paper presents utilization of open-source finite element method (FEM) software for modelling of measurement process on Eddy current tomography setup. Methodology of measurements is presented as well as software for forward tomography transformation. Developed software was based entirely on the open-source programs, which results with high possibility of method implementation in industry. Obtained modelling result presented high compatibility with measurement results, which confirmed correctness of the method.*

## I. INTRODUCTION

Eddy currents are commonly used for non-destructive tests of elements in production process, mainly for the selection of the elements. Reference objects (validated with other measurement method) are measured and their signature response is obtained. Then tested objects are measured and their response is compared with reference objects response. Thus selection of defective objects can be made.

On the other hand, this method does not provide information about the defect size and location and cannot be used for correction of production process. This gap is supplemented by the usage of eddy current tomography [1][2]. This method has typical advantages of eddy current testing (ease of use, simple hardware, no need of safety requirements) as well as possibility of determination of defects size and location as in other tomography methods.

In order to obtain data about the defects in the object, inverse tomography transformation has to be done. Due to significant nonlinearity of eddy current phenomena, it is typically done by FEM-based forward transformation and optimization of modelled objects shape. This paper presents methodology of the forward tomography transformation, which ensures proper reconstruction of measurement process and can be applied to advanced objects shapes, such as motor valve presented in Fig. 1.

*Fig.1. Analyzed object – motor valve placed in measurement holder*

## II. MEASUREMENT METHODOLOGY

Tested object is moved linearly between two coils – exciting and measuring. Exciting coil is powered by alternate current and causes induction of eddy currents in the object, which influence the field measured by second coil. Complete eddy-current tomography measurements are based on

simultaneous measurement of the amplitude and phase of signal on receiving coil in each measurement position. For single linear step, tested object is rotated around its axis, which makes this method more suitable for axisymmetric objects, such as motor valve.

Tested valve was measured in two states – firstly in delivery condition and secondly after making a reference defect –longitudinal incision. Differential analysis of the measurement results confirmed significant influence of defect on the results. The impact of the defect on the distribution of eddy current in the object was confirmed by FEM modelling [4]. This was a motivation for a development of software for complete forward tomography transformation.

## III. FEM MODELLING

The modelling was conducted in ElmerFEM software, which is an open-source computational tool for multi-physics problem. For modelling of eddy-currents phenomena a magnetodynamics solver was selected. It solves Maxwell equations in A-V form [5] basing on Whitney edge elements [6]. In order to perform proper FEM calculations continuous geometry of the modelled objects (exciting and measurement coils, tested valve) has to be discretized to a set of simple sub-domains called mesh. This discretization (meshing) was performed in open-source software - Netgen. Whole procedure of mesh generation and simulation control was implemented in Octave – an open-source software. It may be suitable for application of proper shape optimization algorithm and thus development of inverse tomography transformation.

For proper reconstruction of measurement process simulations had to be conducted for each linear step and every rotation position, which results with over 9 000 modelling steps. To obtain acceptable calculations time a 48-core computational center from the Institute of Metrology and Biomedical Engineering was utilized.

## IV. CONCLUSION

Obtained modelling results present high compatibility with measurements on real objects. Some differences are caused by the numerical noise caused by the transformation of edge (tetrahedral) elements on the Cartesian plane. Also tested object may be placed eccentrically to the axis of rotation which is impossible to take into account during modelling.

Further work should concern development of FEM-based inverse tomography transformation and thus proper determination of the objects defects.

## REFERENCES


[1] Salach J. , Non-destructive Testing of Cylindrical Ferromagnetic and Non-magnetic Materials Using Eddy Current Tomography, *Springer*, 2015

[2] Premel D., Mohammad-Djafari A., Eddy Current Tomography in Cylindrical Geometry, *IEEE Transaction on Magnetics*, 1995

[3] Soleimani M., Lionheart W.R.B., Peyton A.J., Image Reconstruction for High-Contrast Conductivity Imaging in Mutual Induction Tomography for Industrial Applications, *IEEE Transactions on Instrumentation and Measurements*, 2007

[4] Nowak P. et. Al, Utilization of Eddy Current Tomography in Automotive Industry, *Sumbitted do Acta Physica Polonica A*

[5] Raback P. et. Al, Elmer Models Manual, 2016

[6] Bossavit A., Whitney forms: A class of finite elements for three-dimensional computations in electromagnetism., *IEE Proceedings A-Physical Science, Measurement and Instrumentation*, 1988

# TEMPERATURE ERROR OF HALL-EFFECT AND MAGNETORESISTIVE COMMERCIAL MAGNETOMETERS

M. Nowicki[1], M. Kachniarz[2] and R. Szewczyk[1]

[1] Institute of Metrology and Biomedical Engineering, Warsaw University of Technology, sw. Andrzeja Boboli 8, 02-525 Warsaw, Poland; m.nowicki@mchtr.pw.edu.pl, r.szewczyk@mchtr.pw.edu.pl
[2] Industrial Research Institute for Automation and Measurements, al. Jerozolimskie 202, 02-486 Warsaw, Poland; mkachniarz@piap.pl

***Abstract.*** *The paper presents special measurement system for investigation of the temperature influence on the indication of commercially available sensors of magnetic field. Utilizing the developed system, several magnetoresistive and Hall-effect sensors were investigated within the temperature range from -30°C to 70°C. The obtained results indicate that sensitivity of most of the investigated sensors is unaffected, except the basic magnetoresistive device. However, Hall-effect sensors exhibit considerable temperature drift, regardless of manufacturer.*

## I. INTRODUCTION

Additional error induced by the influence of temperature is a very important problem in almost all kind of measurements performed in modern science and industry. Also measurements of magnetic field, widely utilized in many industrial processes, are influenced by the temperature. In this paper, we present the investigation of additional, temperature induced error of various commercially available magnetometers, based on both magnetoresistive effect [1] and Hall effect [2]. Obtained results indicates that for some temperature range, investigated commercial magnetometers are resistant to the influence of the temperature. But for the extremely low or high temperatures, additional error of the measurement is clearly observable.

## II. MEASUREMENT STAND

For this research, special test stand was designed and build, consisting of precision Helmholtz coils used as a magnetic field standard, and 0.01°C precise PolyScience Cryostat. The developed test stand is presented in Fig. 1. The Helmholtz coils were powered from precise laboratory power supply in constant current mode. The current was measured on precise standard 1 Ω resistor with Tonghui TH1961 voltmeter.

*Fig.1. Developed measurement stand for investigation the temperature influence on the magnetometers*

The test stand allowed measuring the magnetometers response in the ±100 μT magnetic field range, in -30° to 70°C temperature range, which is ±50°C from the nominal 20°C operating temperature.

## III. EXPERIMENTAL RESULTS

In the paper, the temperature dependence characteristics of four different magnetometers are presented. There were two triaxial magnetoresistive magnetometers, one triaxial Hall-effect sensor and one one-axis Hall-effect sensor investigated. Basing on the measurement results, linear fitting was performed, and temperature dependence of offset and sensitivity was determined. It was found, that for most magnetometers, except the basic magnetoresistive one, the sensitivity was unaffected by the temperature in the investigated 20°C±50°C range. On the other hand, the offset was negligible for the magnetoresistive sensors, but significant for the Hall-effect sensors, regardless of the manufacturer. In the Fig. 2 the temperature dependence of sensitivity $S$ is presented, relative to the 'nominal' 20°C measurement results $S_{20}$, for magnetoresistive sensor Honeywell HMC 5883L.

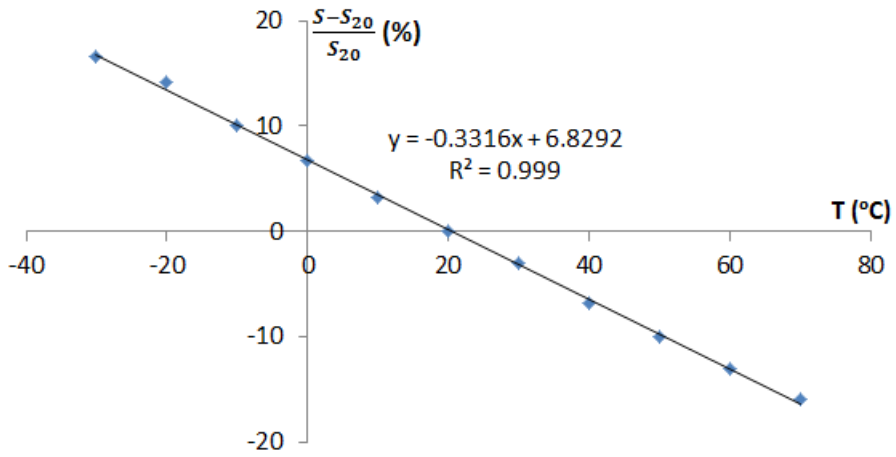


*Fig.2. Temperature dependece of sensitivity in relation to normal operating temperature 20°C for magnetoresistive sensor Honeywell HMC 5883L*

There is a strong, highly linear correlation between sensitivity of the device and operating temperature. HMC 5883L is very simple magnetoresistive sensor, which has no compensation circuit to reduce the influence of temperature on the operation of the device.

## IV. CONCLUSION

Results of the performed investigation indicates that most of the commercially available magnetometers exhibit high resistance to the influence of temperature. However, in simple devices for less demanding applications strong dependence between functional parameters and temperature is observable.

## REFERENCES

[1] Tumański S., Thin film magnetoresistive sensors, *CRC Press*, New York, 2001
[2] Ramsden E., Hall-Effect Sensors: Theory and Application, *Newnes*, Boston, 2006

# MAGNETIC PROPERTIES AND STRUCTURE AFTER CRYSTALLIZATION OF $Fe_{80-x}B_{20}Nb_x$ (x=4,6,10) METALLIC GLASSES

R. Nowosielski[1], M. Kądziołka-Gaweł[2], P. Gębara[3] and R. Babilas[4]

[1] Institute of Engineering Materials and Biomaterials, Silesian University of Technology
Konarskiego 18a, 44-100 Gliwice, Poland, ryszard.nowosielski@polsl.pl
[2] Institute of Physics, University of Silesia, Uniwersytecka 4, 40-007 Katowice, Poland,
mariola.kadziolka-gawel@us.edu.pl
[3] Institute of Physics, Częstochowa University of Technology, al. Armii Krajowej 19, 42-200 Częstochowa, Poland,
pgebara@wip.pcz.pl
[4] Institute of Engineering Materials and Biomaterials, Silesian University of Technology
Konarskiego 18a, 44-100 Gliwice, Poland, rafal.babilas@polsl.pl

***Abstract.*** *The ferromagnetic Fe-based amorphous alloys were studied due to properties for soft magnetic applications. Depending on different Nb addition, the formation of crystalline phases after annealing of amorphous alloys $Fe_{80-x}B_{20}Nb_x$ (x = 4, 6, 10) was studied. The crystallization products as well as the phase structure was determined using Mössbauer spectrometry combined with XRD, DSC and magnetic measurements. Substitution of Fe atoms by Nb led to significant changes in hyperfine magnetic field ($B_{hf}$) distributions in as-cast amorphous alloys $Fe_{80-x}B_{20}Nb_x$, for x = 10 the minimal value of $B_{hf}$ is observed. Addition of Nb caused a shift of crystallization process towards higher temperatures and induced changes in magnetic permeability and disaccommodation of magnetic permeability.*

## I. INTRODUCTION

In recent years a variety of ferromagnetic metallic glasses have been prepared extensively. The Fe-based glassy alloys have been mainly prepared due to the attractive properties for soft magnetic applications. The required magnetic properties are usually large saturation magnetization, low coercive field and high magnetic permeability [1-3].

## II. MATERIAL AND METHODS

The paper presents the structural analysis and magnetic characterization of $Fe_{80-x}B_{20}Nb_x$ metallic glasses (x=4,6,10) in as-cast state and after crystallization. The studies were performed on metallic glasses in the form of ribbons with thickness of 0.05 mm. The structural examinations of the samples in as-cast state and phase analysis of alloys after annealing was carried out by the X-ray diffraction (XRD) methods. Thermal properties associated with onset ($T_x$) and peak ($T_p$) crystallization temperatures was examined by differential scanning calorimetry (DSC). Moreover, Mössbauer spectroscopy (MS) was also used to investigate the local structure and crystallization process of examined alloys. The magnetic properties examination contained initial magnetic permeability ($\mu_r$), disaccommodation ($\Delta\mu/\mu$) of magnetic permeability, coercive force ($H_c$) and saturation magnetization ($J_s$) versus annealing temperature was evaluated.

## III. RESULTS AND CONCLUSIONS

The amorphous structure of Fe-based alloys in as-cast state was confirmed by results of XRD investigations (Fig.1a). The DSC curves (Fig.1b) of studied alloys present the exothermic peaks describing a two-stage of crystallization for $Fe_{70}B_{20}Nb_{10}$ and $Fe_{74}B_{20}Nb_6$ alloys. Moreover, a single crystallization process of $Fe_{76}B_{20}Nb_4$ metallic glass was observed. The $T_x$ = 759 K and $T_p$ = 774 K was achieved for $Fe_{76}B_{20}Nb_4$ alloy. The addition of 10 at.% Nb caused the increase of $T_x$ to 830 K and $T_p$ to 840 K, adequately. Substitution of Fe atoms by Nb led to changes in hyperfine magnetic field ($B_{hf}$) distributions in as-cast state. For $Fe_{70}B_{20}Nb_{10}$ metallic glass the lower value of $B_{hf}$ was observed. Therefore, addition of Nb also caused the improve of magnetic permeability and induced formation of crystalline phases including the α-Fe, $Fe_2B$ and $Fe_3B$ after annealing. The Mössbauer

spectra obtained for annealed samples indicated the presence of $Fe_2B$ and $Fe_3B$ with α-Fe in all alloys. The room temperature Mössbauer spectrum of $Fe_{74}B_{20}Nb_6$ determined after annealing at 773 K for 1 hour is shown in Fig.2a. The corresponding hyperfine magnetic fields distribution p($B_{hf}$) is also presented in Fig.2b. The initial magnetic permeability increased with the increase of annealing temperature and reached a distinct maximum near onset crystallization temperature.

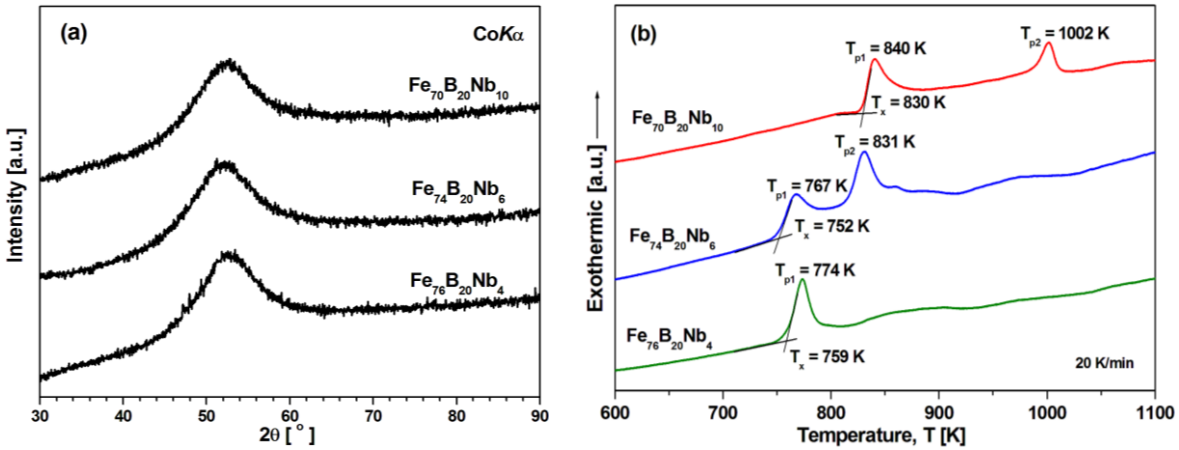


*Fig.1. X-ray diffraction patterns (a) and DSC curves (b) of studied alloys in as-cast state*

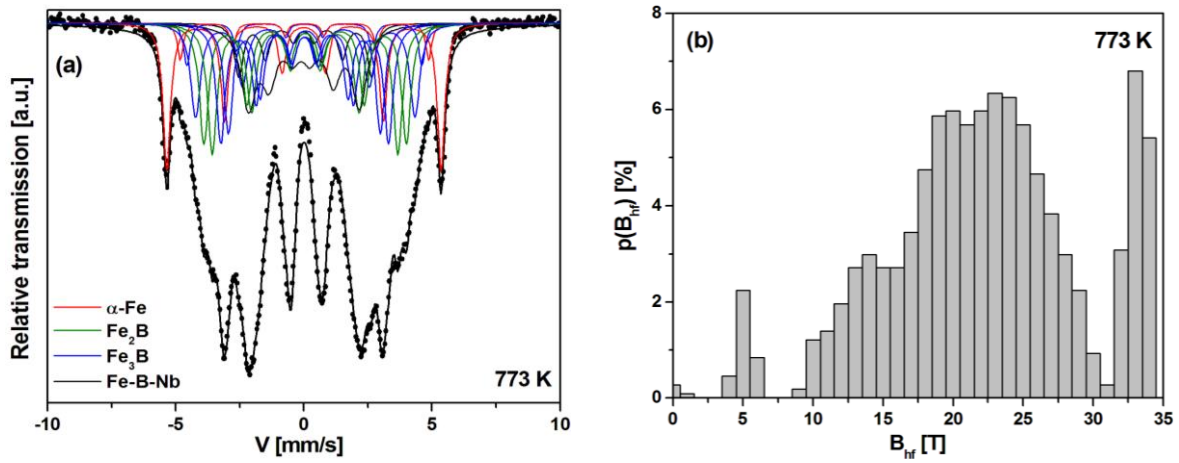


*Fig.2. Transmission Mössbauer spectrum with fittings (a) and hyperfine magnetic field distribution (b) of $Fe_{74}B_{20}Nb_6$ metallic glass after annealing at 773 K/1h*

## ACKNOWLEDGMENT

The work was partially supported by National Science Centre under research project no.: 2011/03/D/ST8/04138.

## REFERENCES

[1] Inoue A., Bulk amorphous and nanocrystalline alloys with high functional properties, *Materials Science and Engineering A* 304-306 (2001) 1-10

[2] Babilas R., Kądziołka-Gaweł M., The influence of Nb atoms on the crystallization process of Fe-B-Nb amorphous alloys, *Acta Physica Polonica A* 127 (2015) 573-575

[3] Babilas R., Kądziołka-Gaweł M., Burian A., Temleitner L., A short-range ordering in soft magnetic Fe-based metallic glasses studied by Mössbauer spectroscopy and Reverse Monte Carlo method, *Journal of Magnetism and Magnetic Materials* 406 (2016) 171-178

# EFFECT OF HEAT TREATMENT ON THE PHASE TRANSFORMATION AND MAGNETIC PROPERTIES OF THE RAPIDLY SOLIDIFIED $Pr_9Fe_{58}Co_{13}Zr_1Nb_4B_{15}$ ALLOY RIBBONS

K. Pawlik

Institute of Physics, Częstochowa University of Technology, al. Armii Krajowej 19,
42-201 Częstochowa, kpawlik@wip.pcz.pl

Pr-Fe-B magnets of low Pr concentration seem to be attractive alternative to more popular Nd-Fe-B counterparts due to a possibility of their applications at low temperatures. The argument for that is the fact that hard magnetic $Nd_2Fe_{14}B$ phase, undergo a significant reduction of magnetocrystalline anisotropy below 150 K due to the spin reorientation in this phase [1]. Replacement of Nd by Pr in the alloy composition results in decrease of the spin-reorientation temperature down to 25 K [2] and maintaining good performance of hard magnetic devices above this temperature. The present studies are focused on evolution of microstructure and magnetic properties of the rapidly solidified ribbons of the $Pr_9Fe_{58}Co_{13}Zr_1Nb_4B_{15}$ alloy subjected to annealing. The samples were produced by controlled atmosphere single roll melt-spinning technique at the velocity of the copper roll surface of 25 m/s. Subsequently the controlled atmosphere heat treatment of fully amorphous samples was carried out at temperatures ranging from 923 K to 1033 K for 5 min. The phase constitution of devitrified specimens was determined by the qualitative analysis of XRD spectra supported by the Rietveld refinement. These studies have shown that precipitation of hard magnetic $Pr_2(Fe,Co)_{14}B$ and paramagnetic $Pr_{1+x}Fe_4B_4$ phases occurs for all specimens heat treated at temperatures higher than 923 K. It was also demonstrated that annealing at 1033 K causes formation of the additional α-Fe phase. Furthermore, the Rietveld refinement has revealed changes in crystal sizes and weight fractions of constituent phases during annealing. In case of specimen heat treated at 923 K, complementary Mö ssbauer studies have shown a presence of large fraction of the amorphous component. The increase of annealing temperature has an effect in optimization of the shape of the magnetic hysteresis loops. The highest values of coercivity ${}_JH_C$, magnetization remanence $J_r$ and maximum energy product $(BH)_{max}$ were determined for the ribbon subjected to annealing at 1003 K. The increase of the annealing temperature up to 1033 K resulted in rise of the saturation magnetization due to the precipitation of the α-Fe phase, however, it has a detrimental effect on both the coercive field and shape of the demagnetization curve. In order to characterize the influence of the phase constitution and microstructure on the magnetization process in annealed ribbons, studies of the switching field distribution (SFD) were performed. The SFDs which are defined as derivatives of the irreversible magnetization remanence with respect to the magnetic field ($dM_{irr}/dH$), were calculated from recoil curves measured on specimens in the initially demagnetized state. This reflects a rate of irreversible magnetization remanence ($M_{irr}$) changes with the increase of maximum applied magnetic fields (H). Additionally, the profile of SFD curve provides the information about the strength of magnetic interactions between grains of magnetic phases.

## REFERENCES

[1] Xue-Fu Zhong, Ching W.Y., Lai W., Calculation of spin reorientation temperature in $Nd_2Fe_{14}B$, *J. Appl. Phys.*, 70, 1991, 6146

[2] Liu Z., Davies H.A., Composition and Microstructure Dependent Spin Reorientation in Nanocrystalline (Nd–Pr)-(Fe–Co)-B Alloys, *IEEE Trans. Magn*. 40, 4, 2004, 2898-2900

# PHASE STRUCTURE AND MAGNETIC PROPERTIES OF THE CO-PRECIPITATED MAGNETITE NANOPARTICLES

P. Pawlik, M. Pruba, K. Pawlik

Institute of Physics, Czestochowa University of Technology, Al. Armii Krajowej 19, 42-200 Częstochowa, Poland

The hyperthermia is a general name for cancer treatments in which the body tissue is exposed to the elevated temperature up to ~42$^{o}$C in order to deteriorate the tumor cells. The advantage of this therapy is the fact that the most of cancer cells reveal lower thermal conductivity than healthy tissue, therefore they are more sensitive to the high temperature. Hyperthermia also known as a thermotherapy frequently used as a whole body treatment is an alternative or complementary medication to chemotherapy. Recently a great interest is focused on application of superparamagnetic nanoparticles as a heat carrier, where the heat is induced in the nanoparticles by the high frequency elektromagnetic field. The advantage of the magnetic hyperthermia is fact that nanoparticles can be focused on selected organs of the body, thus limiting impact on other healthy tissue. The major issue in selection of appropriate medium is the toxicity of the magnetic nanoparticles. Therefore use of magnetic nanoparticles is limited to only few systems. Until now the ferrimagnetic magnetite ($Fe_3O_4$) nanoparticles were accepted for use in human therapies including drug delivery carriers or magnetic particle imaging (MPI). The aim of the present studies is the determination of the influence of processing technique on the microstructure and magnetic properties of the $Fe_3O_4$ used as a potential heat carrier in the magnetic hyperthermia. The samples were produced by co-precipitation method. In this process the iron-oxide nanoparticles were synthesized from aqueous solutions of Fe (II) and Fe (III) salts in the molar ratio 2:1. To the water diluted salts the ammonium hydroxide solution was added dropwise under vigorous stirring. The process was carried out in the nitrogen atmosphere and at the temperature of 60$^{o}$C. A part of synthesized iron-oxide nanoparticles were coated with the silica oxide using Stober process. The X-ray diffractometry was used to determine the phase constitution of the synthesized samples. It was shown that only one $Fe_3O_4$ phase is formed during co-precipitation . To determine the average grain size of the specimens the Rietveld refinement was used. The analysis shown presence of nanocrystallites of the average grain diameter of 10 nm. The Mössbauer spectroscopy confirmed presence of the only one crystalline phase formed during the co-precipitation. However, aggregation of nanoparticles resulted in ferrimagnetic ordering. On the other hand in case of silica coated samples, a presence of paramagnetic component of Mössbauer spectrum suggest isolation of nanoparticles revealing superparamagnetic behavior. Magnetic measurements confirmed changes in the magnetic behavior of silica coated nanoparticles.

## REFERENCES

[1] Pankhurst Q.A., Connolly J., Jones S.K., Dobson J., Applications of magnetic nanoparticles in biomedicine, *Journal of Physics D: Applied Physics*, 36: 167-181 (2003)
[2] Frącek M., Podstawy diagnostyki i terapii nowotworów, *Alfamedica Press* (2008)
[3] Deptała A., Onkologia w praktyce, *Wydawnictwo Lekarskie PZWL* (2007)
[4] Demir A., Baykal A., Sozeri H., Topkaya R., Low temperature magnetic investigation of Fe3O4 nanoparticles filled into multi walled carbon nanotubes, *Synthetic Metals* 187: 75-80 (2014)

# CONCEPTION OF THE THROTTLE-RETURN VALVE FOR THE MAGNETORHEOLOGICAL FLUID

Z. Pilch and J. Domin

Faculty of Electrical Engineering, Mechatronic Department, Silesian University of Technology,
44100 Gliwice, Poland, zbigniew.pilch@polsl.pl, jaroslaw.domin@polsl.pl

***Abstract.*** *The paper presents concept of the throttle-return vale dedicated for magnetorheological fluid.*

## I. INTRODUCTION

Varying viscosity fluids (magnetorheological, electrorheological) belong to one of the groups of a smart materials. This type of fluid in magnetic field works in three different mode (flow mode, compressing mode and clutch mode) [5]. Properties of the magnetorheological fluid are determined by the shear stress τ [6] as a functions of flux density B curve – Fig.1.

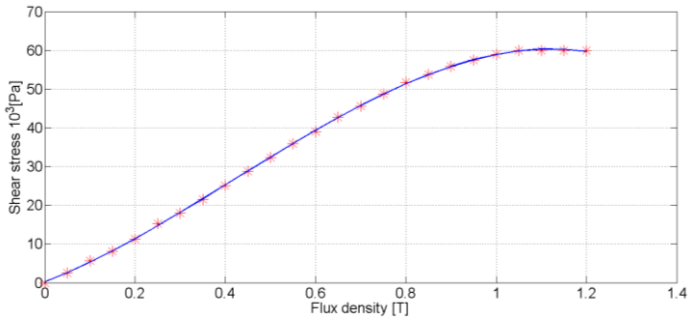


*Fig.1. The shear stress τ as a functions of flux density B curve for MRF-140CG fluid*

## II. CONCEPTION OF THE THROTTLE-RETURN VALVE

Examples of the valve for MR fluids are described in [1]. Throttle-return valves are used to adjust fluid flow in one direction and achieving the free flow in the opposite direction.

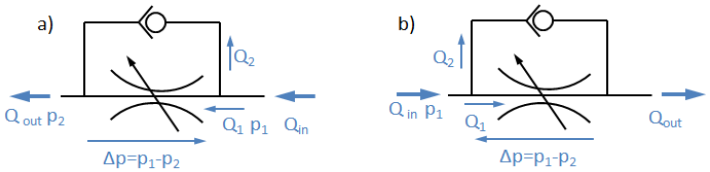


*Fig.2. Symbol of the hydraulic throttle-return valve a)* $Q_{aut} = Q_1$, $Q_2 = 0$, *b)* $Q_{aut} = Q_1 + Q_2$, *where* $Q_2 >> Q_1$

The concept of the throttle-return valve dedicated for magnetorheological fluid (MR fluid) shown in figure below.

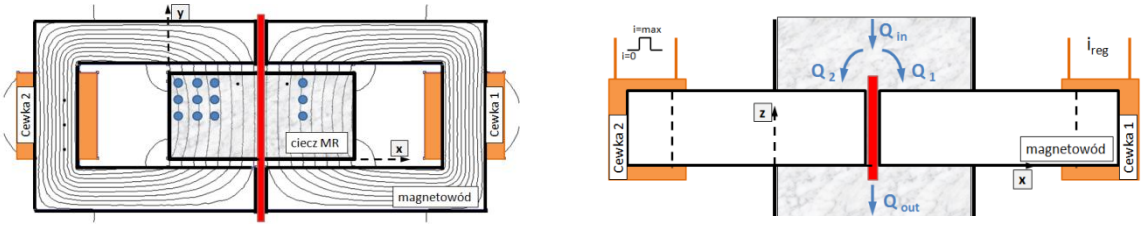


*Fig.3. The concept of the throttle-return vale dedicated for MR fluid*

The valve divides stream of the flowing fluid $Q_{in}$ into two streams $Q_1$ and $Q_2$. The stream $Q_1$ flows through the throttle valve which is responsible for the controlled fluid flow, depending on the current supply coil number 1. The stream $Q_2$ is set to 0 for the current supply coil number 2 equal $I=I_{max}$, or set to maximum value for I=0.

## III. SIMULATION RESULTS

The simulations were performed with using FEMM 4.2 and MATLAB program for: coils current I=3A, number of turns n=400. As a simulations result obtained magnetic field distribution of a duct valve cross section – see Fig.4.

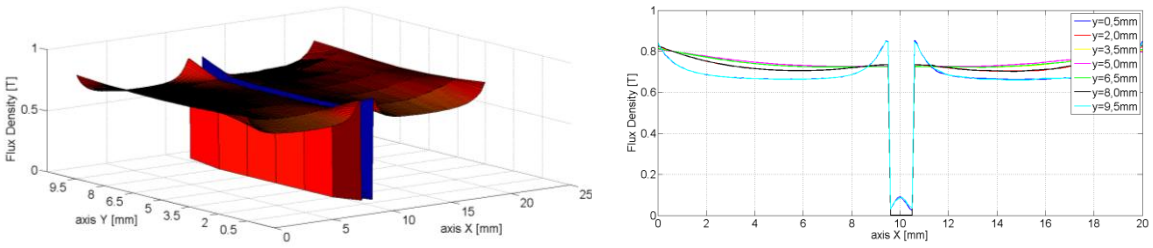


*Fig.4. Flux density distribution for both channel of the throttle-return valve*

Based on magnetic field distribution and with using Bingham's model [1] distribution of the shear stress τ for the valve return channel was determined – Fig.5.

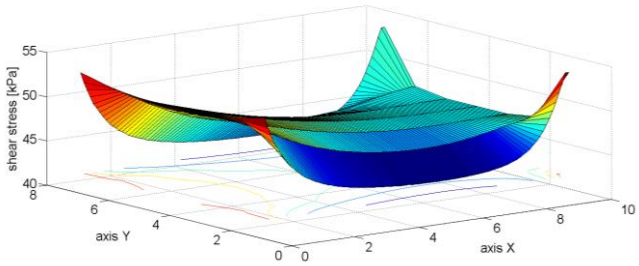


*Fig.5. Distribution of the shear stress τ for the valve return channel*

## IV. SUMMARY

The paper presents novel concept of the throttle-return valve dedicated for magnetorheological fluid. The advantages of this novel concept is lack off moving parts as in the conventional valves and possibility of reverse the stop direction and flow direction without turning the valve.

## REFERENCES


[1] Abd Fatah A.Y., Mazlan S.A., Koga T. Zamzuri H., Zeinali M. Imaduddin F., A review of design and modeling of magnetorheological valve. *International Journal of Modern Physics B* 29(04):1530004 · January 2015. DOI: 10.1142/S0217979215300042

[2] Claracq J., Sarrazin J., Montfort J.p., Viscoelastic properties of magnetorheological fluids. *Rheol Acta* (2004) 43: 38–49 DOI 10.1007/s00397-003-0318-7

[3] Szeląg W.: Electromagnetic converters with magnetorheological fluid (in polish), *Publishing House of Poznan University of Technology*, Poznań, 2010

[4] Information materials LORD Corporation: *www.rheonetic.com*

# RADIATIVE POWER BEAMING USING HIGH POWER MAGNETO-STATIC FREE-ELECTRON MASER

Y. Pinhasi

Ariel University, Faculty of Engineering, P.O. Box 3, Ariel 44837, ISRAEL, yosip@ariel.ac.il

The concept of millimeter wave radiative power transmission in the W-band is presented. The power beaming system consists of a powerful source generating radiation at 94GHz, which is fed to a transmitting dish antenna. The transmitting antenna directs the electromagnetic radiation and focuses it onto a receiving rectifying array. The rectifying antenna (rectenna) converts the received radiation into DC electrical power, which is supplied to a consumer.

Various high power radiation sources have been used in the characterization of the rectenna. Solid states devices produce relatively low power (less than 400mW), while Free-Electron laser and Gyrotrons can produce several tens of kilo-Watts and above. This enables measurements of the rectifying antenna efficiency in different operational regimes.

We will discuss the expected performances of each element, including selection of optimal radiation frequencies as well as possible variable focusing transmitting antenna configuration. The characteristics of a complete power beaming at millimeter waves will be reviewed and design aspects of rectifying antenna array will be demonstrated.

# ANGULAR AND FREQUENCY BEHAVIOR OF SOME PROPERTIES OF ELECTRICAL STEEL SHEETS

W.A. Pluta

Czestochowa University of Technology, Faculty of Electrical Engineering, Al. Armii Krajowej 17, 42-200 Czestochowa, Poland, e-mail: w.pluta@gmail.com

***Abstract.*** *Electrical steel (ES) is one of the most widely used soft magnetic material available at optimal price. Hence, it is used to build magnetic cores of large electrical machines and transformers. At design of these cores it is necessary to take into account anisotropy and frequency influence on magnetic properties of ES. The paper presents angular and frequency behavior of specific total loss and coercivity of ES.*

## I. INTRODUCTION

In the electrical industry the most widely used soft magnetic material is electrical steel. The electrical steel quality influences the efficiency of electrical machines. Magnetic anisotropy resulting from Goss texture has probably the largest influence on magnetic properties the electrical steel sheet. Modeling of both anisotropy and frequency influence on magnetic properties of electrical steel allow optimal and efficient design of electrical machines. The aim of the paper is to present the influence of anisotropy and frequency on remanence flux density, coercivity and specific loss components of electrical steel sheets.

## II. EXPERIMENTAL DATA

The experiment was carried out on grain-oriented (GO) and non-oriented (NO) electrical steel sheets. The measurements of specific total power loss were carried out in a non-standard Single Sheet Tester (SST) on square samples of 100 mm width. Determination of the specific total loss $P_S$ for loss separation purpose has been carried out in computerized system based on LabView$^{TM}$ programming platform. The schematic diagram of the used computerized system is presented in Fig.1.

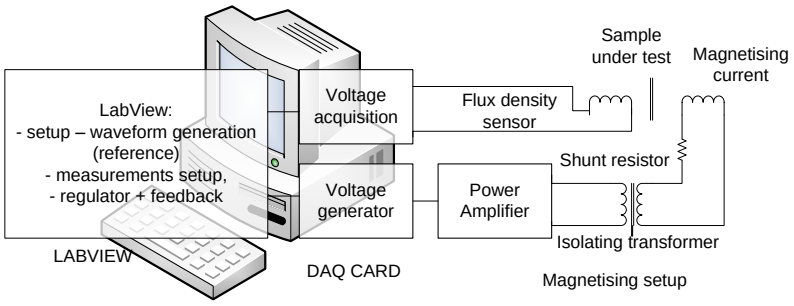


*Fig.1. Schematic diagram of the measurement setup [1]*

The flux density range was varied from 0.1 T to 1.3T - 1.8 T in dependence on magnetization direction. There were chosen 10 to 12 measurement frequencies from the range of 2 Hz to 80 Hz or 100 Hz [1]. The specific total power loss was obtained under controlled sinusoidal magnetic flux waveform and the deviation from sine wave of magnetic flux was kept well under 0.5 %.

The specific total loss of electrical steel consists of three components: hysteresis loss component $P_h$ and both additional $P_a$ and classical $P_e$ eddy current loss components. The additional loss component was described in statistical loss model proposed by G. Bertotti [2]. First two components hysteresis $P_h$ (Fig. 2a) and additional $P_a$ eddy current loss depend on magnetic

anisotropy and carried out calculations [3] show that the statistical loss model could be used also for other directions than RD except the transverse direction (TD) due to different domain structure. Both hysteresis loss $P_h$ and additional loss $P_a$ as a function of the maximum magnetic flux density $B_m$ fulfil power-law relationship.

The power low can be also used for modelling of frequency behaviour of other magnetic properties as for example remanence or coercivity presented in Fig. 2b). The equation describing frequency behaviour of each magnetic property is different but it could be used the same for different magnetisation directions as for RD.

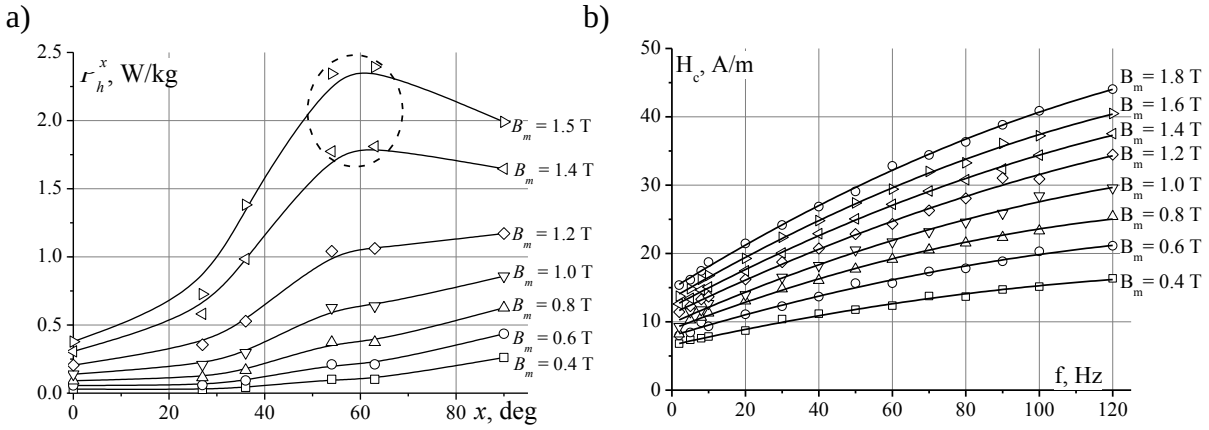


*Fig.2. a) Angular dependence of hysteresis $P_h$ specific total loss component and b) frequency dependence of coercivity measured along RD at different flux densities $B_m$ and at 50 Hz for electrical steel sheet grade M150-27S. Made by a dotted line circles mark the extrapolated points*

Angular dependence of hysteresis $P_h$ component of specific total loss clearly show influence of magnetic anisotropy. The influence of anisotropy can be separated into two regions of flux density differentiate by loss mechanisms that occurs in both regions. At low flux density region, up to about 1.1 T, both hysteresis $P_h$ (Fig. 2a) and additional $P_a$ (not shown) loss components continuously increase with increasing angle *x*. At high flux density region, above about 1.1 T, both components increase with increasing angles *x* up to 45° and then both components decrease up to angle $x = 90°$ and faster as flux density increases.

## III. CONCLUSIONS

An accurate measurement of the specific total loss of electrical steel sheets is important for characterizing and analyzing of electrical steel sheets. The magnetic properties were performed by means of non-standard SST measurement at min 10 frequencies. The magnetic properties of electrical sheets are strongly dependent on magnetic anisotropy and their frequency behaviour can be described using power-low.

## REFERENCES


[1] Pluta W.A.: Measurements of magnetic properties of electrical steel sheets for the aim of loss separation., *Journal of Electrical Engineering*, vol. 12, 2011, 122-127

[2] Berttoti G.: Hysteresis in magnetism. *Academic Press*, 1998

[3] Pluta W., Directional properties of loss components in electrical steel sheets. presented at *12th International Workshop on 1 & 2 Dimensional Magnetic Measurement and Testing*, 2012, Vienna, Austria

# MAGNETIC PROPERTIES AND STRUCTURE AND OF THE Ni-Mn-Co-In WITH THE BORON ADDITION

K. Prusik[1], E. Matyja[2], M. Kubisztal[3], M. Zubko[4], A. Chrobak[5], R. Swadźba[5]

[1,2,3,4] University of Silesia, Institute of Material Science, Bankowa 12, 40-007 Katowice, Poland
[1,2,3,4,5] Silesian Center for Education and Interdisciplinary Research, University of Silesia
75 Pułku Piechoty 1A, 41-500 Chorzów, Poland
[5]A. Chełkowski Institute of Physics, University of Silesia, Uniwersytecka 4, 40-007 Katowice, Poland
[6]Institute for Ferrous Metallurgy, Gliwice, Poland

***Abstract.*** *Series of $Ni_{45.5}$-$xCo_{4.5}Mn_{36.6}In_{13.4}B_x$ (at.%) x=0;0.05;0.1;0.5;1.0 polycrystalline magnetic shape memory alloys (MSMA) were examined in terms of the magnetic properties, structure and transition temperatures. The magnetic properties of the alloys were determined by VSM whereas the X-Ray and TEM, SEM and EBSD techniques were applied to determine the structure of alloys. Boron addition promotes nucleation of the second Co-rich and In-poor phase as well as causes decreasing of the martensitic transformation temperatures.*

## I. INTRODUCTION

Magnetic shape memory alloys exhibit reversible martensitic transformation which may be driven by temperature, external strain or magnetic field resulting in macroscopic shape change. Large recoverable strain and high frequency response make this materials promising magnetic actuators [1]. In polycrystalline alloys obtained by directional solidification, processed by high temperature plastic deformation methods [2], extrusion [3] magnetic shape memory effect can be improved. However, these alloys are very brittle. It is known, that the grain size refinement (realized e.g. by boron addition) results in an improvement of the mechanical properties [4,5]. In this paper the effect of the boron addition on the magnetic properties and structure of the $Ni_{45.5}Co_{4.5}Mn_{36.6}In_{13.4}$ (at.%) alloy was studied.

## II. RESULTS AND DISCUSSION

Polycrystalline $Ni_{45.5-x}Co_{4.5}Mn_{36.6}In_{13.4}Bx$ (at.%) x=0 (B000), 0.05 (B005), 0.1 (B010), 0.5 (B050), 1.0 (B100) alloys were produced by the induction melting and homogenized at 1173 for 24h in vacuum and subsequently quenched into icywater. Depending on the boron addition contents, two type of microstructures were observed: single phase (B000) and two phase microstructure (B010-B100) (Fig.1). The matrix shows a very coarse grain microstructure for which the grains size varies from 200 μm to several millimeters. For the two phase alloys (B005-B100) the volume fraction of precipitates increases with the boron addition. In the B100 (Fig.1b) precipitates creating kind of "subgrains" in the matrix. The average size of the second phase grains is about 1-2 μm. The boron additions also strongly influence the magnetic properties of the studied alloys. Fig. 1 shows thermomagnetization curves (i.e. the effect of applied magnetic field on the magnetization response as a function of temperature) for B000 (Fig.1a) and B100 (Fig.1b) alloys measured under several magnetic fields (0.5-70 kOe). For B000 sample under magnetic field of 500 Oe, the austenite to martensite transformation started at 270 K ($M_s$) and finished at 262 K ($M_f$) upon cooling. The reverse martensite transformation started at 278 K ($A_s$) and finished at around 287 K ($A_f$) upon heating. As one can see up to the 20 kOe transformation is fully reversible with a relatively small thermal hysteresis (about 15 K at 500 Oe). As the applied magnetic field increased from 500 Oe to 70 kOe, the transformation temperatures decreased; e.g., $M_s$ decreased from 270 to 147 K.

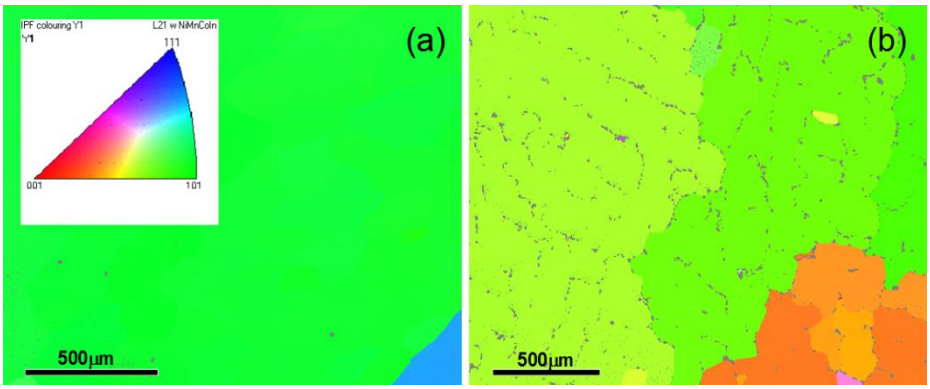


*Fig.1. EBSD Orientation Image Maps of B000 (a) and B100 (b) alloys*

The decrease of the martensite characteristic temperatures with the magnetic field is mainly due to the fact that the applied magnetic field favors the phase with the higher saturation magnetization which for this alloy is austenite. On the other hand, when the content of boron is above the certain value (in this work about 0.5at.%B the transformation is hindered).

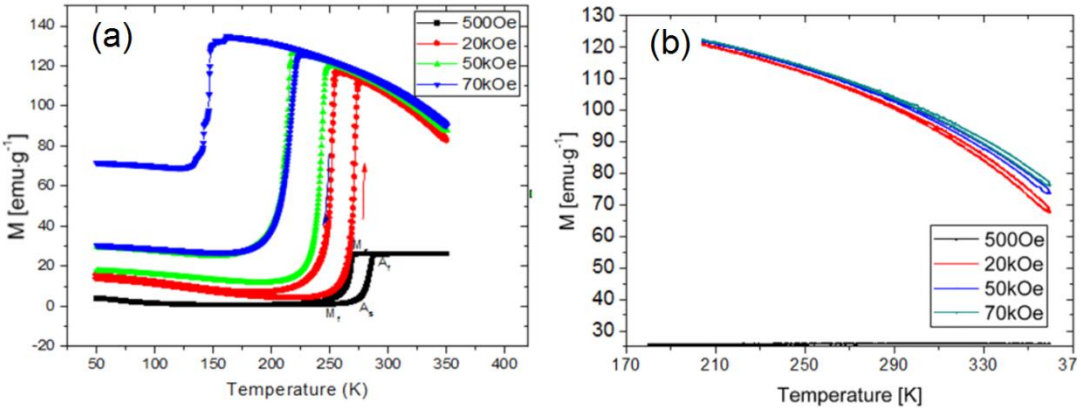


*Fig.2. Magnetization vs temperature curves of B000 (a) and B100 (b) alloys*

So for the alloys B050 and B100 no martensitic transformations were observed (Fig. 2b). This is because during the precipitation process majority of cobalt atoms dissolved in the matrix diffuses to the precipitates and the electron to atom ratio (e/a) of the matrix became lover and as a result the martensitic transformation temperatures decreases as well. It was proved by EDX chemical analysis.

To sum up, the main conclusion is that magnetic and structural properties of the Ni-Co-Mn-In metamagnetic shape memory alloys can be controlled by combination of the applied magnetic field and boron addition.

## REFERENCES

[1] Ulakko K., et. al., *Mater. J. Mater. Engin. Perform.* 5 (1996), 405-409
[2] Morawiec H., Goryczka T., Drdzeń A., Lelątko J., Prusik K., *Solid State Phenomena* Vol. 154 (2009) 133-138
[3] Prusik K., Bałdys K., Stróż D., Goryczka T., Lelątko J., *Solid State Phenomena* 203-204 (2013) 306-309
[4] Tamirisakandala S., et. al., *Scr. Mater.* 53 (2005) 1421–1426
[5] Ramudu M., Satish Kumar A., Seshubai V., *Intermetallics* 28 (2012) 51-57

# MECHANICAL PROPERTIES OF SOFT MAGNETIC COMPOSITES AT THE TEMPERATURE OF LIQUID NITROGEN

M. Przybylski, D. Kapelski and B. Ślusarek

Tele & Radio Research Institute, Ratuszowa 11 St, 03-450 Warsaw, Poland,
marek.przybylski@itr.org.pl, dariusz.kapelski@itr.org.pl, barbara.slusarek@itr.org.pl

***Abstract.*** *Soft magnetic composites are used in a wide range of applications working in different environmental conditions, between others, in different temperatures. Nowadays devices often work at cryogenic temperatures. The paper shows influence of liquid nitrogen temperature on mechanical properties of soft magnetic composites prepared from ABC100.30 iron powder bonded by epoxy resin.*

## I. INTRODUCTION

Soft magnetic materials are used for preparation of magnetic circuits of electromagnetic and electromechanical devices. Nowadays electrical steels are mainly used as soft magnetic material for preparation of magnetic circuits of electric motors. Electric motors manufacturers are looking for new materials with better physical properties or/and easier to technological application in a magnetic core. Powder metallurgy gives possibility to prepare new materials for the development of electric machines.

Soft magnetic composites (SMC), called also dielectromagnetics consists of ferromagnetic particles distributed in a matrix of binding agent. Parts made of magnetic composites are prepared by compression moulding technique which involves compaction of powder in a die under high pressure. In the next step, 'green compacts' are cured in a furnace at melting temperature of binding agent for the increase of their mechanical strength.

The basic material for preparing soft magnetic composites are iron powder. The main feature of these materials is that iron particles are insulated by a thin organic or inorganic coating. Particles insulation can be made during particles making or by preparing mixture of iron powder and e.g. resin powder before compression.

Electric motors in drive of pumps operate in liquid gas atmospheres and are applied in devices for transport and storage of liquid gases such as: nitrogen, hydrogen or oxygen [1-3].

All materials, including magnetic materials change physical properties with changing temperature. Changes of physical properties of magnetic circuit of electric motors influence operational parameters of machines.

## II. EXPERIMENTS

Specimens investigated in the study were produced from commercially available pure iron powder type ABC100.30 (Höganäs AB Company). Preparation of composite elements made of this powder require adding a bonding material. For this purpose epoxy resin Epidian 100 (CIECH Sarzyna S.A.) was selected. Mixture of iron powder, resin in a form of powder and zinc-stearate lubricant (0.1 wt. %) were prepared. The samples with contents 0.25, 0.50 and 0.75 wt. % of resin were made. Then mixture was pressed in a die. The compacting pressure for all samples was 800 MPa. "Green compacts" were hardened in a furnace in a temperature 190°C in air atmosphere, at 120 minutes.

Mechanical properties such as: compressive strength and bending strength were measured at room and liquid nitrogen temperature (-195.8°C).

The results of testing compressive strength of samples are presented in Table 1. For comparison purpose value of compressive strength for soft magnetic composites Somaloy 700

(Höganäs AB Company) and AncorLam (Hoeganaes Corporation) are shown [4]. Somaloy 700 and AncorLam powders have insulation applied on particles in process of preparation of powder.

*Table 1. Compressive Strength of Soft Magnetic Composites at Different Temperatures*

| Type of powder | Content of epoxy resin (wt. %) | Compressive strength at 20°C | Compressive strength at -195.8°C |
|---|---|---|---|
| ABC100.30 | 0.25 | 205 | 578 |
| ABC100.30 | 0.50 | 223 | 601 |
| Somaloy 700 | - | 513 | 804 |
| AncorLam | - | 304 | 779 |

Bending strength called also transverse rapture strength (TRS) of prepared samples from ABC.100.30 was measured in room and liquid nitrogen temperature. Results are presented in table 2. There are presented in the table values of transverse rapture strength composites from Somaloy 700 and AncorLam powders for comparison purpose [4].

Table 2. Transverse Rupture Strength (TRS) of Soft Magnetic Composites at Different Temperatures

| Type of powder | Content of epoxy resin (wt. %) | TRS at 20°C | TRS at -195.8°C |
|---|---|---|---|
| ABC100.30 | 0.25 | 62.8 | 118.4 |
| ABC100.30 | 0.50 | 77.7 | 150.4 |
| ABC100.30 | 0.75 | 99.4 | 159.6 |
| Somaloy 700 | - | 37.5 | 54.9 |
| AncorLam | - | 32.9 | 55.3 |

## III. CONCLUSION

The results of investigation show that mechanical properties of soft magnetic composites increase with decreasing temperature from room to liquid nitrogen temperature. It means that this type of material, from this point of view can be used in devices working in nitrogen temperatures. The changes of mechanical properties of soft magnetic composites depend on the type of binding agent and method of preparing powder with binding material, by covering iron powder by binder during production of powder or by preparing mixture of iron powder with binding agent before compression.

## REFERENCES


[1] Walker I.R., Small dc motor for producing motion in a cryogenic environment, and a method for monitoring its orientation, *Review of Scientific Instruments*, vol. 64, no. 3, 1993, pp. 814-820

[2] Kołowrotkiewicz J., Barański M., Szeląg W., Długiewicz L., FE analysis of induction motor working in cryogenic temperature, *COMPEL: The International Journal for Computation and Mathematics in Electrical and Electronic Engineering*, vol. 26, no. 4, 2007, pp. 952-964

[3] Abe Y., Nakagawa A., Watada M., Torii S., Yamane K., Ebihara D., Basic characteristics of linear oscillatory actuator for liquid hydrogen pump, *IEEE Transactions on Magnetics*, vol. 32, no. 5, 1996, pp. 5025-5027

[4] Kapelski D., Jankowski B., Przybylski M., Ślusarek B., The influence of the temperature of liquid nitrogen on the physical properties of powder magnetic composites, *Archives of Metallurgy and Materials*, vol. 60, no. 2, 2015, pp. 1323-1326

# AN INFLUENCE OF THE TEMPERATURE AND MAGNETIC CORE SATURATION ON THE INDUCTANCE FREQUENCY CHARACTERISTIC OF AN INDUCTION MACHINE

J. Rolek[1], G. Utrata[2] and A. Kaplon[1]

[1] Kielce University of Technology, Power Electronic, Electrical Machines and Drives Chair, Aleja 1000-lecia Panstwa Polskiego 7, 25-314 Kielce, Poland, e-mail: jrolek@tu.kielce.pl, akaplon@tu.kielce.pl
[2] Czestochowa University of Technology, Institute of Environmental Engineering, J.H. Dabrowskiego 73, 42-201 Czestochowa, Poland, e-mail: gutrata@is.pcz.pl

***Abstract.*** *Algorithms for induction machine angular velocity, torque and flux estimation, developed by the authors of the article, are based on the knowledge of the primary inductance frequency characteristic (PIFCh) of the machine. The authors analyze the influence of the temperature and magnetic core saturation on the shape of the frequency characteristic and provide a way to take into account changes of these parameters in the secondary multi-loop equivalent circuit of an induction machine*

## I. INTRODUCTION

The PIFCh most fully reproduces variability of electromagnetic parameters of an induction machine and therefore can be used for estimating of selected electromagnetic and mechanical quantities of this machine required in regulation and control systems of sensorless AC drives. The variability of electromagnetic parameters, caused mainly by the the skin effect in rotor bars, follows also from that fact that these parameters are also a function of the electrical conductivity and magnetic permeability.

A good approximation of the inductance frequency characteristic is obtained by means of a machine secondary multi-loop equivalent circuit of the (Fig. 1). The method of construction of such equivalent circuit is given in [1].

## II. PRIMARY INDUCTANCE FREQUENCY CHARACTERISTIC

The PIFCh, which is defined as the ratio of the magnetic flux linkage of the primary winding in the air gap to the current flowing trough that winding, can be determined by computational methods. The degree of adequacy of the obtained characteristics in relation to the measured ones depends on the adopted computational model of induction machine.

This characteristic can also be achieved by measurement according to the formula (1):

$$\frac{\underline{U}_1\ \omega_1\ /\underline{I}_1\ \omega_1, s\ -R_1}{\mathrm{j}\omega_1} = \underline{L}_1\ \omega_2\ = L_{1\sigma} + \underline{L}_{1\delta}\ \omega_2 \tag{1}$$

where: $\underline{U}_1(\omega_1)$, $\underline{I}_1(\omega_1,s)$ – stator voltage and current space vectors, respectively, $\omega_1$ – stator supply angular frequency, $s$ – motor slip, $R_1$, $L_{1\sigma}$ – stator phase winding resistance and leakage inductance, respectively, $\underline{L}_{1\delta}(\omega_2)$ – inductance associated with the magnetic flux in the motor air gap, $j^2$=-1.

Study was carried out for the induction motor SG 132S-4 with parameters: 5.5 kW, 400 V, 11 A, 1450 rpm, rotor length 114 mm, rotor diameter 133.3 mm, air gap length 0.35 mm. The magnetic core of the motor is made of steel M600-50A. The variability of the module and argument of the actual motor inductance in the motor slip range of $|s|\leq 0.2$ and the corresponding circle-shaped characteristic are depicted in Fig. 3 and 2, respectively, by the black line. They are in the good agreement with the characteristics obtained from the equivalent circuit with eight two-terminals on the secondary ($N_0 = 8$, Fig. 1), [2], [3]. These characteristics are the reference ones for which the assumed temperature and relative permeability are 30˚C and 6678, respectively.

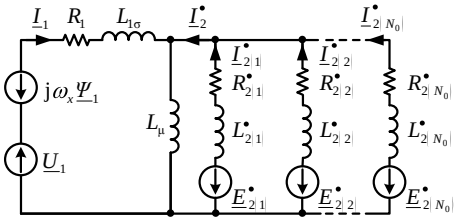


*Fig.1. Machine secondary multi-loop equivalent circuit*

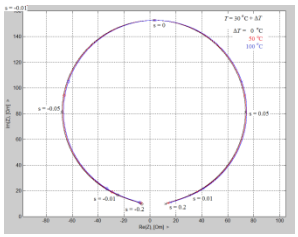

*Fig.2. Circle-shaped characteristic*

*a)* *b)*

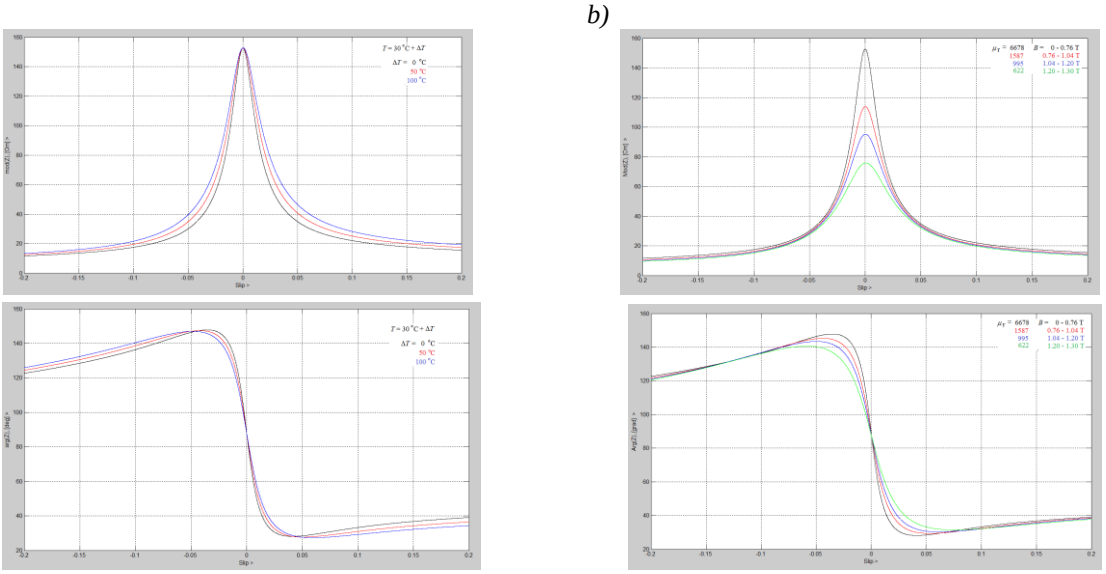

*Fig.3. Primary inductance frequency characteristics as a function of: a) temperature, b) permeability*

In these figures, the effect of the machine heating and of the magnetic core saturation is also shown by changing the parameters in equivalent circuit according to the formulas: for resistance $R_{(30+\Delta T)} = R_{30}(1+\alpha_{Al}\cdot\Delta T)$ and for inductance $L_{\mu_{rp}} = L_{\mu_r}\ (l_\delta + l_{Fe}/\mu_r)/(l_\delta + l_{Fe}/\mu_{rp})$, where: $\alpha_{Al}$ - resistance temperature coefficient [K$^{-1}$], $l_\delta$, $l_{Fe}$ - path length for the magnetic flux in the air gap and iron, respectively [m], $\mu_r$, $\mu_{rp}$ - relative permeability.

## III. CONCLUSIONS

Temperature of the electric circuits and saturation of the magnetic core of the induction machine affect its slip dependent characteristics of the primary inductance module and argument.

For the estimation of electromechanical quantities in the range of angular velocity corresponding to the slip $|s| \le s_n$ it is convenient to use the inductance argument, while for the slip $|s| > s_n$ the inductance module.

## REFERENCES


[1] Kapłon A., Estymacja parametrów elektromagnetycznych określających stany elektrodynamiczne maszyn prądu przemiennego analizowanych za pomocą modeli wielowarstwowych, Monografia, *Wydawnictwo PŚk*, Kielce, 2003, str. 171

[2] Utrata G., Rolek J., Kaplon A., The Genetic Algorithm for an Electromagnetic Parameters Estimation of an Induction Motor Secondary Multi-Loop Equivalent Circuit", *IREE*, vol. 9 no. 6, 2014, pp. 1111-1118,. DOI:10.15866/iree.v9i6.4599

[3] Rolek J. , Utrata G. , Kaplon A. , Estimation of Electromagnetic Parameters of an Induction Motor Multi-loop Equivalent Circuit Based on the Machine Inductance Frequency Characteristic, *Proc. of WZEE 2015*, Kielce, 2015, Poland, pp. 141-146, DOI:10.1109/WZEE.2015.7394018

# RECENT STATE OF RESEARCH ON COMPRESSIVE AND TENSILE STRESSES INFLUENCE ON MAGNETIC PROPERTIES OF AMORPHOUS MATERIALS

J. Salach

Institute of Metrology and Biomedical Engineering, Warsaw University of Technology,
Warsaw, Poland, j.salach@mchtr.pw.edu.pl

***Abstract.*** *The paper presents the recent state of research on compressive and tensile stresses influence on the magnetic properties of selected amorphous materials with different composition. The materials represent the most important group of magnetic materials allowing to generalize the impact of stress on the magnetic properties of metallic glasses.*

## I. INTRODUCTION

The development of amorphous magnetic materials created new possibilities with regard to further development of magnetoelastic sensors. The main differences between amorphous magnetic materials and crystalline magnetic materials are their higher magnetic permeability μ, lower coercive field intensity $H_c$ and higher mechanical strength. Mechanical strength is particularly significant in case of magnetoelastic sensor core use. Magnetically soft amorphous magnetic materials are usually built in form of a thin ribbon, about 25μm thick, or a wire of about 125 μm diameter, which results in limiting the shape of cores made of those materials to rings made of ribbons. Ring-shaped cores are commonly used in constructing inductive components. However, using them as magnetoelastic sensor cores causes serious difficulties. It is a problem to obtain a closed magnetic circuit and uniform stress distribution in the core at the same time. Only solution proposed by the author allowed fulfilling both of these conditions.

## II. TECHNICAL INSTRUCTIONS

In the papers up to now concentrated on researching magnetoelastic properties of state of the art magnetic materials – amorphous alloys. Within the scope of presented research author show a general description of magnetoelastic $B(\pm\sigma)_H$ characteristics for this magnetic material class. The research described in papers covered amorphous magnetic materials with various physical and chemical properties:

- cobalt based [1], with low negative saturation magnetostriction coefficient $\lambda_s$ (below 1μm/m) and very high magnetic permeability $\mu_r$ in the region of $10^6$,
- cobalt based with addition of iron [3], with saturation magnetostriction coefficient $\lambda_s$ close to zero and very high magnetic permeability $\mu_r$ in the region of $5 \cdot 10^4$,
- iron based [2, 4, 6, 9, 10], with high positive saturation magnetostriction coefficient $\lambda_s$ (over 35 μm/m) and high saturation induction $B_s$, up to 1,5 T,
- iron and nickel based [2, 5, 7, 8, 11], with positive saturation magnetostriction coefficient $\lambda_s$ (around 15 μm/m) and possibility to create induced magnetic anisotropy under thermal relaxation.

The comparison of conducted research with regard to alloys both as-quenched and after thermal relaxation carried out in selected cases with external magnetic field present. The investigated amorphous magnetic materials represent the most significant amorphous magnetic material groups varying in terms of physical and chemical composition, as well as in terms of varying saturation magnetostriction coefficient $\lambda_s$. Varying saturation magnetostriction coefficient $\lambda_s$ is important because of the function of magnetostriction in a magnetoelastic phenomenon, since sign and value of this coefficient define the position of the Villari point in magnetoelastic $B(\pm\sigma)_H$ characteristics.

With regard to amorphous magnetic materials, the conducted research made it possible to provide a general description of magnetoelastic $B(\pm\sigma)_H$ characteristics and new guidelines regarding choosing the composition of these alloys for magnetoelastic sensor cores. As the result of described works a completely new method for assessment of the influence of stresses on processing characteristics of current transformers was developed [1]. The developed methodology makes it possible to relate magnetoelastic characteristics of current transformer cores to their processing characteristics during current measurement. It was proved that such alloys are fit for current transformer cores only under the condition that they are not to be subjected to influence of tension from external forces. The magnetic material proposed in the publication has high magnetoelastic sensitivity, which makes it potentially fit for use as a stress sensor core.

## REFERENCES


[1] Salach J., Stresses influence on magnetic characteristics of amorphous ring cores for current transducers, *Journal of Electrical Engineering*, 2015, Vol. 66, No. 7s, 41–44

[2] Salach J., Magnetoelastic effect for three type magnetic materials under torque load, *Advances in Intelligent Systems and Computing*, 2015, Vol. 393, 515–520

[3] Salach J., Szewczyk R., Svec Sr P., Bieńkowski A., Jackiewicz D., Svec P., Nowicki M., Winiarski W., Kachniarz M. and Gruszecka M. The influence of thermomagnetic treatment on the magnetoelastic characteristics of Fe61Co19Si5B15 amorphous, *Acta Physica Polonica A*, 2015, Vol. 127, 617–619

[4] Salach J., Jackiewicz D., Bieńkowski A., Szewczyk R., Gruszecka M., Amorphous soft magnetic Fe80B11Si9 alloy in tensile stress sensors application, *Acta Physica Polonica A*, 2014, Vol. 126, 102–103

[5] Salach J., Szewczyk R., Bieńkowski A., Frydrych P., Methodology of testing the magnetoelastic characteristics of ring-shaped cores under uniform compressive and tensile stresses, *Journal of Electrical Engineering*, 2010, Vol. 61, No. 7s,93–95

[6] Salach J., Jackiewicz D., Bieńkowski A., Nowicki M., Gruszecka M., Influence of tensile force on magnetic properties of amorphous $Fe_{80}B_{11}Si_9$ alloys in different states of thermal relaxation, *Advances in Intelligent Systems and Computing*, 2014, Vol. 267, 665–675

[7] Szewczyk R., Švec Sr. P., Salach J., Svec P., Bieńkowski A., Hosko J., Jackiewicz D., Kamiński M., Winiarski W., Influence of thermomagnetic treatment on magnetoelastic properties of FeNiMoB amorphous alloy, *Acta Physica Polonica A*, 2014. Vol. 126, No.1, 52–53

[8] Bieńkowski A., Salach J., Szewczyk R., Kolano R. The magnetoelastic characteristics of $Fe_{70}Ni_8Si_{10}B_{12}$ amorphous alloy subjected to thermo-magnetic treatment, *Acta Physica Polonica A*, 2008, Vol. 113, 87–91

[9] Salach J., Szewczyk R., Bieńkowski A., Jackiewicz, D. Possibilities of application of amorphous $Fe_{77}Cr_2B_{16}Si_5$ alloys in different states of thermal relaxation as magnetic tensile force sensors, *Solid State Phenomena*, 2013, Vol. 198, 388–393

[10] Salach J., Szewczyk R., Bieńkowski A., Nowicki M. Tensile stress sensor with amorphous ring shape core, *Solid State Phenomena*, 2015, Vol. 220–221, 515–519

[11] Szewczyk R., Bieńkowski A., Salach J., The temperature dependence of the magnetoelastic characteristics of cores for force sensors utilizing $Fe_{70}Ni_8Si_{10}B_{12}$ amorphous alloy, *PRAMANA Journal of Physics* 2008, Vol. 71, 591–597

# SIMULATION AND INVESTIGATION OF THE MICRO-DISPLACEMENT ACTUATOR WITH MAGNETOSTRICTIVE ROD

D. Stachowiak and A. Demenko

Poznań University of Technology, Piotrowo 3a, 61-138 Poznań, Poland,
e-mail: Dorota.Stachowiak@put.poznan.pl, Andrzej.Demenko@put.poznan.pl

***Abstract.*** *The paper presents the experimental and numerical investigation of the output characteristics of the giant magnetostrictive actuator. To determine the distribution of the magnetic and the mechanical fields the finite element method was used. In the proposed model the coupling of magnetic and mechanical field has been taken into account. The obtained results of simulations and their comparison with the measurements show that the applied method is sufficiently accurate.*

## I. INTRODUCTION

The most popular giant magnetostrictive material (GMM) is the Terfenol-D, an alloy made of iron (Fe) and two rare earth elements terbium (Tb) and dysprosium (Dy). The two main areas of Terfenol-D applications are actuators and sensors. Giant magnetostrictive actuators (GMA) are used in high-class industrial devices (linear motors, micropumps, microvalves, micropositioners, etc.), biomedical applications and arm industry [1].

Magnetostriction is the change in shape of materials under the influence of an external magnetic field. The simplest form of the GMA consists of a cylindrical rod which is magnetically excited by a coil surrounding the rod to generate strain and force. The GMA exhibits nonlinear behavior and magneto-mechanical coupling characteristic. In order to design the GMA, an accurate modeling of their characteristic is necessary. Usually, to determine the distribution of the magnetic and the mechanical fields the finite element method was used.

The paper presents a finite element (FE) model of the GMA. The model is based on the equations of electromagnetic field and Navier's equations for mechanical systems. The equations are coupled using a nonlinear magneto-mechanical constitutive law for Terfenol-D.

## II. MAGNETO-MECHANICAL EQUATIONS

In magnetostrictive material the strain $\boldsymbol{\varepsilon}$ and the magnetic flux density $\boldsymbol{B}$ are functions of the stress $\boldsymbol{\sigma}$ and the magnetic field intensity $\boldsymbol{H}$. The behavior of magnetostrictive materials is described with nonlinear relations $\boldsymbol{\varepsilon} = \boldsymbol{\varepsilon}(\sigma, \boldsymbol{H})$, $\boldsymbol{B} = \boldsymbol{B}(\sigma, \boldsymbol{H})$ [1]. Here, the total strain tensor $\boldsymbol{\varepsilon}$ is the sum of the elastic strain $\boldsymbol{\varepsilon}_e$ and the magnetostrictive strain $\boldsymbol{\varepsilon}_{ms}$, i.e. $\boldsymbol{\varepsilon} = \boldsymbol{\varepsilon}_e + \boldsymbol{\varepsilon}_{ms}$. Only the elastic strain contributes to mechanical stress [1, 2]. According to Hook's law, the stress tensor $\boldsymbol{\sigma}$ is described as follows,

$$\boldsymbol{\sigma} = \boldsymbol{C}\boldsymbol{\varepsilon}_e = \boldsymbol{C}\boldsymbol{\varepsilon} - \boldsymbol{C}\boldsymbol{\varepsilon}_{ms}\,, \tag{1}$$

where $\boldsymbol{C}$ is the 6x6 stiffness tensor widely used in structural analysis. The second component of (1) represents blocked stress $\boldsymbol{\sigma}_{block}$ of a material, $\boldsymbol{\sigma}_{block} = -\boldsymbol{C}\,\boldsymbol{\varepsilon}_{ms\_\max}$.

Very often the magnetostrictive strain is modeled using the linear constitutive relation $\boldsymbol{\varepsilon}_{ms} = \boldsymbol{d}\,\boldsymbol{H}$, where $\boldsymbol{d}$ is the piezo-magnetic strain matrix. However, in reality, the relation between strain $\boldsymbol{\varepsilon}_{ms}$ and intensity $\boldsymbol{H}$ is nonlinear. In the paper, the relation proposed in [3] is applied.

$$\boldsymbol{\varepsilon}_{ms} = \frac{3}{2}\boldsymbol{\lambda}_S\left(\frac{\boldsymbol{\chi}_m \boldsymbol{H}}{M_S}\right)^2, \tag{2}$$

where $\boldsymbol{\lambda}_S$ is the saturation magnetostriction, $M_S$ is the saturation magnetization, and $\boldsymbol{\chi}_m$ is the magnetic susceptibility [3]. The relationship between the strain and displacement $\boldsymbol{u}$ has been expressed as, $\boldsymbol{\varepsilon} = \boldsymbol{D}\boldsymbol{u}$, where $\boldsymbol{D}$ is the strain-displacement (symmetric-gradient) matrix [2].

## III. RESULTS AND CONCLUSIONS

The brittle nature of Terfenol-D and its poor machinability restricts its availability to geometries like cylindrical rods (Fig. 1). The axisymmetrical GMA has been considered. The main components of the actuator consist of a cylindrical Terfenol-D rod, a wound excitation coil and a prestress spring washer. Application of proper compressive prestress increases the value of the maximum strain. The computations have been performed in an axial-symmetric domain with cylindrical coordinates ($r$, $z$, $\vartheta$). The elaborated nonlinear magnetostrictive model has been implemented in the commercial FE package. It has been assumed that GMA is supplied from a DC power source. It should be noted that the calculation have been preceded by the measurement of nonlinear characteristics of the materials applied in the FE model - Fig. 2.

In Figs. 3 and 4 the selected results of calculation have been given. The calculated values of the output displacement of the GMA have been compared with measured values – see Fig. 3. Fig. 4 shows the blocked force of the GMA as a function of supply current. To determine a blocked force, the Terfenol-D rod is considered to be clamped.

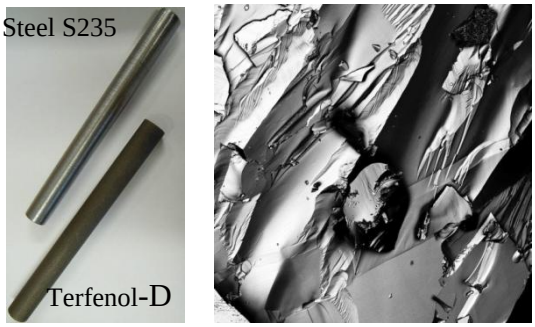


*Fig.1. The sample of Terfenol D and steel S235 (a), Kerr microscope image of surface of Terfenol D (b)*

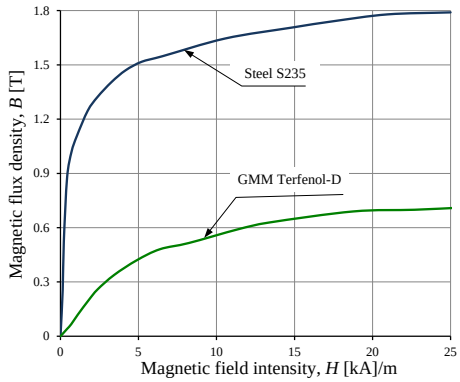


*Fig.2. Measured magnetization characteristic of the materials used in the FE model*

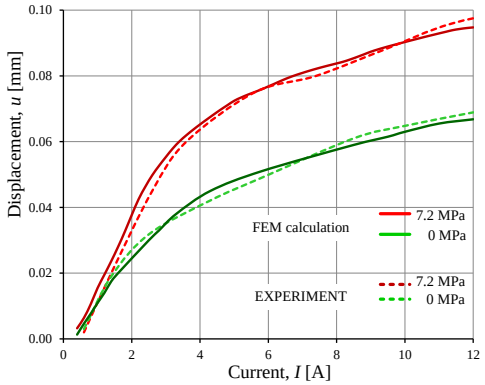


*Fig.3. The displacement of the GMA vs. the supply current*

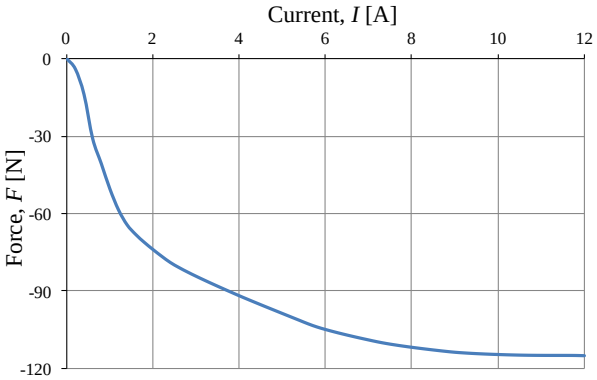


*Fig.4. The blocked force of the GMA vs. the supply current*

The obtained results and their comparison with the measurements show that the proposed model is sufficiently accurate. Thus, the model can be successfully applied in the analysis and design of axisymmetrical magnetostrictive actuators.

## REFERENCES


[1] Engdahl G., Handbook of giant magnetostrictive materials. San Diego, USA, *Academic Press*, 2000

[2] Stachowiak D., Finite element analysis of the active element displacement in a giant magnetostrictive transducer, *COMPEL*, Vol. 35 Iss. 4, pp.1371 - 1381, 2016

[3] Cullity B.D., Graham C.D., Introduction to Magnetic Materials, *Wiley-IEEE Press*, 2008

# HOW TO PERFORM THE ACCURATE MAGNETIC MEASUREMENTS – PHYSICAL INTERPRETATION AND PRACTICAL IMPLEMENTAION

A. Stupakov

Institute of Physics, Czech Academy of Sciences, Na Slovance 2, 18221 Prague, Czech Republic
stupak@fzu.cz, www.fzu.cz\~stupak

Recently we developed a unique system for physically accurate measurement of the magnetic hysteresis, the magnetic Barkhausen noise (BN) and the magneto-acoustic emission. A novelty of this setup consists in a combination of two main features: a precise local determination of the magnetic field and a feedback control of the magnetization process. First, the tangential components of the surface magnetic field are measured by two Hall sensors at different distances above the sample. The sample field is determined by a linear extrapolation of these measured fields to the sample surface (see Fig. 1). Second, a digital feedback loop adjusts the time dependence of the magnetic induction or field. The feedback algorithm combines two classical methods of magnetizing signal adjustment: linear corrections of the magnetizing voltage amplitude and phase. This measurement approach provides stable and physically accurate results, which are independent of a specific experimental configuration. In particular, the measurements can be correctly performed in the magnetically open configurations, which was considered to be a real technical challenge so far (see Fig. 2) [1,2].

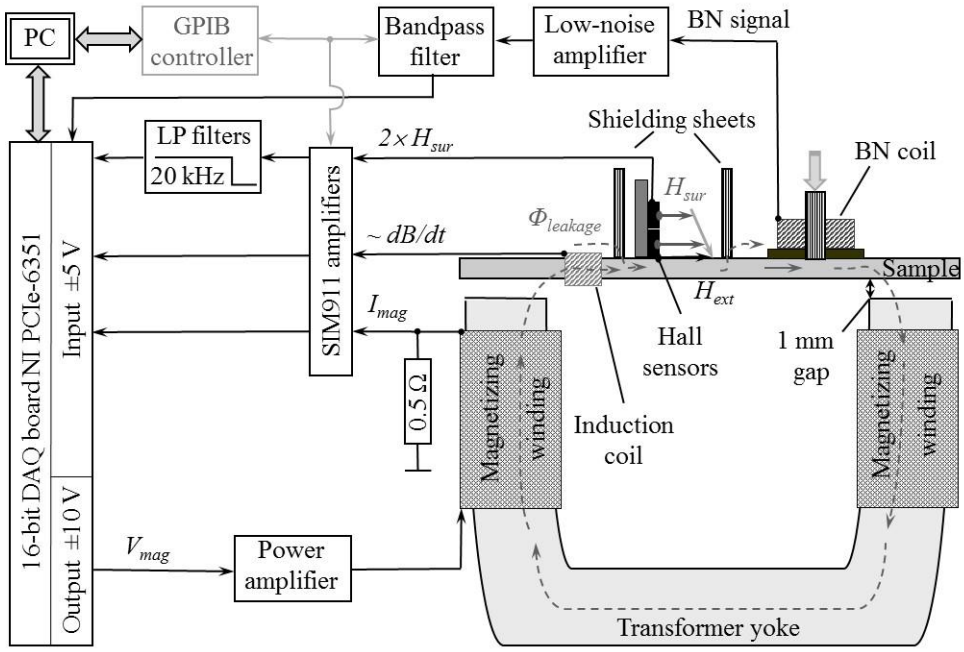


*Fig.1. Block schemes of the magnetizing–sensing unit and the measurement setup*

An efficiency of the developed measurement system was extensively tested for a wide scale of the magnetization conditions: different open/closed magnetization circuits, the sinusoidal/triangular shapes of the controlled field/induction waveforms, magnetizing frequencies in the range 0.1-200 Hz as well as for different industrial materials from the magnetically softest melt-spun ribbons and electrical steels to the relatively hard spring/TRIP steels. This gave principally new results, which should activate debates about the principles of the industrial magnetic testing, further development of the measurement standards and the magnetic non-destructive techniques. In particular, a strong linear relation between our hysteresis measurements of the soft electrical steels

in the magnetically open configurations and the standard single sheet tester data was obtained [2]. The BN signal was also stabilized with respect to an air gap between the magnetizing yoke and the tested sample (see Fig. 2). An introduced BN parameter demonstrated an improved stability to a lift-off of the sensing BN coil as well as a strong linear correlation with the hysteresis coercive field [3,4]. Our latest results demonstrated that the micro-magnetic responses, BN and the magneto-acoustic emission, are driven by the rate of change of the magnetic field *dH/dt* but not by the induction rate of change *dB/dt* as was considered before. However, the differential permeability of the tested material has an additional influence on rms profiles of the micro-magnetic signals [4].

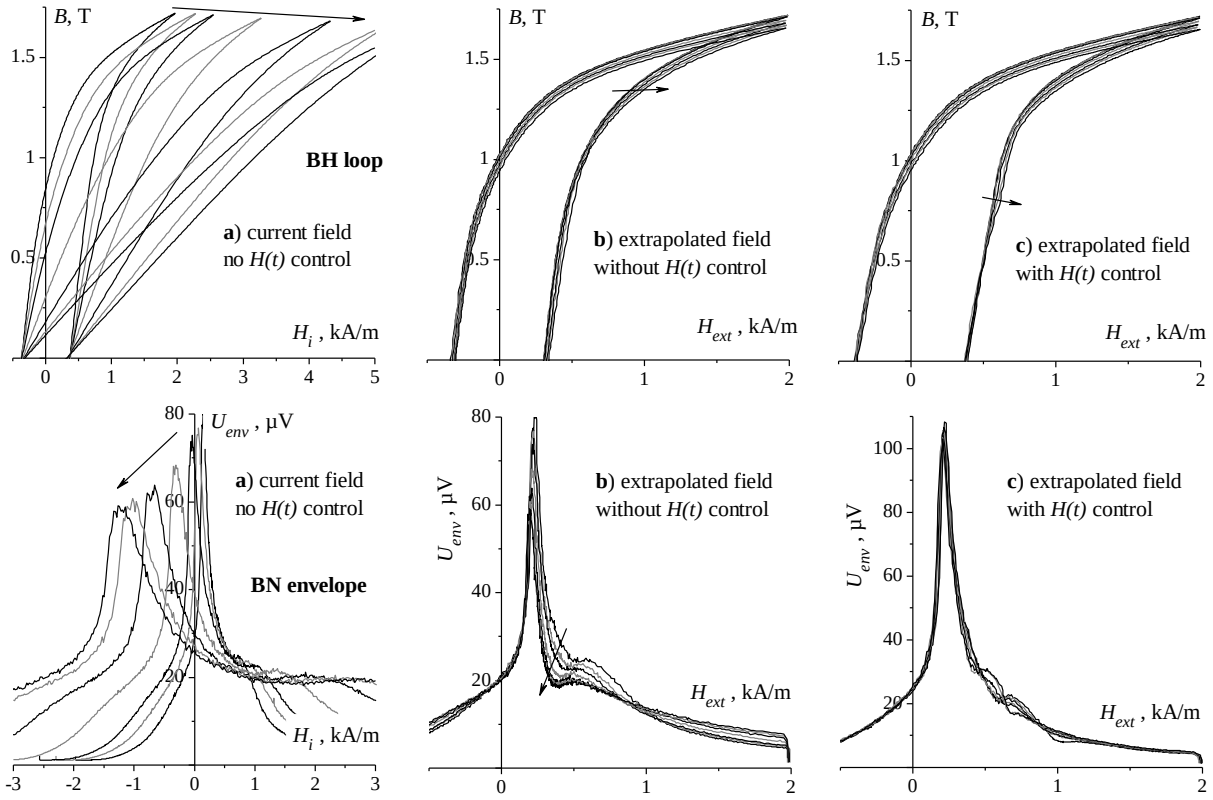


*Fig.2. Top: magnetic hysteresis loops B(H) obtained with increasing air gap between the magnetizing yoke and the tested sample for the different measurement conditions. (a) Common current field method $H_i$~$I_{mag}$ without the field waveform H(t) control. (b) Field extrapolation method $H_{ext}$ without the H(t) control. (c) Field extrapolation method $H_{ext}$ with the triangular H(t) control. Bottom: corresponding BN rms profiles $U_{env}$(H) obtained for the same measurement conditions. The yoke-sample gap is set to 0, 0.1, 0.2, 0.5, 0.75, 1.1, and 1.5 mm. The arrows indicate how the results are changed with air gap increase*

## REFERENCES


[1] Stupakov A., Perevertov O., Zablotskii V., A system for controllable magnetic measurements of hysteresis and Barkhausen noise, *IEEE Trans. Instrum. Measur.*, 65, 5, 2016, 1087 - 1097

[2] Stupakov O., Controllable magnetic hysteresis measurement of electrical steels in a single-yoke open configuration, *IEEE Trans. Magn.*, 48, 12, 2012, 4718 – 4726

[3] Stupakov O., Local non-contact evaluation of the ac magnetic hysteresis parameters of electrical steels by the Barkhausen noise technique, *J. Nondestruct. Eval.*, 32, 4, 2013, 405 – 412

[4] Stupakov O., Stabilization of Barkhausen noise readings by controlling a surface field waveform, *Measur. Sci. Technol.*, 25, 1, 2014, 015604 (8pp)

# OPEN SOURCE ELMER SOFTWARE BASED FEM MODELLING OF WAVEGUIDES AND RESONANT CAVITIES FOR MICROWAVE HEATING AND DRYING DEVICES

J. Szałatkiewicz[1], R. Szewczyk[2], M. Kalinowski[1], J. Kataja[3], P. Råback[3], J. Ruokolainen[3] and M. Kachniarz[2]

[1] Industrial Research Institute for Automation and Measurements PIAP, Al. Jerozolimskie 202,02-486 Warsaw, Poland
[2] Institute of Metrology and Biomedical Engineering, Warsaw University of Technology, sw. A. Boboli 8; 02-525 Warsaw, Poland, szewczyk@mchtr.pw.edu.pl
[3] CSC - CSC – IT center for science, P.O Box 405, FI-02101 Espoo, Finland

***Abstract.*** *Microwave devices are widely used in the industry and in the specialized laboratory analyses. Development of such devices require possibility of modeling of microwave energy distribution in the specific resonant chambers. Until now, such modeling was possible only with the use of commercial software or was limited to specific cases.*
*Paper presents open-source module for ELMER software for solving time-harmonic Maxwell's equations, allowing modelling of microwave waveguide lines. Three test cases of different resonant chambers are investigated at 2.45GHz frequency. Modelling results obtained from open-source ELMERVectorial Helmholtz module show that application of this software can be effective in R&D works, enabling high-tech small and medium enterprises involvement in advanced microwave technology.*

## I. INTRODUCTION

Modelling of key elements of developed devices is important part of development process, reducing it cost and increasing efficiency. The most flexible method of this modeling, commonly implemented in commercial development tool chains is finite element method (FEM). However, development of special devices, such as microwave chambers for heat drying e.g. in the food industry [1], require specialized modelling software, which is expensive. As a result development of special microwave devices is monopolized by large-scale companies, which are able to cover significant investment costs at the beginning of development process.

Recently, the open source modeling software becomes more and more important alternative, opening development niches for small enterprises. One of such solution is ELMER FEM, enabling modeling of mechanical, thermal, electrical and magnetic systems. However, until now, it was not possible to model microwave systems with this software, which makes microwaves as one of last area, where FEM modeling during the development of devices was limited by necessity of large investment in commercial modeling software.

This paper present the solution overcoming this problem. Open source ELMER finite element method oriented software was equipped in module enabling calculation of microwave distribution in the resonant chamber. Open source Delaunay tetrahedral meshing modules, visualization software and solvers using conjugate gradient-oriented algorithms previously available in ELMER were applied to solve proposed set of differential equations.

## II. METHOD OF MODELLING

Real technical cases, described by the full set of differential Maxwell equations, are very difficult to be modelled, even using advanced methods and high power computers. For this reason, Maxwell equations are reduced to describe the specific cases, such as magnetostatic, magnetodynamic, optics or microwaves.

In developed module time-harmonic Maxwell equations system is given as [2]:

$$\mu^{-1}\nabla \times \vec{E} = i\omega\vec{H} \quad (1)$$

$$\nabla \times \vec{H} = -i\omega\vec{E} + \vec{J} \quad (2)$$

$$\omega = 2\pi f \quad (3)$$

$$\mu = \mu_0\mu_r \quad (4)$$

$$\varepsilon = \varepsilon_0\varepsilon_r \quad (5)$$

where $f$ is the frequency of the electromagnetic field, $\mu_0$ is magnetic constant, $\mu_r$ is relative permeability, $\varepsilon_0$ is permittivity of vacuum and $\varepsilon_r$ is relative permittivity of material. $E$, $H$ and $J$ are electric field, magnetic field and impressed current distributions respectively. In the developed module the Leontovich impedance boundary and the first order absorbing boundary conditions are implemented together with the port feed described as the Robin boundary.

## III. RESULTS AND CONCLUSION

Figure 1 presents the results of simulations of the same WR340 waveguide for 2.45GHz with two different cylindrical cavities attached to one of its end. It can be clearly seen, that the resonance and distribution of the electric field in the cavities depends on its diameter.

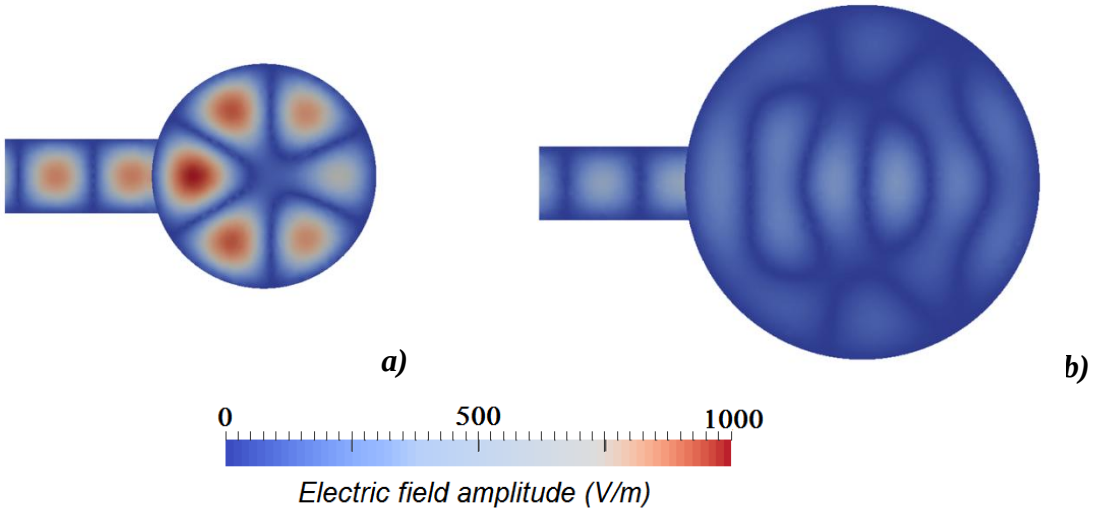


*Fig.1. Distribution of electric field in cylindrical cavities attached to WR340 waveguide (frequency f = 2.45 GHz). Cavity with diameter: a) 250 mm, b) 400 mm*

Presented results confirm, that it is possible to perform 3D simulations of microwave devices using open-source software for finite elements method. Such simulations are especially important for small, high-tech companies involved in microwave technology.

## REFERENCES


[1] Krokida M.K., MaroulIs Z.B., Effect of microwave drying on some quality properties of dehydrated products, *Drying Technology*, 17(1999) 449

[2] Råback P., Malinen M., Ruokolainen J., Pursula A., Zwinger T. (Eds.), Elmer Models Manual, *CSC – IT Center for Science*, March 30, 2016.

# ANALYSIS OF THE APPLICABILITY OF 3D MAGNETIC FILAMENT TECHNOLOGY IN ELECTRICAL AND ELECTROMECHANICAL DEVICES

M. Szczygieł[1], Z. Pilch[1], J. Domin[1], T. Trawiński[1], K. Kluszczyński[1], M. Przybylski[2], B. Ślusarek[2]

[1] Faculty of Electrical Engineering, Mechatronic Department, Silesian University of Technology, 44100 Gliwice, Poland, jaroslaw.domin@polsl.pl, krzysztof.kluszczynski@polsl.pl, zbigniew.pilch@polsl.pl, marcin.szczygiel@polsl.pl, tomasz.trawinski@polsl.pl

[2] Tele and Radio Research Institute, 03450 Warszawa, Poland, marek.przybylski@itr.org.pl, barbara.slusarek@itr.org.pl

***Abstract.*** *In the paper the initial results of experiments with new material dedicated to 3D printing filament technology are presented. Authors compared properties of new material polylactide (PLA) doped with Nd-Fe-B) with standard material which are used in electromechanical devices.*

## I. INTRODUCTION

Nowadays additive production is identified with 3D printing process. The 3D printing methods can be divided into: powder or resin printing, lamination and Fused Filament Fabrication (FFF) method (realized by using paste or wire). The FFF method of 3D printing was developed in 80's of 20th century but only in recent years devices for 3D printing were designed and control methodology of these devices were done. Actually FFF method of 3D printing is the cheapest from the rest of 3D printing methods.

3D printing process is connected with a rapid prototyping method for production of individual parts of devices for their verification in pre-production.

Elements performed by FFF method have a layered structure, which is important in relation to the strength parameters [2]. The development of this technology has contributed to the interest of this technology by universities and scientific research centres. Actually trends in the development of 3D printing are focused on devices that ensure high repeatability and reliability as well as high precision of printed elements.

## II. CONCEPTION OF MAGNETIC FILAMENT TECHNOLOGY

Conception of magnetic filament technology based on the typical technology which used in FFF method but wire for printing is a Nd-Fe-B doped magnetic material. The material was produced on single screw extruder and result is wire with a diameter 1.75 mm dedicated to standard 3D printer.

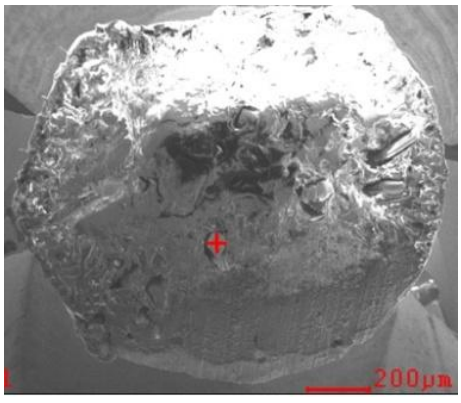


*Fig.1. Cross section of a wire for printing PLA doped Nd-Fe-B*

## III. INITIAL RESULTS OF EXPERIMENT – 8 POLE PERMANANT MAGNET OF SPINDLE MOTOR USED IN HARD DISC DRIVE

Spindle motors (SM) used in modern storage devices (hard disk drives) belong to the class of brushless DC motors. The rotors of these motors composed of a ring of permanent magnet and yoke of the magnetic circuit (rotor yoke) are fixedly connected to the spindle (on which are deposited the hard drive platters) [1]. Spindle motors used in modern storage devices have different internal design features, but the most commonly used configuration between the number of poles of the permanent magnet ring and the number of stator teeth are as follow: 8 poles / 9 teeth, 8 poles / 12 teeth. In Fig.2 the internal structures of those above mentioned configuration are shown. In Fig.2. the magnetic yoke of the stator with stator tooth are denoted by (1), by (2) the magnetic yoke of the rotor is denoted and finally the permanent magnet ring is denoted by (3). For depictive purposes in Fig.2 the magnetic ring was partitioned into magnetic poles.

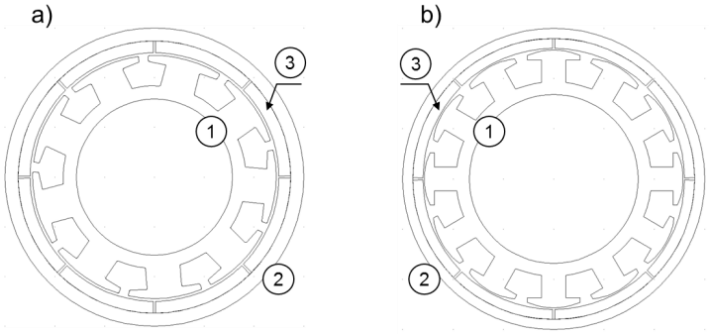


*Fig.2. Simplified internal structure of a modern spindle motor (stator windings is removed): a) - 8 pole / 9 teeth configuration, b) – 8 pole / 12 teeth configuration*

During experiment SM motor magnet was made in the filament technology and result is presented in Fig.3. After magnetization process the permanent magnet of rotor will be mounted in rotor of a SM motor. Results of measurements of operational parameters of a model motor will be presented.

*Fig.3. Results of experiment: rotor of SM motor with original permanent magnet and (on right side) magnet produced in the filament technology.*

## REFERENCES


[1] Kołton W., Trawiński T., Badania drgań silników wrzecionowych pamięci masowych, *Przegląd Elektrotechniczny*, ISSN 0033-2097, R. 87 NR 12b/2011, s.188-191

[2] Tymrak B.M., Kreiger M., Pearce J.M., Mechanical properties of components fabricated with open-source 3-D printers under realistic environmental conditions, *Materials and Design* 58 (2014) 242–246. www.elsevier.com/locate/matdes

# METHOD OF MOMENTS IN JILES-ATHERTON MODEL BASED MAGNETOSTATIC MODELLING OF THIN LAYERS

R. Szewczyk

Institute of Metrology and Biomedical Engineering, Warsaw University of Technology,
sw. A. Boboli 8; 02-525 Warsaw, Poland, szewczyk@mchtr.pw.edu.pl

***Abstract.*** *Method of moments enables effective magnetostatic modelling of thin layers, where thickness of the layer should be considered. This paper presents the non-linear extension for this method of modelling.Initial magnetization curve, necessary for modelling, was reconstructed from saturation hysteresis loops on the base of Jiles-Atherton model. Finally, the set of non-linear equations was stated, and example of solution for square-shaped magnetic thin layer is presented.*

## I. INTRODUCTION

Method of Moments is an important alternative for Finite Elements Method in the case of magnetostatic simulations of thin layers. For the thin layers, tetrahedral meshing leads to radical increase of the numbers of elements, which creates calculation problems. In the case of Method of Moments, thin layer may be described by 2D uniform mesh with given thickness and the set of linear equations.

However, commonly used linear simplification of description of soft magnetic material with constant value of magnetic permeability may lead to significant errors. To overcome this problem, shape of initial magnetization curve should be considered.

## II. RECONSTRUCTION OF INITIAL MAGNETIZATION CURVE

Measurement of initial magnetization curve is difficult from technical point of view. For these reason initial magnetization curve and its relative permeability $\mu$ versus magnetization $M$ dependence is rarely presented for soft magnetic materials. However, it was previously proven [1], that Jiles-Atherton model very well reconstructs initial magnetization curve on the base of saturation magnetic hysteresis loop. In such a case, the parameters of Jiles-Atherton model determined on the base of magnetic saturation hysteresis loops may be used to calculate both initial magnetization curve as well as relative permeability $\mu$ versus magnetization $M$ dependence. Example of such calculations for isotropic 3H13 steel is given in the figure 1.

Due to the necessity of application of the Runge-Kutta method for solving ordinary differential equations stating Jiles-Atherton model, such calculations are time consuming. For this reason, the results of modelling of relative permeability $\mu$ versus magnetization $M$ dependence were stored in the lookup table. Exact values were determined by interpolation.

## III. METHOD OF THE MOMENTS FOR THIN LAYERS

Generalization of magnetostatic Method of moments for thin layers with regular rectangular grids was presented previously [2]. To consider nonlinear dependence of relative permeability $\mu$ versus magnetization $M$ equations stated the Method of moments (for the x axis direction) should be extended to the following form:

$$M_x(k_x,k_y) + \sum_{iy=1}^{N}\sum_{ix=0}^{M}\left[\left(\mu_{rel}(M_x(k_x,k_y))-1\right)\cdot dH_{xx}(i_x,i_y,k_x,k_y)\right] + \\ + \sum_{ix=1}^{n}\sum_{iy=0}^{n}\left[\left(\mu_{rel}(M_x(k_x,k_y))-1\right)\cdot dH_{xy}(i_x,i_y,k_x,k_y)\right] = \left(\mu_{rel}(M_x(k_x,k_y))-1\right)\cdot H_x \quad (1)$$

Where $\mu_{rel}(M_x(k_x, k_y))$ is spline-based interpolation of relative permeability $\mu$ versus magnetization $M$ dependence in initial magnetization curve. Solution of such set of nonlinear equations was implemented with OCTAVE 4.0 software on the base of Powell'strust-region dogleg algorithm.

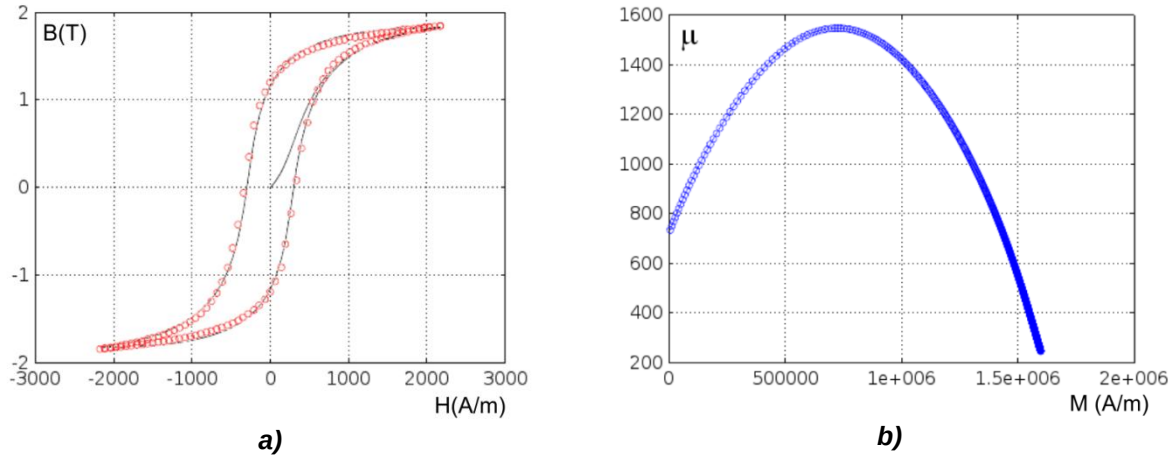


*Fig.1. Results of modelling based on the Jiles-Atherton model: a) reconstructed hysteresis loop with the initial magnetization curve (solid line), results of measurements (dotted line), b) reconstructed relative permeability $\mu$ versus magnetization M dependence*

## IV. RESULTS OF MODELLING AND CONCLUSIONS

Results of modelling of square-shaped thin film element are presented in the figure 2. The length of the element was 10 mm, whereas its thickness was 30 μm. Magnetizing field strength was 1000 A/m.Relative permeability $\mu$ versus magnetization $M$ dependence for 3H13 steel was used for simulation.

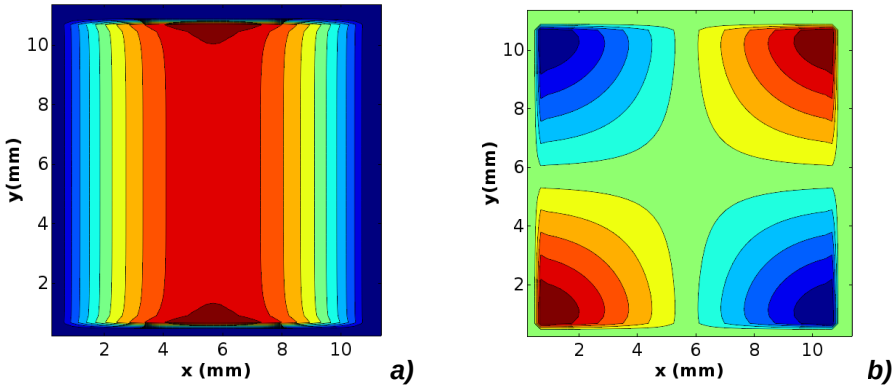


*Fig.2. Results of magnetostatic modelling of square-shaped thin film element: flux density B in: a) x-axis, b) y-axis*

Results of simulation confirm that nonlinear permeability dependence may be considered in reasonable time of calculation and significantly improve the accuracy of simulations.

## REFERENCES


[1] Roubal Z., Smejkal V., Determination of parameters in the Jiles - Atherton model for measured hysteresis loops, *9th International Conference MEASUREMENT 2013*, Smolenice, Slovakia

[2] Szewczyk R., Generalization of magnetostatic Method of moments for thin layers with regular rectangular grids, *16th Czech and Slovak Conference on Magnetism 2016*, Košice, Slovakia

# COMPLEX CHARACTERISTICS OF SINTERED Nd-Fe-B MAGNETS FROM SCRAP HDDs

M. Szymański[1], B. Michalski[1], M. Leonowicz[1] and Z. Miazga[2]

[1] Warsaw University of Technology, Faculty of Materials Science and Engineering, 141 Woloska Street, 02-507 Warsaw, Poland, m.szymanski@inmat.pw.edu.pl, m.michalski@inmat.pw.edu.pl, mkl@inmat.pw.edu.pl
[2] P.P.H.U. Polblume Zbigniew Miazga, 35 11-tego Listopada Street, Piaseczno, Poland, polblume@polblume.pl

***Abstract.*** *Sintered Nd-Fe-B magnets were dismantled – by the P.P.H.U. Polblume company – from scrap hard disc drives (HDDs), thermally demagnetized at 400°C and analyzed in terms of their chemical composition, structure and magnetic properties. It was noticed that the magnets have bipolar magnetizing. All of the magnets were covered with a nickel or nickel-cooper coating (around 50 μm in thick), which however was often discontinuous and deeply scratched. What is more, the majority of the magnets were partially destroyed (broken or corroded). The examined magnets were basically made of iron (65±1%$_{wt.}$) and neodymium (30±2%$_{wt.}$) however they differed with a concentration of alloying elements such as Co (1-2.5%$_{wt.}$), Dy (0-1%$_{wt.}$) or Pr (0-5%$_{wt.}$). Magnets were textured thus their XRD pattern (for bulk, as received magnets) did not match with a relevant one for the $Nd_2Fe_{14}B$ (φ) phase. A typical XRD pattern of the Nd-Fe-B magnets was achieved for a powder obtained after mechanical crushing of the magnets. The grey grains of $Nd_2Fe_{14}B$ (φ) phase and a thin Nd-rich grain boundary phase were observed in the magnets by SEM. The magnets exhibited excellent magnetic properties: maximum energy product above 300 kJ/m$^3$, remanence above 1 T and coercivity above 1000 kA/m, slightly varying between each magnet. What is more, the magnets were strongly anisotropic possessing the best properties when measured perpendicular to their flat surface.*

## I. INTRODUCTION

It is a commonly known fact that a noble and precious metals can be recovered from the Waste of Electric and Electronic Equipment (WEEE). This is due to both economic and environmental reasons. The WEEE has to be precisely characterized in order to allow for developing reasonable recovery methods, dedicated for particular type of the e-scrap. Present work is focused on characterization of a neodymium-iron-boron magnets which are the important products made of rare earths elements (with respect to a concentration/volume ratio) and are available in quite large amounts. The rare earths metals (Nd, Pr, Dy, Tb etc.) are recognized as critical raw materials for the UE and that is why there is an urgent need for studies focused on recycling technologies for these elements [1,2]. The Nd-Fe-B magnets are parts of electric motors, detection systems, loudspeakers etc. Currently, one of the biggest application of Nd-Fe-B magnets are Voice Coil Motors (VCM) in computer Hard Disc Drives (HDDs) – there are 2 sintered Nd-Fe-B magnets in the VCM of HDD (for more details see [3]). Old computers are replaced by newer in around 5 years period. Thus, a constant inflow of scrap HDDs (including magnets) occurs [4]. The WEEE can be recognized as an "urban ore" and can be a source of rare earth metals (urban mining concept) [5]. Taking all of these into account, a full characteristic of scrap Nd-Fe-B magnets was carried out hoping that this will help for further processing of these materials.

## II. EXPERIMENTAL

The magnets were provided by the P.P.H.U. Polblume Zbigniew Miazga company. Visual observations were carried out in order to estimate size, shape, mass and general look of the magnets. A magnetic field viewer film was placed into the magnets revealing they have bipolar magnetizing. Subsequently, the magnets were thermally demagnetized under an inert atmosphere at 400°C. Coatings of the magnets were examined using both light and scanning electron microscopy. Chemical composition of the magnets was investigated with two techniques: an Energy-Dispersive Spectroscopy (EDS/SEM) and an X-Ray Fluorescent spectroscopy (XRF). Results from the XRF analysis were provided by PANalytical company thanks to courtesy of Katarzyna Stepaniuk and Sonia Vicente Dols at PANanalytical B.V. Almelo, Netherlands. Phase structure was analyzed

using an X-Ray Diffraction technique and microstructure was observed by a Scanning Electron Microscope (SEM). In order to measure magnetic properties cubic samples (1.5-1.5-1.5 mm) were cut from the magnets, magnetized at 6 T pulse field magnetizer along each of the three orthogonal axes and then demagnetized along the same directions using the Vibrating Sample Magnetometer. So, as a result, three second-quadrants of the hysteresis loop were gathered for each magnet, referring to the three perpendicular directions of magnetization/demagnetization (X, Y and Z).

## III. RESULTS

The magnets from VCMs are flat and "C" shape (horseshoe) due to the way of working in HDDs. The magnets are covered with Ni or Ni-Cu coating – around 50 μm thick. The coating protects the magnets against corrosion and prevents from crumbling individual grains. The mass of the magnets varies between 10-20 g depending on their size. The chemical composition of the magnets is dominated by iron (65±1%wt.) and neodymium (30±2%wt.). However, alloying elements such as Co (1-2.5%wt.), Dy (0-1%wt.) or Pr (0-5%wt.) are incorporated into the material in order to improve the magnetic properties. In this work the three randomly chosen magnets were investigated, but one should notice that there is a variety of alloying elements for Nd-Fe-B magnets [6]. Furthermore, the chemical composition of the magnets changes with time and is not reproducible by one supplier [7].

The magnets exhibit bipolar magnetizing due to the way of working in the VCMs. The magnets are anisotropic and exhibit excellent properties in a direction perpendicular to the flat surface.

## REFERENCES


[1] http://ec.europa.eu/growth/sectors/raw-materials/specific-interest/critical/index_en.htm (access on June 26th, 2016)

[2] Massari S., Ruberti M., Rare earth elements as critical raw materials: Focus on international markets and future strategies, *Resources Policy*, 38, issue 1, 2013, pp. 36-43

[3] http://hddscan.com/doc/HDD_from_inside.html (access on June 26th, 2016)

[4] Walton A., Han Yi., Rowson N.A., Speight J.D., Mann V.S.J., Sheridan R.S., Bradshaw A., Harris I.R., Williams A.J., The use of hydrogen to separate and recycle neodymium-iron-boron-type magnets from electronic waste, *Journal of Cleaner Production,* 104, 2015, pp. 236-241

[5] Katagiri N., Ijima K., Halada K., Production of Urban Ores Using Ball Mill for Saving Time and Effort, *NIMS NOW International*, vol. 7, no. 5, 2009, p. 9

[6] http://erean.eu/wordpress/additives-in-ndfeb-magnets (access on June 26th, 2016)

[7] https://ec.europa.eu/growth/tools-databases/eip-raw-materials/sites/rawmaterials/files/3%20-%20Walton%20EIP%20talk%20for%20ERECON.pdf (access on June 26th, 2016)

# RELATIVISTIC ENGINE BASED ON A PERMANENT MAGNET

M. Tuval[1] and A. Yahalom[2]

[1] Atidron Ltd., San Martin 15, Ramat Gan 52237, Israel
[2] Ariel University, Kiriat Hamata POB 3, Ariel 40700, Israel
concepts@israel.net, asya@ariel.ac.il

***Abstract.*** *The purpose of this paper is to describe and analyze a relativistic engine based on a permanent magnet. Newton's third law states that any action is countered by a reaction of equal magnitude but opposite direction. The total force in a system not affected by external forces is thus zero. However, according to the principles of relativity a signal can not propagate at speeds exceeding the speed of light. Hence the action cannot be generated at the same time with the reaction due to the relativity of simultaneity, thus the total force cannot be null at a given time. The above conclusion leads to the possibility of a relativistic engine based on a permanent magnet. The analysis is based on a previous paper [1] in which we studied the relativistic effects in a system of two current conducting loops. It should be emphasized that although momentum can be created in the material part of the system as described in the following work momentum can not be created in the physical system, hence for any momentum that is acquired by matter an opposite momentum is attributed to the electromagnetic field.*

## I. INTRODUCTION

Among the major achievements of Sir Isaac Newton is the formulation of Newton's third law stating that any action is countered by a reaction of equal magnitude but opposite direction [2, 3]. The total force in a system not affected by external forces is thus zero. This law has numerous experimental verifications and seems to be one of the corner stones of physics. However, by the middle of the nineteenth century Maxwell has formulated the laws of electromagnetism in his famous four partial differential equations [4, 5, 7] which were formulated in their current form by Oliver Heaviside [8]. One of the consequences of these equations is that an electromagnetic signal cannot travel at speeds exceeding that of light. This was later used by Albert Einstein [5, 7, 9] (among other things) to formulate his special theory of relativity which postulates that the speed of light is the maximal allowed velocity in nature. According to the principles of relativity no signal (even if not electromagnetic) can propagate at superluminal velocities. Hence an action and its reaction cannot be generated at the same time because of the relativity of simultaneity. Thus the total force cannot be null at a given time. In consequence, by not holding rigorously the simultaneity of action and reaction Newton's third law cannot hold in exact form but only as an approximation. Moreover, the total force within a system that is not acted upon by an external force would not be rigorously null since the action and reactions are not able to balance each other and the total force on a system which is not affected by an external force in not null in an exact sense.

Most locomotive systems of today are based on open systems. A rocket sheds exhaust gas to propel itself, a speeding bullet generates recoil. A car pushes the road with the same force that is used to accelerate it, the same is true regarding the interaction of a plane with air and of a ship with water. However, the above relativistic considerations suggest's a new type of motor in which the open system is not composed of two material bodies but of a material body and field. Ignoring the field a naive observer will see the material body gaining momentum created out of nothing, however, a knowledgeable observer will understand that the opposite amount of momentum is obtained by the field. Indeed Noether's theorem dictates that any system possessing translational symmetry will conserve momentum and the total physical system containing matter and field is indeed symmetrical under translations, while every sub-system (either matter or field) is not.

The purpose of this paper is to describe and analyze a relativistic engine based on a permanent magnet. Here we will use Jefimenko’s equation [6] to study the force between a current loop and a permanent magnet. In this respect the current paper differs from a previous one [1] which discussed the case of two current carrying coils, but is nevertheless based on this previous analysis. The

current configuration may seem attractive for some purposes since a permanent magnet does not require a power source.

## REFERENCES


[1] Tuval M., Yahalom A., Newton's Third Law in the Framework of Special Relativity, *Eur. Phys. J. Plus* (11 Nov 2014) 129: 240 DOI: 10.1140/epjp/i2014-14240-x. (arXiv:1302.2537 [physics.gen-ph])

[2] Newton I., *Philosophiæ Naturalis Principia Mathematica* (1687)

[3] Goldstein H., Poole Jr. C.P., Safko J.L., Classical Mechanics, *Pearson*, 3 edition (2001)

[4] Maxwell J.C., A dynamical theory of the electromagnetic field, *Philosophical Transactions of the Royal Society of London* 155: 459–512 (1865)

[5] Jackson J.D., Classical Electrodynamics, Third Edition. *Wiley*: New York, (1999)

[6] Jefimenko, O.D., Electricity and Magnetism, *Appleton-Century Crofts*, New York (1966); 2nd edition, Electret Scientific, Star City, WV (1989)

[7] Feynman R.P., Leighton R.B., Sands M.L., Feynman Lectures on Physics, *Basic Books*; revised 50th anniversary edition (2011)

[8] Heaviside O., On the Electromagnetic Effects due to the Motion of Electrification through a Dielectric, *Philosophical Magazine*, (1889)

[9] Einstein A., On the Electrodynamics of Moving Bodies, *Annalen der Physik* 17 (10): 891–921, (1905)

# DESCRIPTION OF SOURCES OF MAGNETIC FIELD USING EDGE VALUES OF CURRENT VECTOR POTENTIAL

R.M. Wojciechowski and C. Jędryczka

Poznan University of Technology, ul. Piotrowo 3, 60-965 Poznań, rafal.wojciechowski@put.poznan.pl, cezary.jedryczka@put.poznan.pl

***Abstract****. The paper discusses the method of description of magnetic field sources in systems with the stranded windings. The sources are determined on basis of given distribution of edge values of current vector potential* $\boldsymbol{T}_0$*. The formulas describing the magnetic field sources in the finite element space have been given. The approach for determining the* $\boldsymbol{T}_0$ *distribution in stranded windings with simple and complex geometry has been proposed.*

## I. INTRODUCTION

One of the important aspects ensuring high credibility of the numerical calculations of systems with magnetic field is proper and accurate method for the field sources description. It can be said that among the group of magnetic fields sources in finite element space the most difficult is proper description of the sources for windings of complex geometry. In the open literature many methods of filed sources description for systems with windings can be found [1,2]. Nevertheless most of them lead to complex and time consuming calculations for windings of complex geometries. In the paper authors present and describe an alternative way to define the field sources that is universal end computational effective for simple as well as for complex current paths in the windings. In the discussed approach it is assumed that distribution of the turns in the system can be treated as distribution of current paths inside the region described by the contour of a winding which are defined by means of current flow field equations. For description of the winding the current vector potential $\boldsymbol{T}_0$ can be successfully applied and on basis of obtained the $\boldsymbol{T}_0$ distribution the magnetic field sources can be determined for both the scalar potential $\Omega$ as well as the vector potential $\boldsymbol{A}$ formulations. The expressions describing the magnetic field source have been given.

## II. DESCRIPTION OF THE WINDING USING $T_0$ FORMULATION

In the proposed approach the distribution of current vector potential $\boldsymbol{T}_0$ for winding region, for example simple coil shown in Figure 1, can be determined using following formulas:

$$\nabla\times\rho\nabla\times\boldsymbol{T}_0 = 0\big|_{\Omega_c} \quad \text{and} \quad \nabla\times\nabla\times\boldsymbol{T}_0 = 0\big|_{\Omega_n} \tag{1a,b}$$

taking into account boundary conditions:

$$\boldsymbol{T}_0 = \boldsymbol{\tau}_0\big|_{\Gamma_{To}} \quad \text{and} \quad \boldsymbol{T}_0 = 0\big|_{\Gamma_0+\Gamma_\Omega} \tag{2a,b}$$

where: $\rho$ is tensor describing the material resistivity, and $\tau_0$ is function that describes the distribution of $\boldsymbol{T}_0$ on the boundary surface $\Gamma_{To}$.

The values of boundary function $\tau_0$ can be determined numerically. The simplest way is to use the relation between magnetomotive force $\theta$, current density vector $\boldsymbol{J}_0$ passing thought the cross-section surface of the coil $\boldsymbol{S}_c$ and potential $\boldsymbol{T}_0$ along line $L$ surrounding the surface $\boldsymbol{S}_c$ (Fig. 1):

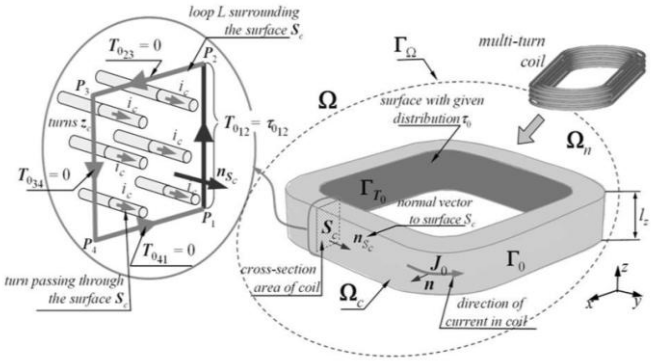


*Fig.1. An example of multi-turn winding*

$$\theta = z_c i_c = \int_{S_c} \boldsymbol{J}_0 \, \mathrm{d}\boldsymbol{s} = \oint_{L(S_c)} \boldsymbol{T}_0 \mathrm{d}\boldsymbol{l} = \boldsymbol{\tau}_{0_{12}} l_z \tag{3}$$

and following condition:

$$\nabla \times \boldsymbol{\tau}_0 \cdot \boldsymbol{n} = 0 \tag{4}$$

where: $i_c$ is value of the current in the winding, $\tau_{012}$ is value of the boundary function assigned to edge $P_1P_2$ of loop $L$ (Fig.1), $l_z$ is length of the edge $P_1P_2$ representing the height of the winding, and $\boldsymbol{n}$ is the normal vector to the considered boundary surface. In order to solve equations (1) i.e. to determine the distribution of $\boldsymbol{T}_0$, the edge formulation of finite element method has been applied [3]. The correctness of discussed approach has been verified among others in [4].

## III. MAGNETIC FIELD SOURCE CALCULATION

The starting point for determining the magnetic field sources is obtained distribution of current vector potential $\boldsymbol{T}_0$ i.e. distribution of edge values of currents $\boldsymbol{i}_0$. In the case of formulation using scalar potential $\Omega$, the finite element (FE) equations are equivalent to the nodal equations of magnetic edge network (MEN). In the MEN the field sources, i.e. magnetomotive forces (*mmf*'s), are assigned to edges of elements. Because the edge values of currents $\boldsymbol{i}_0$ are also assigned to the branches of MEN, they directly from the vector of branch *mmf*'s $\Theta$, i.e.:

$$\boldsymbol{\Theta} = \boldsymbol{i}_0 \tag{5}$$

The field sources description is different for case when magnetic field in considered system is described by the magnetic vector potential $\boldsymbol{A}$. In such case FE equations are equivalent to the magnetic facet network equations (MFN). The field sources are described by loop magnetomotive forces *mmf*'s $\theta_o$ assigned to loops of MFN. In order to calculate the loop *mmf*'s on basis of edge values of $\boldsymbol{T}_0$ potential the transformation of the edge quantities to values assigned to facets of elements must be applied first. In the next step these values are transformed to the magnetomotive forces assigned to the loops of MFN. The source vector of loop *mmf*'s $\theta_o$ can be determined using fallowing formulas:

$$\theta_o = \boldsymbol{k}_s^T \boldsymbol{K} \boldsymbol{i}_0 = \boldsymbol{K}^T \boldsymbol{k}_s \boldsymbol{i}_0 \tag{6}$$

where: $\boldsymbol{k}_s$ is matrix transforming the values assigned with element edge into the values assigned to the element facets in the MFN; whereas $\boldsymbol{K}$ is the matrix converting quantities associated with edges of the elements to quantities associated with facets of the elements.

## IV. CONCLUSION

The universal and flexible method for determining the field sources in FE space using current vector potential $\boldsymbol{T}_0$ has been proposed and briefly described. The method has been tested on number of numerical examples. The detailed explanation as well as numerical examples showing the superiority of proposed method over commonly used approached based on application of Biot-Savart law will be given in the extended version of the paper.

## REFERENCES


[1] Ohnishi T., Takahashi N., Effective optimal design of 3-D magnetic device having complicated coil using edge element and Biot - Savart method, *IEEE Trans. Magn.*, 38(2), 2002, 1021 – 1024

[2] Bui V., Le Floch Y, Meunier G., Coulomb J., A new 3D scalar finite element method to compute $\boldsymbol{T}_0$. *IEEE Trans. Magn.*, 42(4), 2006, 1035-1038

[3] Demenko A., Sykulski J., Wojciechowski R.M., Network representation of conducting regions in 3D finite-element description of electrical machines, *IEEE Trans. Magn*, 44(6), 2008, 714-717

[4] Wojciechowski R.M., Description of distribution of windings made from filamentary conductors using electric vector potential $\boldsymbol{T}_0$, *Przegl. Elektrotech.*, 9/2013, 58 – 61

# MAGNETIC SIGNATURE OF LAND VEHICLES

M. Wołoszyn, M. Chojnicki and M. Nowak

Faculty of Electrical and Control Engineering, Gdańsk University of Technology,
11/12 Narutowicza Street, Gdańsk, 80-233, Poland, mirwolos@pg.gda.pl

***Abstract.*** *The results of numerical simulations of the magnetic field surrounding of land vehicles' models have been presented in this paper. Vehicle containing of ferromagnetic elements distorts the Earth's magnetic field. This distortion can be measured by magnetometers. It is possible to detect and identify an object on the basis of its magnetic signature.*

## I. INTRODUCTION

In order to protect different areas, for safety reasons, there is a need to detect and identify moving objects consisting of ferromagnetic components. Vehicles, ships, and airplanes can be considered as such objects.

Magnetometric method is one of the techniques of detection and identification of the objects. Every object comprising of ferromagnetic components perturbs the homogeneity of the Earth magnetic field around it. This perturbation can be measured with the use of magnetometers (fluxgate, GMR or scalar magnetometers [1]). Moving objects in the protected area can be detected this way. Numerical simulations' results of the magnetic field of different land vehicles models have been presented in this paper.

## II. NUMERICAL MODELS OF VEHICLES

Every object composed of ferromagnetic materials perturbs the homogeneity of the Earth magnetic field. Ferromagnetic components of the object possess permanent and induced magnetization. Induced magnetization depends on the direction in which the vehicle moves, while permanent magnetization is independent of the direction. Magnetic field of a ferromagnetic object such as a vehicle is a composite function of its dimensions, shape, magnetic properties of the materials, ferromagnetic history of components (permanent magnetization) and the direction in which the vehicle moves. Numerical calculations of the magnetic field of vehicles models were performed in the Opera 3D software. The numerical calculations were made for a model of a bicycle, car and a truck. The example of the sedan car model and the vertical component of the magnetic flux density are presented in Fig.1. By introducing different values for the external magnetic field in the numerical model it is possible to analyze magnetic signatures of objects for any magnetic direction.

The vertical component of the magnetic flux density is the characteristic magnetic signature of the vehicles [2]. This signature for the compact construction of the vehicle includes one extreme value and does not depend on the direction in which the vehicle moves. The values of perturbation of magnetic field for the vehicles of the same dimensions can differ, mainly as a result of a different degree of permanent magnetization and amount of ferromagnetic elements.

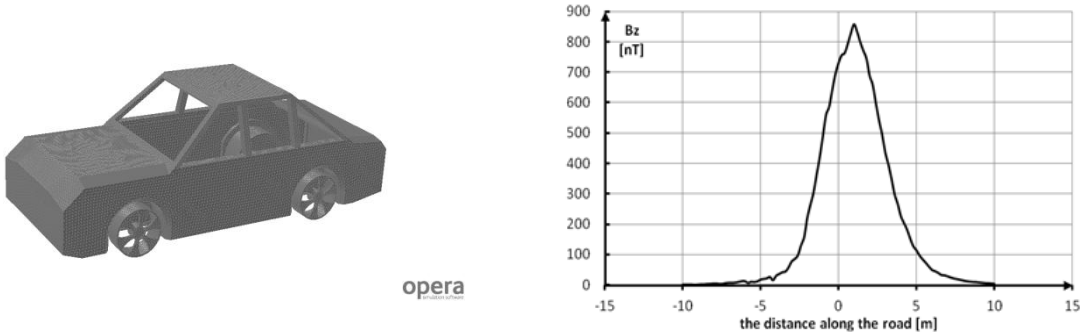


*Fig.1. Model of a sedan vehicle with mesh and a result of numerical analysis - vertical magnetic flux density*

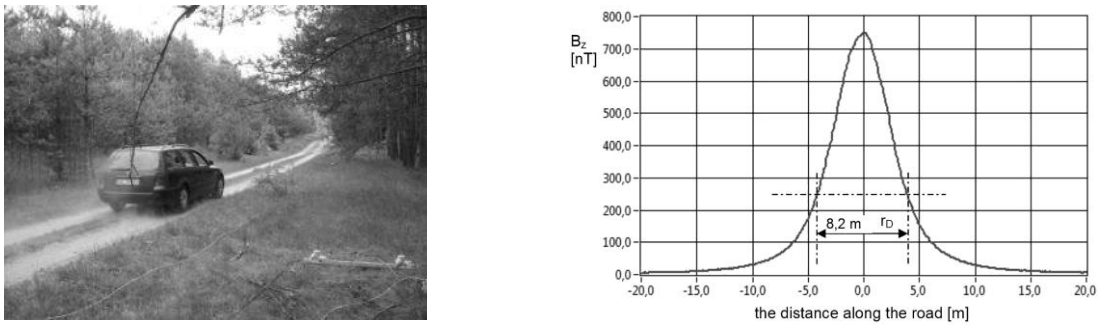


*Fig.2. Measured distribution of the vertical magnetic flux density of vehicle (for cars $r_o$ = 3m).*

## III. CONCLUSIONS

Presented results of the researches in the field of the deformation of magnetic field near to the vehicles have been presented in this paper. On the basis of the tests of the distributions of perturbation of the Earth magnetic field performed for different vehicles, the following conclusions can be formulated:

- changes in the quantity and the quality of the distributions of the magnetic field distortions of different vehicles are more diversified for smaller distances between the magnetic sensors and the vehicle;
- for the vehicles with a trailer or a semitrailer there occur several (most frequently two) local extreme values in the magnetic induction distribution. Local extrema disappear, joining to become one extreme value, as the distance between the magnetic sensors and the road increases;
- the measurement of magnetic flux density in a differential circuit eliminates natural and industrial magnetic interferences;

## REFERENCES

[1] Tumański S., Czujniki pola magnetycznego, *Przegląd Elektrotechniczny*, 2013 nr 10, s. 1- 11
[2] Jakubiuk K., Jankowski P., Wołoszyn M.: System of wireless magnetic sensors for detection and identification of ferromagnetic vehicles. *Acta Technica*, no 2, pp.171-184., 2014

# EXAMPLE OF VANISHING ANISOTROPY AT HIGH ROTATIONAL MAGNETISATION OF GRAIN-ORIENTED ELECTRICAL STEEL

S. Zurek

Megger Instruments Ltd, Archcliffe Road, Dover, CT17 9EN, Kent, United Kingdom, stan.zurek@ieee.org

***Abstract.*** *This paper presents experimental data measured up to 2.0 T under rotational circular flux density. The results show that at lower excitations there is significant anisotropy of permeability. However at 2.0 T the anisotropy collapses so that the permeability varies only ±14% from the average value. On a qualitative level the results are very similar to the directional curves for single-crystal samples for the three significant crystallographic directions [100], [110] and [111] shown previously in the literature.*

## I. INTRODUCTION

A crystallite has a cubic shape for which the planes and directions can be defined as shown in Fig. 1. The alignment of crystallites in grain-oriented electrical steels (GO) is controlled during production so that one "easy" magnetisation direction is produced [1]. In this so-called Goss structure the crystallites are aligned in such a way that all three important crystallographic directions are located within the plane of the sheet (Fig. 1). The "easy" direction is along the rolling direction (RD) and it caused by all the crystallites having their *[100]* directions aligned with it. The direction *[110]* is the face diagonal (Fig. 1a) and is in the transverse direction (TD, perpendicular to RD). The direction *[111]* is the cube diagonal.

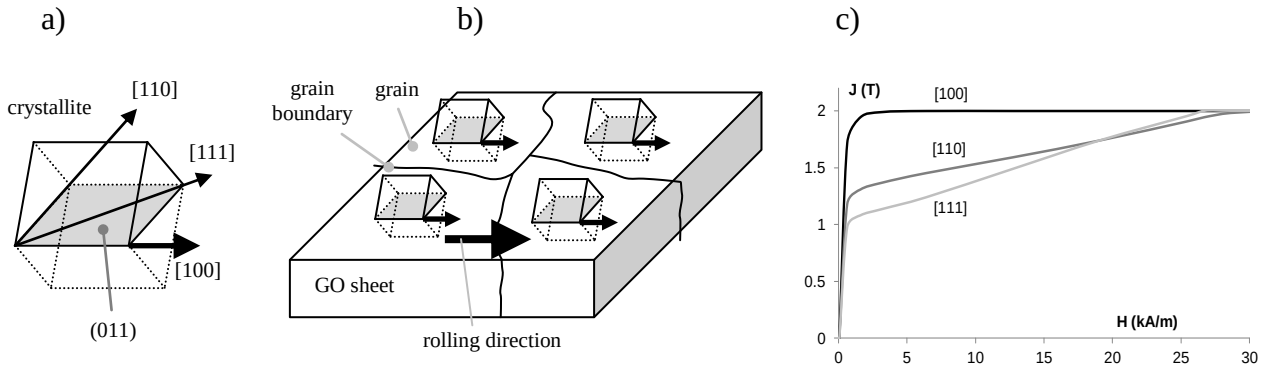


*Fig.1. Goss structure in GO: a) directions in a crystallite, b) alignment of crystallites in GO sheet, c) directional properties [3,4]*

*B-H* curves measured for the three crystallographic directions for a single crystal are shown in Fig. 2 [1-3]. At lower excitations, within practically applicable range, the *[100]* direction (0° with respect to RD) has the highest permeability. The *[110]* direction (90° with respect to RD) has significantly lower permeability, and *[111]* has the lowest permeability (55° with respect to RD, and other corresponding symmetrical directions: 125°, 235° and 305°).

## II. RESULTS AT VERY HIGH FLUX DENSITY

According to the curves shown in Fig. 1c at sufficiently high excitation the material should saturate. This corresponds to conditions in which for each direction permeability will be the same or similar – thus the anisotropy of permeability should vanish, or at least be significantly reduced.

Rotational measurements under controlled *B* rotation [4,5] are quite difficult to carry out in practice, especially at high *B*. Values above 1.9 T required using an especially adjusted rotational

magnetisation system with two power amplifiers for the magnetising phase working in the TD direction, and a third power amplifier for the RD direction [5].

The results are shown in Fig. 2. Only data for 1.7 T and above are shown, because for lower excitation the behaviours is well known. The *B* loci (Fig. 2a) remain circular because this was the quantity controlled by a digital feedback [6,7].

Interesting behaviour occurs above 1.8 T (Fig. 2b). At 1.9 T the *H* loci begins to significantly "swell" in all directions, including TD and RD. And at 2.0 T the *H* loci loses its original "butterfly" shape and develops into a shape whose instantaneous radius varies much less than for lower excitations. The corresponding directional permeability curves are shown in Fig. 6. At 0° and 180° the *B* vector passes through RD or the "easy" direction so permeability is high.

It should be noted that it was required to generate in excess of 30 kA/m in order to reach 2.0 T in all directions. This is also supported by the curves from Fig. 1c. At such excitation the anisotropy of permeability reduces to rather small variation, changing only from relative amplitude permeability $\mu_r$ = 40.0 to 53.6. Therefore the change is only ±14% from the average value through the whole rotation.

The excitation at 2.0 T is still far from full saturation, for which it would be $\mu_r$ = 1. However, it can be observed from Fig. 2c that at 2.0 T around 55° (and 125°, 235° 305°) the instantaneous permeability is *higher* than at 90° (and and 270°). Again, this is supported by the curves in Fig. 1c in which at 20-30 kA/m the *[111]* curve overtakes the *[110]* curve.

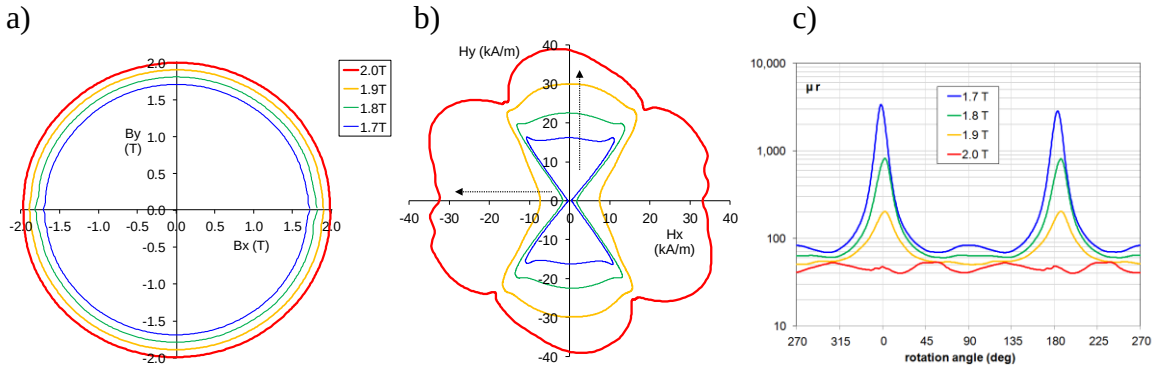


*Fig.2. Rotational results for conventional grain-oriented electrical steel M089-27N, at 50 Hz: a) controlled circular B loci, b) corresponding H loci, c) corresponding directional $\mu_r$ with vanishing anisotropy at 2.0 T*

## REFERENCES


[1] Beckley P., Electrical steels, *European Electrical Steels*, Newport, UK, 2000

[2] Soinski M., Magnetic materials in technology, (in Polish: Materiały magnetyczne w technice), *Centralny Ośrodek Szkolenia i Wydawnictw SEP*, 2001

[3] Tumanski S., Handbook of magnetic measurements, *CRC Press*, 2011

[4] Zurek S., et al., Rotational power losses and vector loci under controlled high flux density and magnetic field in electrical steel sheets, *IEEE Trans. Magnetics*, Vol. 42 (10), 2006, p. 2815

[5] Zurek S., Two-dimensional magnetisation problems in electrical steels, *PhD thesis, Wolfson Centre for Magnetics Technology*, Cardiff University, Cardiff, United Kingdom, 2005

[6] Zurek S., et al., Use of novel adaptive digital feedback for magnetic measurements under controlled magnetising conditions, *IEEE Trans. Magnetics*, Vol. 41 (11), 2005, p. 4242

[7] Zurek S., Practical implementation of universal digital feedback for characterisation of soft magnetic materials under controlled ac waveforms, presented at *Symposium of Magnetic Measurements & Modeling*, Czestochowa – Siewierz, Poland, 2016

# PRACTICAL IMPLEMENTATION OF UNIVERSAL DIGITAL FEEDBACK FOR CHARACTERISATION OF SOFT MAGNETIC MATERIALS UNDER CONTROLLED AC WAVEFORMS

S. Zurek

Megger Instruments Ltd, Archcliffe Road, Dover, CT17 9EN, Kent, United Kingdom, stan.zurek@ieee.org

***Abstract.*** *Practical implementation of digital feedback (DF) for waveshape control is described in the paper. It is shown that if the system has intrinsically sufficient phase margin then operation of DF can be controlled by changing just the DF gain even though the system gain can vary more than 2 orders of magnitude. Practical tips as well as typical difficulties are also discussed. The provided description should be sufficient to implement DF in any programming language and hardware configuration.*

## I. INTRODUCTION

International standards define sinusoidal magnetising conditions for measurement of magnetic properties of soft magnetic materials [1-3]. At high excitations the specimen exhibits strongly non-linear behaviour which produces distorted output signal if uncontrolled. Desired waveshape can be obtained e.g. by the means of analogue or digital negative feedback [4].

## II. DIGITAL FEEDBACK

The concept of digital feedback (DF) closely follows that of the analogue feedback shown in Fig. 1. The output waveform is compared with the reference waveform and an appropriate correction is applied to the generated waveform in order to reduce any discrepancy. Because of the iterative operation, the algorithm dwells at each amplitude with continuously applied alternating current for at least one cycle, and usually more than one.

DF algorithm can be summarised in the self-explanatory block diagram as shown in Fig. 1, and can be implemented with the corresponding block diagram of Fig. 2.

For a given measurement point, the virtual target waveform $\boldsymbol{T}$ (produced virtually in the software) is kept constant in amplitude and phase. Therefore, the natural approach is to trigger the controlled real waveform $\boldsymbol{V_{out}}$ (synonymous with the digitised waveform $\boldsymbol{R}$) to have the same phase as the target waveform $\boldsymbol{T}$. Then the difference waveform $\boldsymbol{D}$ can be calculated by a direct subtraction of $\boldsymbol{R}$ from $\boldsymbol{T}$ in step 3 (Fig. 1).

In a general case there will be significant phase shift between the generated and the controlled signal so that the zero crossing will not coincide. This is important because if $\boldsymbol{R}$ is always triggered at the assumed zero crossing then its phase will by definition be the same as $\boldsymbol{T}$. But the generated signal $\boldsymbol{V_{gen}}$ needs to have its phase shifted accordingly so that the required waveshape control takes place. It turns out that the phase of the digital waveform held in the buffer for generation of $\boldsymbol{G}$ might or might not be directly related to the actual phase of the generated signal.

If the phase correlation between the physical voltages cannot be derived from just the digital information inside the software then it will be required to re-measure the just-generated waveform $\boldsymbol{V_{gen}}$. This can be achieved by simply connecting the same signal to the power amplifier input as well as simultaneously to another analogue input (Fig. 1). This completely defines the phase information for all the signals relevant to DF, because $\boldsymbol{T}$ has the arbitrarily set phase, $\boldsymbol{R}$ is triggered to have the same phase as $\boldsymbol{T}$ and $\boldsymbol{G}$ is re-measured with the actual phase difference between $\boldsymbol{R}$ and $\boldsymbol{G}$.

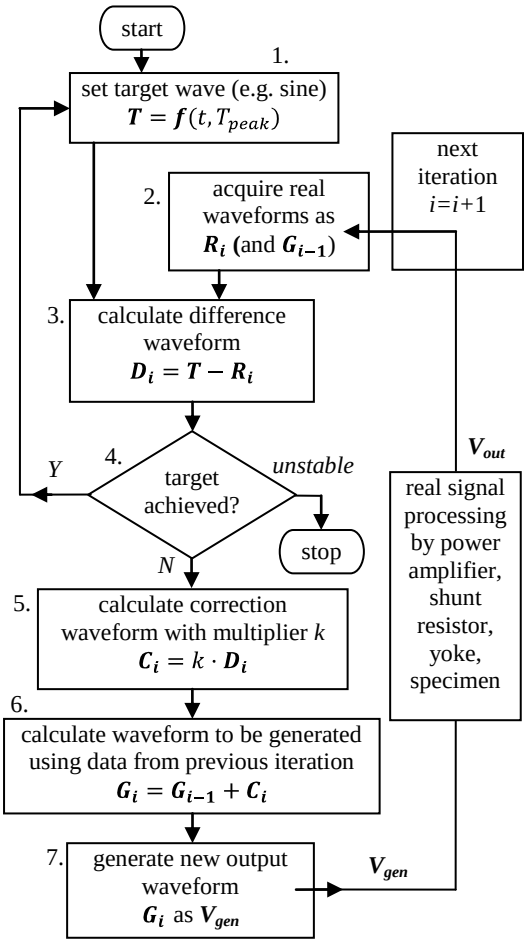


*Fig.1. Digital feedback algorithm, i – iteration*

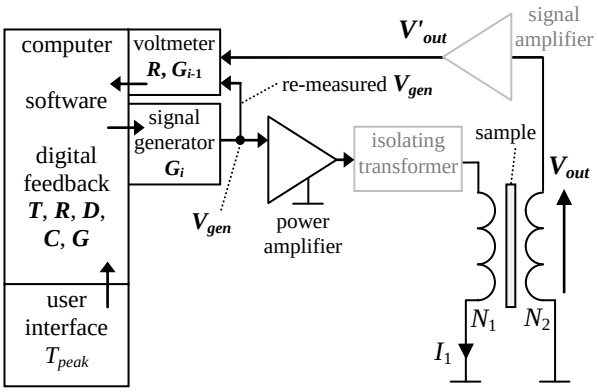


*Fig.2. Block diagram of magnetising setup with DF: **R** corresponds to $V_{out}$ and **G** to $V_{gen}$ (optional components are shown in grey)*

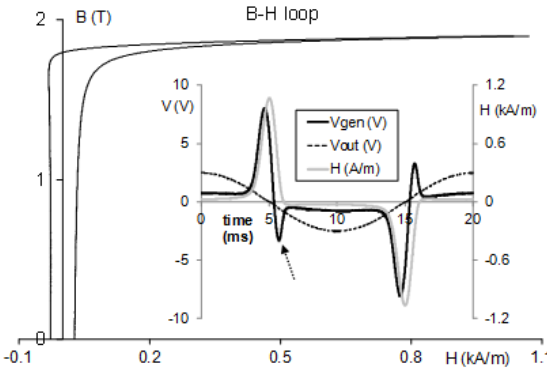


*Fig.3. Data measured with controlled sine at 50 Hz, 1.9 T for toroidal sample of grain-oriented steel*

The system gain *s* was varied from 0.294 to 28.4, which is around 2 orders of magnitude. Yet, it was sufficient just to change the value of the *k* multiplier (Fig. 1) in order to obtain stable operation in all cases, with and without an isolating transformer for blocking DC offset in the primary current.

The relation between the DF gain *g*, the system gain *s* and the feedback multiplier *k* is explained in the full paper. Also detailed discussion is provided on: triggering, universality issues, current glitches, convergence, phase and amplitude performance, multi-channel feedback and protection against instability.

## REFERENCES


[1] IEC 60404-3:1992 (Single Sheet Tester)
[2] IEC 60404-2:1998 (Epstein frame)
[3] IEC 60404-6:2003 (Ring specimen)
[4] Beckley P., Electrical steels, A handbook for producers and users, *European Electrical Steels*, Newport, UK, 2000, ISBN 0-9540039-0-X

# PARTICIPANTS OF
# XII SYMPOSIUM OF MAGNETIC MEASUREMENTS & MODELING
## Częstochowa – Siewierz, 17th – 19th October 2016

| | |
|---|---|
| Anna Abramowska | EBSCO Sp. z o.o.<br>Krakowskie Przedmieście 79, 00-079 Warszawa, Poland<br>e-mail: AAbramowska@ebsco.com |
| Babilas Rafał | Silesian University of Technology<br>Institute of Engineering Materials and Biomaterials<br>Konarskiego 18a, 44-100 Gliwice, Poland<br>e-mail: rafal.babilas@polsl.pl |
| Bajorek Jerzy | R&J Measurement, Lipowa 48, Borowa, Poland<br>e-mail: bajorek@rjmeasurement.com.pl |
| Bereźnicki Michał | Częstochowa University of Technology<br>Faculty of Electrical Engineering<br>Al. Armii Krajowej 17, 42-200 Częstochowa, Poland<br>e-mail: bereznickim@interia.pl |
| Borowik Lech | Częstochowa University of Technology<br>Faculty of Electrical Engineering<br>Al. Armii Krajowej 17, 42-200 Częstochowa, Poland<br>e-mail: borowik@el.pcz.czest.pl |
| Burlikowski Wojciech | Silesian University of Technology<br>Faculty of Electrical Engineering, Department of Mechatronics<br>ul. Akademicka 10a, 44-100 Gliwice, Poland<br>e-mail: wojciech.burlikowski@polsl.pl |
| Chwastek Krzysztof | Częstochowa University of Technology<br>Faculty of Electrical Engineering<br>Al. Armii Krajowej 17, 42-200 Częstochowa, Poland<br>e-mail: krzysztof.chwastek@gmail.com |
| Demenko Andrzej | Poznań University of Technology<br>Faculty of Electrical Engineering<br>Piotrowo 3A, 60-965 Poznan, Poland<br>e-mail: andrzej.demenko@put.poznan.pl |
| Domin Jarosław | Silesian University of Technology<br>Faculty of Electrical Engineering, Department of Mechatronics<br>ul. Akademicka 10a, 44-100 Gliwice, Poland<br>e-mail: jaroslaw.domin@polsl.pl |
| Garstka Tomasz | Częstochowa University of Technology<br>Faculty of Production Engineering and Materials Technology<br>Al. Armii Krajowej 19, 42-200 Częstochowa, Poland<br>e-mail: tomasz.garstka@wip.pcz.pl |

| | |
|---|---|
| Gaworska-Koniarek Dominika | Electrotechnical Institute<br>Division of Electrotechnology and Materials Science<br>ul. 55/61 Sklodowskiej-Curie, 50-369 Wroclaw, Poland<br>e-mail: gaworska@iel.wroc.pl |
| Gębara Piotr | Częstochowa University of Technology, Faculty of Production Engineering and Materials Technology, Institute of Physics<br>al. Armii Krajowej 19, 42-200 Częstochowa, Poland<br>e-mail: pgebara@wip.pcz.pl |
| Giżyński Tomasz | Warsaw University of Technology<br>Faculty of Materials Science and Engineering<br>ul. Wołoska 141, 02-507 Warsaw, Poland<br>e-mail: tomasz.gizynski@inmat.pw.edu.pl |
| Gozdur Roman | Technical University of Lodz<br>Department of Semiconductor and Optoelectronic Devices<br>211/215 Wolczanska St., 90-924 Łódz, Poland<br>e-mail: gozdur@p.lodz.pl |
| Guzmán Octavio | National University of Colombia<br>Faculty of Science, Magnetic Materials and Nanostructures Group<br>Carrera 45 # 44-85, Bogota, Colombia<br>e-mail: oguzman12@hotmail.com |
| Haneczok Grzegorz | University of Silesia, Institute of Materials Science<br>ul. 75 Pułku Piechoty 1A, 41-500 Chorzów, Poland<br>e-mail: grzegorz.haneczok@us.edu.pl |
| Hasiak Mariusz | Wrocław University of Science and Technology<br>Department of Mechanics and Materials Science<br>ul. Smoluchowskiego 25, 50-370 Wrocław, Poland<br>e-mail: Mariusz.Hasiak@pwr.edu.pl |
| Hiergeist Robert | Magnet-Physik Dr. Steingroever GmbH<br>Emil-Hoffmann-Straße 3, 50996 Köln, Germany<br>e-mail: robert.hiergeist@magnet-physik.de |
| Jackiewicz Dorota | Warsaw University of Technology<br>Institute of Metrology and Biomedical Engineering<br>ul. Andrzeja Boboli 8, 02-525 Warsaw, Poland<br>e-mail: d.jackiewicz@mchtr.pw.edu.pl |
| Jakubas Adam | Częstochowa University of Technology<br>Faculty of Electrical Engineering<br>Al. Armii Krajowej 17, 42-200 Częstochowa, Poland<br>e-mail: adam.jakubas@gmail.com |

| | |
|---|---|
| Kachniarz Maciej | Warsaw University of Technology<br>Institute of Metrology and Biomedical Engineering<br>ul. Andrzeja Boboli 8, 02-525 Warsaw, Poland<br>e-mail: m.kachniarz@mchtr.pw.edu.pl<br><br>Industrial Research Institute for Automation and Measurements<br>al. Jerozolimskie 202, 02-486 Warsaw, Poland<br>e-mail: mkachniarz@piap.pl |
| Kapelski Dariusz | Tele & Radio Research Institute<br>ul. Ratuszowa 11, 03-450 Warszawa, Poland<br>e-mail: dariusz.kapelski@itr.org.pl |
| Kapłon Andrzej | Kielce University of Technology<br>Power Electronic, Electrical Machines and Drives Chair<br>Aleja 1000-lecia Panstwa Polskiego 7, 25-314 Kielce, Poland<br>e-mail: akaplon@tu.kielce.pl |
| Kawalec Damian | Rzeszow University of Technology<br>Faculty of Electrical and Computer Engineering<br>ul. W. Pola 2, 35-959 Rzeszów, Poland<br>e-mail: damkaw@prz.edu.pl |
| Kielan Paweł | Silesian University of Technology<br>Faculty of Electrical Engineering, Department of Mechatronics<br>ul. Akademicka 10a, 44-100 Gliwice, Poland<br>e-mail: pawel.kielan@polsl.pl |
| Kluszczyński Krzysztof | Silesian University of Technology<br>Faculty of Electrical Engineering, Department of Mechatronics<br>ul. Akademicka 10a, 44-100 Gliwice, Poland<br>e-mail: krzysztof.kluszczynski@polsl.pl |
| Kotynia Katarzyna | Częstochowa University of Technology, Faculty of Production Engineering and Materials Technology, Institute of Physics<br>al. Armii Krajowej 19, 42-200 Częstochowa, Poland<br>e-mail: kkotynia@wip.pcz.pl |
| Kowalik Zygmunt | Silesian University of Technology<br>Faculty of Electrical Engineering, Department of Mechatronics<br>ul. Akademicka 10a, 44-100 Gliwice, Poland<br>e-mail: zygmunt.kowalik@polsl.pl |
| Kowol Paweł | Silesian University of Technology<br>Faculty of Electrical Engineering, Department of Mechatronics<br>ul. Akademicka 10a, 44-100 Gliwice, Poland<br>e-mail: pawel.kowol@polsl.pl |
| Krawczyk Damian | Silesian University of Technology<br>Faculty of Electrical Engineering, Department of Mechatronics<br>ul. Akademicka 10a, 44-100 Gliwice, Poland<br>e-mail: damian.krawczyk@polsl.pl |

| | |
|---|---|
| Kubisztal Marian | University of Silesia, Institute of Materials Science<br>ul. 75 Pułku Piechoty 1A, 41-500 Chorzów, Poland<br>e-mail: Marian.Kubisztal@us.edu.pl |
| Kurzawa Milena | Poznań University of Technology<br>Faculty of Electrical Engineering<br>Piotrowo 3A, 60-965 Poznan, Poland<br>e-mail: milena.kurzawa@put.poznan.pl |
| Kwapuliński Piotr | University of Silesia, Institute of Materials Science<br>ul. 75 Pułku Piechoty 1A, 41-500 Chorzów, Poland<br>e-mail: piotr.kwapulinski@us.edu.pl |
| Majocha Andrzej | Technical University of Lodz<br>Department of Semiconductor and Optoelectronic Devices<br>211/215 Wolczanska St., 90-924 Łódz, Poland<br>e-mail: andrzej.majocha@p.lodz.pl |
| Mazur Damian | Rzeszów University of Technology<br>Faculty of Electrical and Computer Engineering<br>ul. W. Pola 2, B206, 35-959 Rzeszów, Poland<br>e-mail: mazur@prz.edu.pl |
| Melikhov Yevgen | Polish Academy of Sciences, Institute of Physics<br>Al. Lotnikow 32/46, 02-668 Warsaw, Poland<br>e-mail: melikhov@ifpan.edu.pl<br><br>Cardiff University<br>Wolfson Centre for Magnetics, School of Engineering<br>Cardiff, CF24 3AA, United Kingdom<br>e-mail: melikhov@cardiff.ac.uk, melikhov@ifpan.edu.pl |
| Mendoza Barón Aminta | National University of Colombia<br>Faculty of Science, Magnetic Materials and Nanostructures Group<br>Carrera 45 # 44-85, Bogota, Colombia<br>e-mail: gamendozab@unal.edu.co |
| Nadolski Roman | Kielce University of Technology<br>Power Electronic, Electrical Machines and Drives Chair<br>Aleja 1000-lecia Panstwa Polskiego 7, 25-314 Kielce, Poland<br>e-mail: r.nadolski@tu.kielce.pl |
| Najgebauer Mariusz | Częstochowa University of Technology<br>Faculty of Electrical Engineering<br>Al. Armii Krajowej 19, 42-200 Częstochowa, Poland<br>e-mail: najgebauer@el.pcz.czest.pl |
| Nowak Paweł | Warsaw University of Technology<br>Institute of Metrology and Biomedical Engineering<br>ul. Andrzeja Boboli 8, 02-525 Warsaw, Poland<br>e-mail: p.nowak@mchtr.pw.edu.pl |

| | |
|---|---|
| Nowakowski Andrzej | Tele & Radio Research Institute<br>ul. Ratuszowa 11, 03-450 Warszawa, Poland<br>e-mail: andrzej.nowakowski@itr.org.pl |
| Nowicki Michał | Warsaw University of Technology<br>Institute of Metrology and Biomedical Engineering<br>sw. Boboli 8, 02-525 Warsaw, Poland<br>e-mail: m.nowicki@mchtr.pw.edu.pl<br><br>Industrial Research Institute for Automation and Measurements<br>al. Jerozolimskie 202, 02-486 Warsaw, Poland<br>e-mail: mkachniarz@piap.pl |
| Pasko Marian | Silesian University of Technology<br>Faculty of Electrical Engineering<br>ul. Akademicka 10a, 44-100 Gliwice, Poland<br>e-mail: marian.pasko@polsl.pl |
| Pawlik Katarzyna | Częstochowa University of Technology<br>Faculty of Production Engineering and Materials Technology<br>Al. Armii Krajowej 19, 42-200 Częstochowa, Poland<br>e-mail: kpawlik@wip.pcz.pl |
| Pilch Zbigniew | Silesian University of Technology<br>Faculty of Electrical Engineering, Department of Mechatronics<br>ul. Akademicka 10a, 44-100 Gliwice, Poland<br>e-mail: zbigniew.pilch@polsl.pl |
| Pinhasi Yosef | Ariel University, Faculty of Engineering<br>Department of Electrical and Electronic Engineering<br>Kiriat Hamata POB 3, Ariel 40700, Israel<br>e-mail: yosip@ariel.ac.il |
| Pluta Wojciech A. | Częstochowa University of Technology<br>Faculty of Electrical Engineering<br>Al. Armii Krajowej 17, 42-200 Częstochowa, Poland<br>e-mail: w.pluta@gmail.com |
| Pruba Marcin | Częstochowa University of Technology, Faculty of Production Engineering and Materials Technology, Institute of Physics<br>al. Armii Krajowej 19, 42-200 Częstochowa, Poland<br>e-mail: mpruba@wip.pcz.pl |
| Prusik Krystian | University of Silesia, Institute of Materials Science<br>ul. Bankowa 12, 40-007 Katowice, Poland<br>e-mail: prusik.krystian@gmail.com<br><br>University of Silesia<br>Silesian Center for Education and Interdisciplinary Research,<br>75 Pułku Piechoty 1A, 41-500 Chorzów, Poland |
| Przybylski Marek | Tele & Radio Research Institute<br>ul. Ratuszowa 11, 03-450 Warszawa, Poland<br>e-mail: marek.przybylski@itr.org.pl |

| | |
|---|---|
| Salach Jacek | Warsaw University of Technology<br>Institute of Metrology and Biomedical Engineering<br>ul. Andrzeja Boboli 8, 02-525 Warsaw, Poland<br>e-mail: j.salach@mchtr.pw.edu.pl |
| Smusz Robert | Rzeszów University of Technology<br>Department of Thermodynamics and Fluid Mechanics<br>ul. Powstańców Warszawy 12, 35-959 Rzeszów, Poland<br>e-mail: robsmusz@prz.rzeszow.pl |
| Stachowiak Dorota | Poznań University of Technology<br>Faculty of Electrical Engineering<br>Piotrowo 3A, 60-965 Poznan, Poland<br>e-mail: dorota.stachowiak@put.poznan.pl |
| Stupakov Alexandr | Czech Academy of Sciences, Institute of Physics<br>Na Slovance 2, 18221 Prague, Czech Republic<br>e-mail: stupak@fzu.cz |
| Szczurek Paweł | Stalprodukt S.A.<br>ul. Wygoda 69, 32-700 Bochnia, Poland<br>e-mail: pawel.szczurek@stalprodukt.pl |
| Szczygieł Marcin | Silesian University of Technology<br>Faculty of Electrical Engineering, Department of Mechatronics<br>ul. Akademicka 10a, 44-100 Gliwice, Poland<br>e-mail: marcin.szczygiel@polsl.pl |
| Szczygłowski Jan | Częstochowa University of Technology<br>Faculty of Electrical Engineering<br>Al. Armii Krajowej 17, 42-200 Częstochowa, Poland<br>e-mail: jszczyg@gmail.com |
| Szewczyk Roman | Warsaw University of Technology<br>Institute of Metrology and Biomedical Engineering<br>ul. Andrzeja Boboli 8, 02-525 Warsaw, Poland<br>e-mail: szewczyk@mchtr.pw.edu.pl |
| Szymański Mateusz | Warsaw University of Technology<br>Faculty of Materials Science and Engineering<br>141 Woloska Street, 02-507 Warsaw, Poland<br>e-mail: m.szymanski@inmat.pw.edu.pl |
| Ślusarek Barbara | Tele & Radio Research Institute<br>ul. Ratuszowa 11, 03-450 Warszawa, Poland<br>e-mail: barbara.slusarek@itr.org.pl |
| Wojciechowski Rafał M. | Poznań University of Technology<br>Faculty of Electrical Engineering<br>Piotrowo 3A, 60-965 Poznan, Poland<br>e-mail: rafal.wojciechowski@put.poznan.pl |

| | |
|---|---|
| Wołoszyn Mirosław | Technical University of Gdańsk<br>Faculty of Electrical and Control Engineering<br>ul. G. Narutowicza 11/12, 80-233 Gdańsk, Poland<br>e-mail: miroslaw.woloszyn@pg.gda.pl, mirwolos@pg.gda.pl |
| Wysłocki Jerzy J. | Częstochowa University of Technology, Faculty of Production Engineering and Materials Technology, Institute of Physics<br>al. Armii Krajowej 19, 42-200 Częstochowa, Poland<br>e-mail: wyslocki@wip.pcz.pl |
| Yahalom Asher | Ariel University, Faculty of Engineering<br>Department of Electrical and Electronic Engineering<br>Kiriat Hamata POB 3, Ariel 40700, Israel<br>e-mail: asya@ariel.ac.il |
| Żurek Stan | Megger Instruments Ltd<br>Archcliffe Road, Dover, CT17 9EN, Kent, United Kingdom<br>e-mail: stan.zurek@ieee.org |